Western University

Scholarship@Western

5-11-2021 4:30 PM

4DCT to Examine Carpal Motion

Sydney M. Robinson, *The University of Western Ontario*

Supervisor: Lalone, Emily, *The University of Western Ontario*

A thesis submitted in partial fulfillment of the requirements for the Master of Engineering Science degree in Biomedical Engineering
© Sydney M. Robinson 2021

Recommended Citation

Abstract

Four-dimensional computed tomography (4DCT) is a novel imaging modality initially used in cardiac imaging but recently applied to the musculoskeletal system; although its methodology has been developed, it is still in its infancy as a powerful clinical tool. Currently, scapholunate interosseous ligament (SLIL) tears, whose early symptoms are elucidated through dynamic movement, are diagnosed with static techniques that cannot visualize dynamic motion; hence, a tool is needed that is responsive and dynamic to visualize subtle abnormal carpal movements indicative of SLIL tears. It is hypothesized that 4DCT can visualize subtle dynamic carpal movements to define uninjured motion as well as differentiate between that and motion from those with SLIL tears. Understanding uninjured wrist motion was done by calculating scaphoid centroid translation and joint surface area (JSA) from kinematic 4DCT scans. The findings agreed with previously reported outcomes. The 4DCT tool was validated against a gold standard (micro-CT). Lastly, the 4DCT tool was provocatively tested to determine kinematic differences between uninjured and SLIL tear cohorts, as well as between types of SLIL tears. The helical axes of the scaphoid and lunate were calculated from 4DCT bone models using custom MATLAB code. Findings suggest that 4DCT shows promise as a diagnostic tool for dynamic injuries and that volar SLIL tears may negatively impact carpal motion.

Keywords

Four-dimensional computed tomography, wrist, kinematics, scapholunate interosseous ligament tears, joint surface area, helical axes, carpal rotation

Summary for Lay Audience

Currently, there is no universally-agreed-upon theory for how the wrist moves; the wrist is made of nine bones and two forearm bones, and so its motion is complex. One reason for why there is no such theory is a lack of data; it is difficult to image wrist motion because a lot of methods for imaging the wrist are static. Static imaging methods, such as the common x-ray, are methods that can only visualize how the bones are positioned when the wrist is stationary. This presents a large problem when diagnosing injuries. Certain injuries, such as ligament tears, wherein a ligament connects bone to bone, have symptoms that are only apparent when the wrist is in motion. Ligament tears are painful, and it is important to medically intervene early for the best results. A tool is needed to visualize wrist motion for two reasons: to measure uninjured wrist motion and to determine the differences between that and wrist motion in individuals with ligament tears. This thesis proposes the use of four-dimensional computed tomography (4DCT) to address both needs because 4DCT scans can create a movie of moving 3D bone models.

The 4DCT tool was used to measure uninjured wrist movement, specifically the translation of a wrist bone and the amount of contact between neighbouring bones. Once it was determined that 4DCT could successfully take such measurements, it was validated against a gold standard method (micro-CT) for 3D scanning bones. Micro-CT creates high-quality 3D models of the wrist bones, but it is a static imaging method. The comparison confirmed that 4DCT was valid, and so it was applied to a more challenging situation: detecting differences between uninjured wrist motion and that of individuals with ligament tears. It was hypothesized that the type of tear would determine how wrist motion differed from uninjured motion. The 4DCT scans were used to measure wrist bone rotation and contact between neighbouring bones. The results showed that 4DCT could detect a difference in these measurements. All types of ligament tears may impact wrist motion and may need to be repaired, as only some types are currently surgically repaired.

Co-Authorship Statement

Chapter 1:

Sydney Robinson – Sole author

Chapter 2:

Sydney Robinson – Study design, data collection, statistical analysis, wrote manuscript

Lauren Straatman – Data collection, statistical analysis

Ting-Yim Lee – Study design

Nina Suh – Study design, reviewed manuscript

Emily Lalone – Study design, reviewed manuscript

Chapter 3:

Sydney Robinson – Study design, data collection, statistical analysis, wrote manuscript

Elizabeth Norman – Study design, data collection, statistical analysis

Nina Suh – Study design, reviewed manuscript

Emily Lalone – Study design, reviewed manuscript

Chapter 4:

Sydney Robinson – Study design, wrote MATLAB code, data collection, statistical analysis, wrote manuscript

Elizabeth Norman – Study design, data collection

Michael Rainbow – Assisted with MATLAB coding, reviewed manuscript

Emily Lalone – Study design, reviewed manuscript

Nina Suh – Study design, reviewed manuscript

Chapter 5:

Sydney Robinson – Sole author

Acknowledgments

I would like to thank everyone whose help and support was instrumental to my completion of this work. Foremost, I would like to thank my supervisor, Dr Emily Lalone, for her exceptional guidance and support, as well as constructive criticism that helped me grow as a researcher. I would like to thank Dr Nina Suh for her insights and probing questions that ensured these studies are relevant and interesting. I would also like to thank Dr Dan Langohr for being instrumental in the technical elements of my data analysis and validation. I would also like to thank my lab for their support and friendship, especially Elizabeth Norman and Lauren Straatman for their assistance with this work. Lastly, I would like to thank my friends and family for their unfailing love and support.

Table of Contents

List of Tables

List of Figures

List of Appendices

List of Abbreviations

ABS – acrylonitrile butadiene styrene

ADL – activities of daily living

APL – abductor pollicis longus

BVF – biplane videofluoroscopy

CMC – carpometacarpal

CT – computed tomography

D – dorsal

Di – distal

DICOM – digital imaging and communications in medicine

DISI – dorsal intercalated segment instability

DLP – dose length product

DRUJ – distal radioulnar joint

DTM – Dart Thrower's Motion

ECRB – extensor carpi radialis brevis

ECRL – extensor carpi radialis longus

ECU – extensor carpi ulnaris

EDC – extensor digitorum communis

EDQ – extensor digiti quartus

EIP – extensor indicis proprius

EPB – extensor pollicis brevis

EPL – extensor pollicis longus

FCR – flexor carpi radialis

FCU – flexor carpi ulnaris

FDS – flexor digitorum superficialis

FDP – flexor digitorum profundus

FE – flexion extension

FPL – flexor pollicis longus

HU – Hounsfield units

ICP – iterative closest point

IP – interphalangeal

ISB – International Society of Biomechanics

JSA – joint surface area

LCS – local coordinate system

MP – metacarpophalangeal

MRI – magnetic resonance imaging

NVR – neurovascular relationship

P – proximal

PL – palmaris longus

PQ – pronator quadratus

R – radial

RUD – radioulnar deviation

SL – scapholunate

SLAC – scapholunate advanced collapse

SLIL – scapholunate interosseous ligament

STL – stereolithography

TWA – total wrist arthroplasty

U – ulnar

V – volar

VTK – visualization toolkit

2D – two-dimensional

3D – three-dimensional

3DCT – three-dimensional computed tomography

4DCT – four-dimensional computed tomography

Chapter 1

1 Introduction

This thesis focuses on the implementation of four-dimensional computed tomography (4DCT) as a novel tool for examining carpal motion. Joint contact relationships and kinematics of the wrist joint are evaluated in normal conditions, and in the case of scapholunate interosseous ligament tears; the provocative application of 4DCT to differentiate between healthy and injured populations tests the capabilities of this tool. This chapter reviews the anatomy, kinematics, and biomechanics of the wrist. Methods for assessing joint kinematics and joint contact are discussed, followed by a summary of the study rationale, objectives, and hypotheses.

1.1 The Wrist

The wrist is one of the most complex and functionally important joints in the upper extremity. Comprised of many carpal bones which allow for many articulations, the wrist allows for three primary planar motions[1], which enable many complex combined motions such as Dart Thrower's Motion or circumduction[2]. There are four groupings of bones in the wrist and hand: the forearm (2 bones), the carpus (8 bones), the metacarpus (5 bones), and the phalanges (14 bones) (Figure 1.1). Due to the high number of bones, there are also many joints of varying orientations and size. The wrist is the most susceptible to injury of all upper extremity joints[3] and there are conflicting theories about its mechanisms of motion[4].
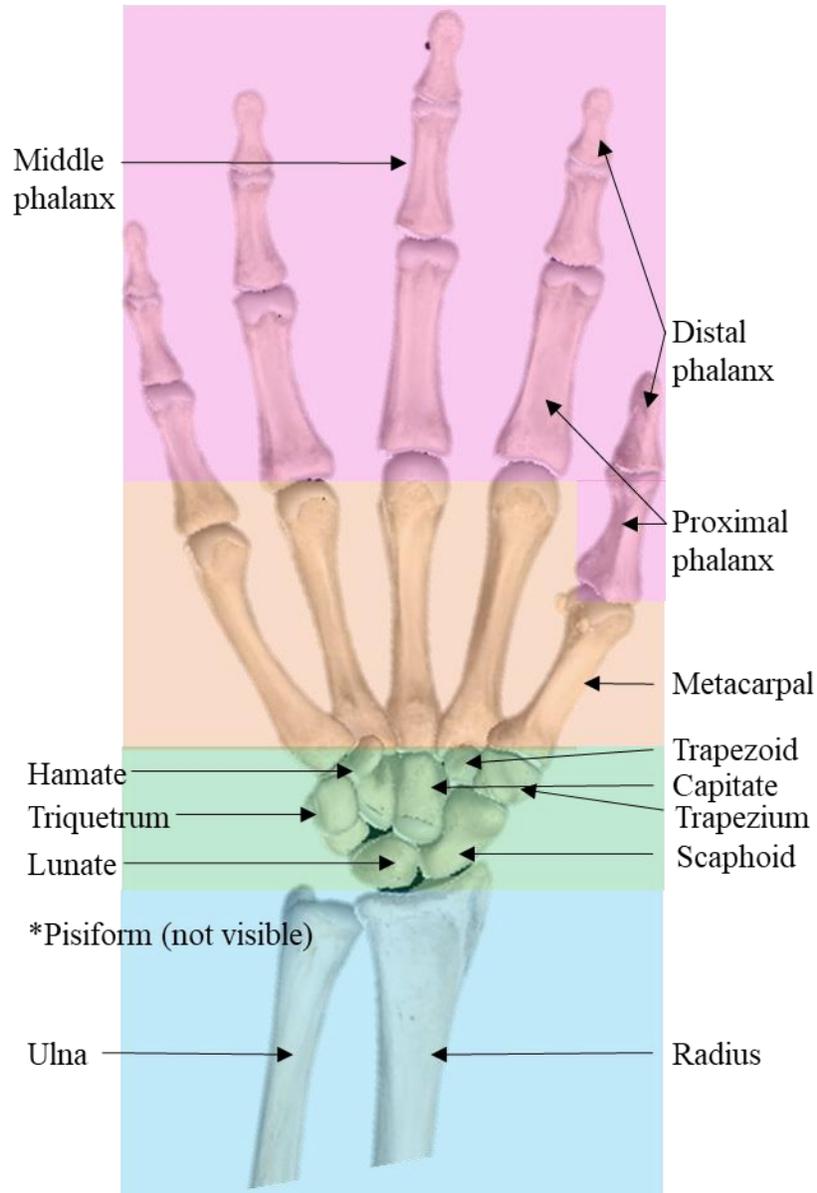
Figure 1.1: Bones of the hand. The groups of the bones are as follows: pink are the phalanges, orange are the metacarpals, green are the carpals, and blue are the forearm[5].

1.2 Anatomy of the Wrist

1.2.1 Bony Anatomy

<u>Structure</u>. Bones are comprised of various tissues (osseous tissue, cartilage, dense connective tissue, epithelium, adipose tissue, nervous tissue) that work together to form the skeletal system[1]. The wrist's functions primarily include support (of soft tissues and providing points of attachments

for tendons and ligament), protection from injury, and facilitation of movement (through the contraction of forearm muscles attached to the carpus)[1]. To execute these functions, there are several types of bones: long bones, short bones, and sesamoid bones (Figure 1.2). Long bones have greater length than width, consist of a diaphysis and some number of epiphyses, are curved for strength, and contain compact bone as well as spongy bone; in the wrist, the long bones are the radius, ulna, metacarpals, and phalanges. Short bones are approximately equal in all dimensions and are comprised of spongy bone surrounded by a thin layer of compact bone; most carpal bones are short bones. Sesamoid bones are found in tendons that experience high forces and stress to protect the tendons from excessive wear and improve mechanical advantage through alteration of force direction through a tendon. In the wrist, the pisiform is the best-known sesamoid bone, while others include those found in the tendons of the adductor pollicis and flexor brevis muscles at the thumb joint.
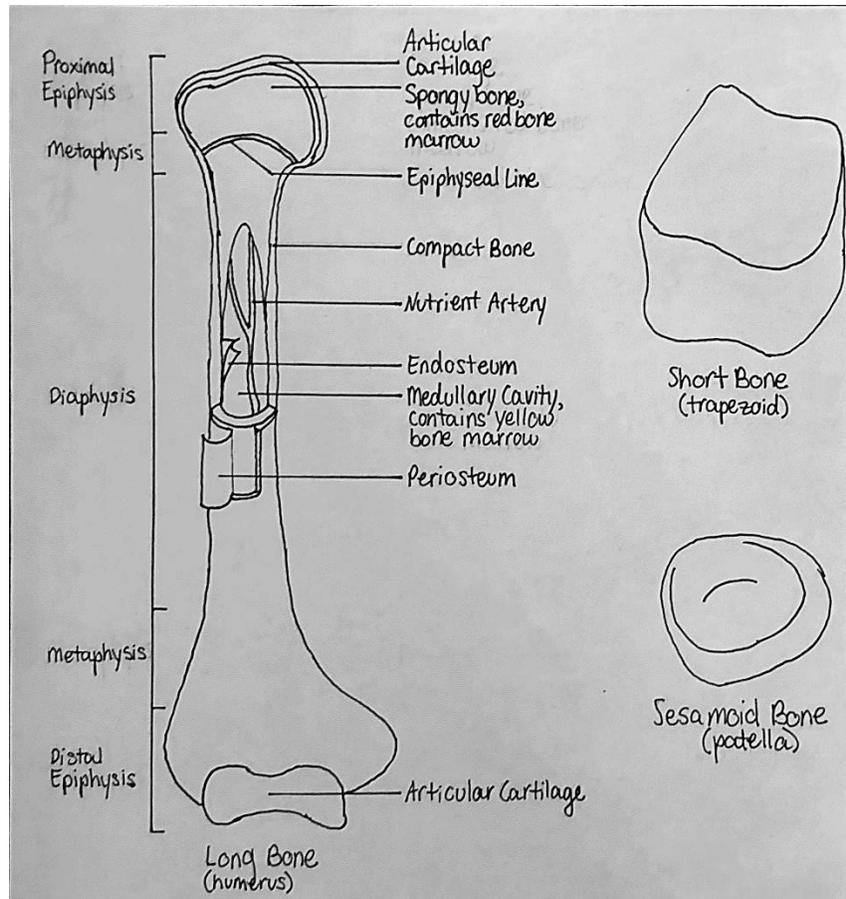
Figure 1.2: Anatomy of bones; gross geometry of a representative long bone, short bone, and sesamoid bone.

While there are different shapes of bones, all bones are comprised of mostly the same components (Figure 1.2). The diaphysis is the shaft of the bone, which contains a medullary cavity filled with bone marrow and lined with the endosteum, a layer of bone-forming cells and connective tissue[1]. The epiphyses are the proximal and distal extremities of the bone, and the metaphyses are the regions in between the diaphysis and epiphysis, which contain the epiphyseal plate (growth plate) in growing bones and the epiphyseal line (fused growth plate) in mature bones. A thin layer of hyaline cartilage called articular cartilage surrounds the epiphysis where the bone articulates with other bones to reduce friction and absorb shock in the joint. Due to its avascular nature, articular cartilage is limited in its ability to repair and regenerate. Where a bone is not covered in articular cartilage, it is covered in the periosteum, which is a tough vascular sheath of connective tissue that

protects the bone, assists in fracture repair, provides nourishment, and provides an attachment point for tendons and ligaments.

Radius. Located on the lateral side of the forearm, the radius is shorter than the ulna and widens from a narrow proximal end to a broad distal end (Figure 1.3)[1]. The proximal end articulates with the capitulum of the humerus and the radial notch of the ulna. The styloid process is where the shaft of the radius widens on the lateral side of the distal end. One study identified four shapes of the articular surface of the distal radius sigmoid notch: flat-faced (no curve to the sigmoid notch, parallel to the dorsal-volar axis), C-type (deepest concave curve and lowest sagittal slope of the sigmoid notch), S-type (concave curve and exaggerated dorsal lip of the sigmoid notch), and ski-slope (no curve to the sigmoid notch, oblique to the dorsal-volar axis) variants[6].
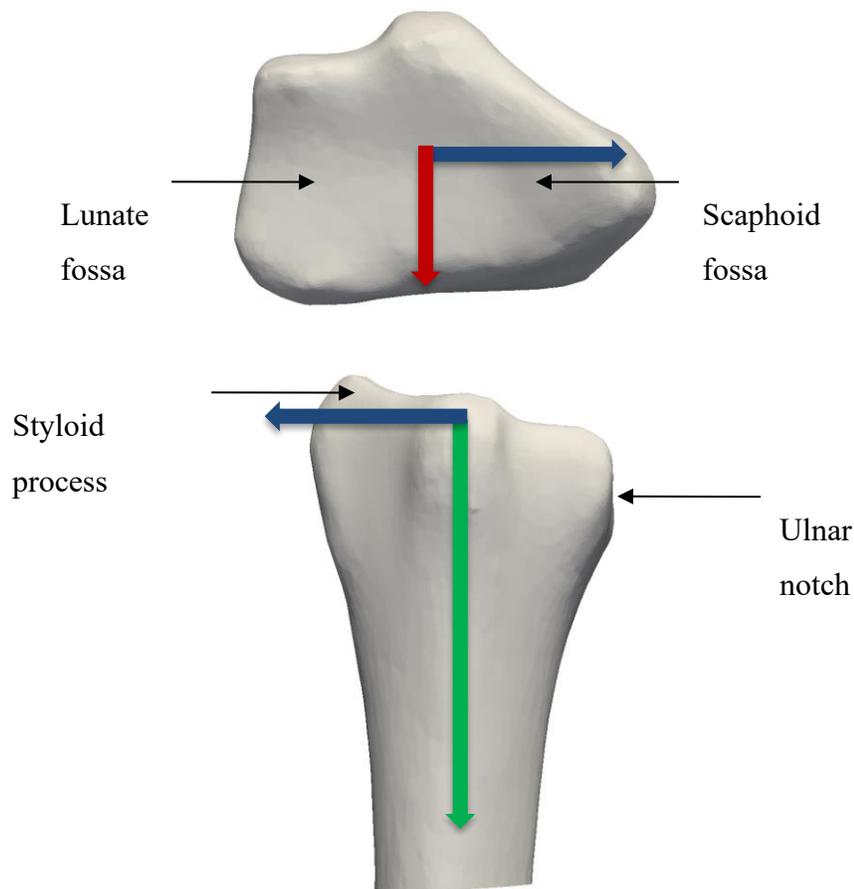
Figure 1.3: Osteology of the radius, distal articular surface (top) and posterior view (bottom). The ISB coordinate system is included: x-axis (red) points volar and describes radioulnar deviation, y-axis (green) points proximal and describes pronation supination, and z-axis (blue) points radial and describes flexion extension.

Ulna. Located on the medial side of the forearm, the ulna is longer than the radius with a thick, notched proximal end and a narrow, cylindrical distal end (Figure 1.4)[1]. The proximal end is comprised of the olecranon (the prominence of the elbow), the trochlear notch (receives the trochlea of the humerus as part of the elbow joint), the coronoid process (anterior projection distal to the trochlear notch), the radial notch (lateral and inferior to the trochlear notch, articulates with the radius), and the ulnar tuberosity (inferior to the coronoid process). The distal end is comprised of a head with a disc of fibrocartilage and a styloid process on the posterior side.
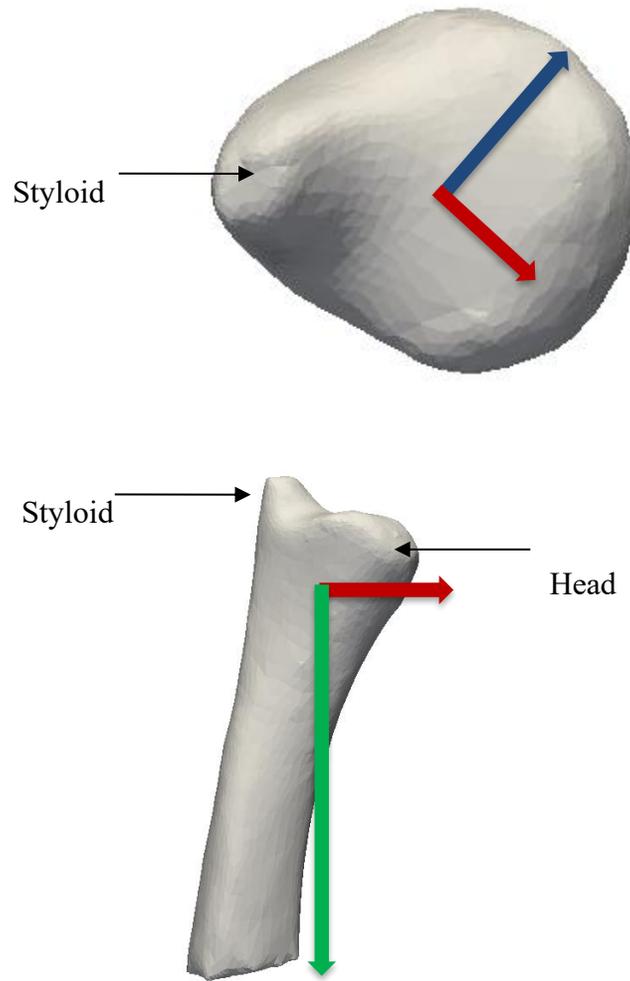
Figure 1.4: Osteology of the ulna, distal articular surface (top) and ulnar view (bottom). The ISB coordinate system is included: x-axis (red) points volar and describes radioulnar deviation, y-axis (green) points proximal and describes pronation supination, and z-axis (blue) points radial and describes flexion extension.

Carpus. The carpus is comprised of seven short bones (lunate, scaphoid, capitate, hamate, trapezium, trapezoid, triquetrum) and a sesamoid bone (pisiform) connected by ligaments, and connects the distal radius and ulna to the metacarpals (Figure 1.1)[1,7]. The carpals can be categorized into two rows: the proximal row (from lateral to medial: scaphoid, lunate, triquetrum, pisiform) and the distal row (from lateral to medial: trapezium, trapezoid, capitate, hamate).

Lunate. The lunate is a moon-shaped bone and is involved in the radiocarpal joint (Figure 1.5)[1]. Lunates are classified into two types: type one has a single distal facet, and type two has two distal

facets wherein the additional one allows for articulation with the hamate (Figure 1.6)[8-10]. In one carpal mechanics study, lunate type was responsible for a change in the distal articular midpoint of the triquetrum relative to the midpoint of the lunate[11]; the sliding distance was greater in type 2 lunates than in type 1. Five main modes of variation within the lunate have been described: ratio between width and height, angle between sides adjacent to scaphoid and triquetrum and height of the lunate along the long axis of the capitate, skewness in the coronal plane, higher volar or dorsal bone end, and extra facet adjacent to hamate[12]. However, insignificant findings between such classifications indicate the lunate can still only be reliably grouped as type 1 or type 2.
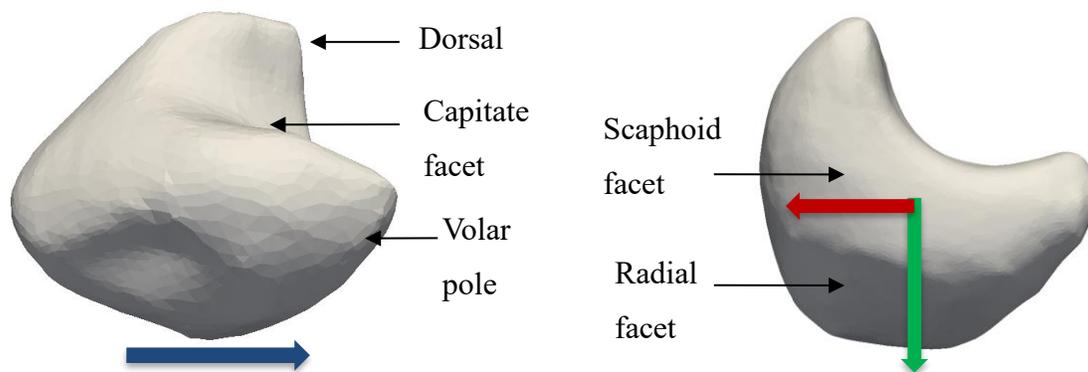
Figure 1.5: Osteology of the lunate, oblique view (left) and radial view (right). The ISB coordinate system is included: x-axis (red) points volar and describes radioulnar deviation, y-axis (green) points proximal and describes pronation supination, and z-axis (blue) points radial and describes flexion extension.

Figure 1.6: Type 1 lunate (left, no articulation with the hamate) vs. Type 2 lunate (right, articulation with the hamate).

<u>Scaphoid.</u> The scaphoid is a boat-shaped bone in the radiocarpal joint[1]. Very few studies have examined the morphologic shapes of carpals, which is necessary for prosthesis design[12], and those that have mostly focus on the lunate and seldom on the scaphoid. Van de Giessen et al. found five main modes of variation within the scaphoid: height of the waist, length of the tubercle, volume ratio between the proximal and distal poles, orientation and length of the distal ridge, and anteroposterior instrascaphoid angle[12]. There were no significant differences between these scaphoid shapes which suggest that although these landmarks can be seen in the scaphoids and do change between specimens, there are no distinct types such as in the lunate.
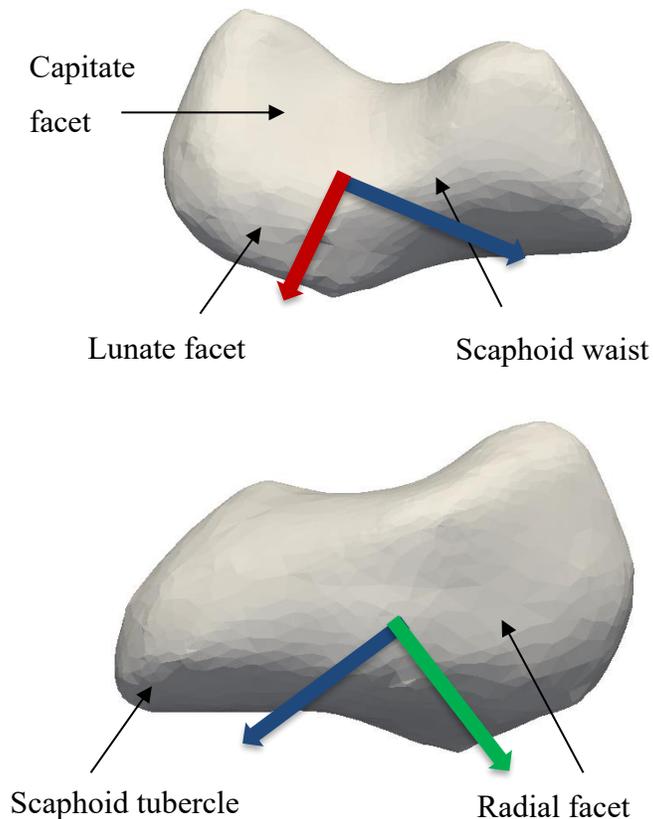
Figure 1.7: Osteology of the scaphoid, superior/volar view (top) and dorsal view (right). The ISB coordinate system is included: x-axis (red) points volar and describes radioulnar deviation, y-axis (green) points proximal and describes pronation supination, and z-axis (blue) points radial and describes flexion extension.

Capitate. The capitate is the largest carpal bone with a rounded head that articulates with the lunate (Figure 1.8)[1]. Kramer et al. used plain radiographs to analyze the midcarpal joint, and classified the capitate into two types, wherein type one had a spherical proximal facet and type two had a flat proximal facet[8]. They subsequently defined two wrist types: type one had a type one lunate and capitate while type two wrists had a type two lunate and capitate. From the radiographs, they determined differences in contact area between the lunate and capitate, capitate and third metacarpal, lunate and hamate, and capitate and hamate depending on wrist type. This would suggest that the capitate can be grouped into morphologic shapes akin to the lunate.
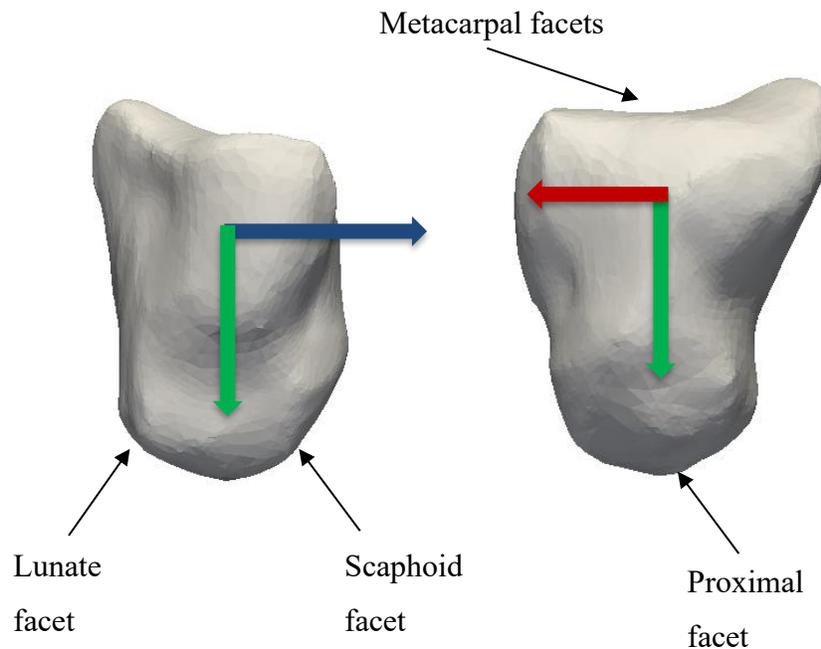
Figure 1.8: Osteology of the capitate; volar view (left) and radial view (right). The ISB coordinate system is included: x-axis (red) points volar and describes radioulnar deviation, y-axis (green) points proximal and describes pronation supination, and z-axis (blue) points radial and describes flexion extension.

Remaining Carpals. The shapes of the remaining carpal bones (Figure 1.1) are reflected in their names and have not been classified into morphologic shapes in the current literature: the triquetrum is three-cornered, the pisiform is pea-shaped, the trapezium is four-sided with no two sides parallel, the trapezoid is four-sided with two sides parallel, and the hamate has a large hook-shaped projection on its anterior surface[1].

Metacarpals. The five bones (numbered one to five, lateral to medial) in the intermediate region of the hand are called the metacarpals, which all consist of a proximal base, a shaft, and a distal head (Figure 1.1)[1].

Phalanges. The 14 bones which comprise the digits of the hand at the most distal region are called the phalanges; the digits are numbered one to five from radial to ulnar, wherein a single bone in the digit is a phalanx (Figure 1.1)[1]. While the thumb has two phalanges (proximal and distal

phalanges), the rest of the digits have three (proximal, middle, and distal phalanges) and are commonly called the index, long, ring and small fingers moving radial to ulnar.

1.2.2   Joints

Structure. A joint is a point of contact or articulation between bones and while there are many types, those in the wrist are synovial joints (Figure 1.9) that have a distinct joint cavity and use cartilage between the bones to articulate with reduced friction[1]. The specific types of synovial joints found in the wrist include plane joints (back-and-forth, side-to-side, and sometimes rotational motion; bi- or triaxial), hinge joints (a bone's convex surface articulates within another bone's concave surface; uniaxial), pivot joints (rounded surface of one bone pivots around a ring comprised of another bone and ligament; uniaxial), condyloid joints (convex surface of one bone fits into the concave surface of another but the surfaces are oval instead of rounded; biaxial), and saddle joints (one bone is saddle-shaped and another bone fits into that shape; biaxial) (Figure 1.9).
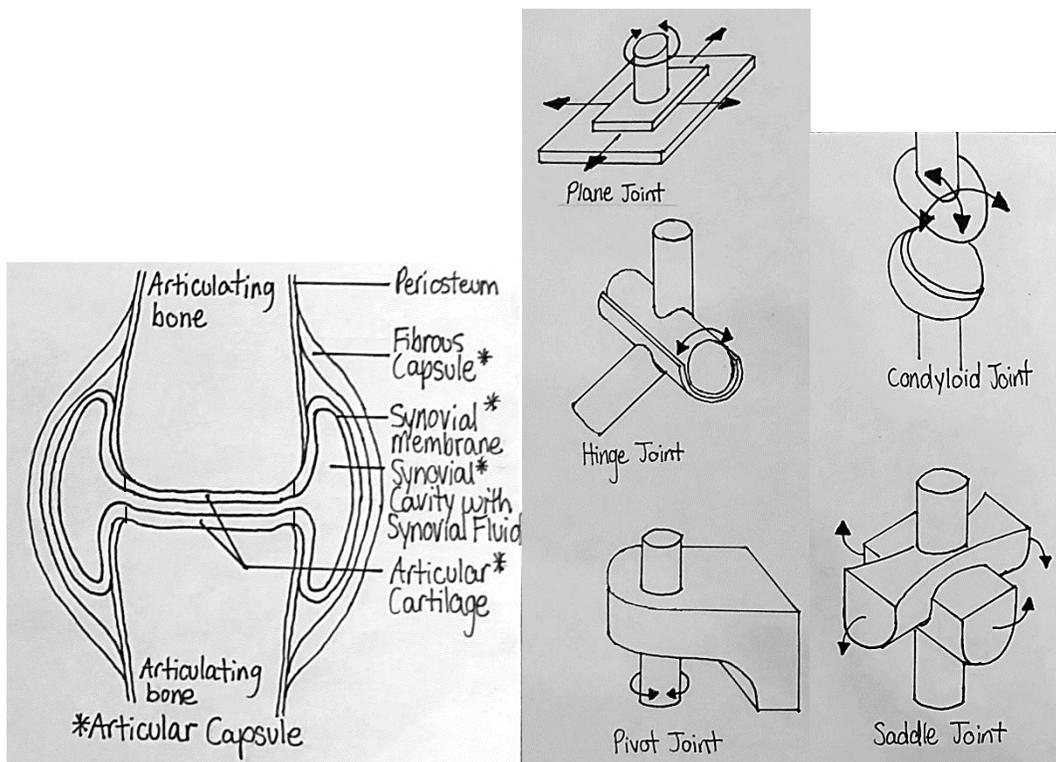
Figure 1.9: Anatomy of synovial joints and five subtypes found in the wrist. Structures with the symbol * are part of the articular capsule.

Anatomy. There are six joints or groups of joints in the wrist (Figure 1.10). The distal radioulnar joint (DRUJ), where the convex head of the ulna articulates with the concave sigmoid notch of the distal radius[1], is a pivot joint critical for facilitating forearm rotation and maintaining wrist stability[6]. The radiocarpal joint is where the distal end of the radius articulates with the lunate, scaphoid, and triquetrum of the carpus[1]. It is classified as a condyloid joint and allows for flexion-extension, abduction-adduction, circumduction, and slight hyperextension of the wrist. The intercarpal joints are the articulations between carpal bones, are comprised of plane and saddle joints, and allow for gliding motion as well as flexion-extension, abduction-adduction, and slight rotation at the midcarpal joint. The carpometacarpal (CMC) joints are the articulations between the bases of the metacarpals with the distal row of the carpals, are comprised of saddle and plane joints, and allow for flexion-extension, abduction-adduction, and circumduction of the digits, as well as gliding at all digits except for the thumb[1]. The metacarpophalangeal (MP) joints are the articulations between the heads of the metacarpals and the proximal ends of the phalanges, commonly known as the "knuckles"[1]. The MP joints are condyloid joints and allow for flexion-extension, abduction-adduction, and circumduction of the phalanges. The interphalangeal (IP) joints are the articulations between phalanges in the form of hinge joints that allow for flexion-extension of the phalanges[1].
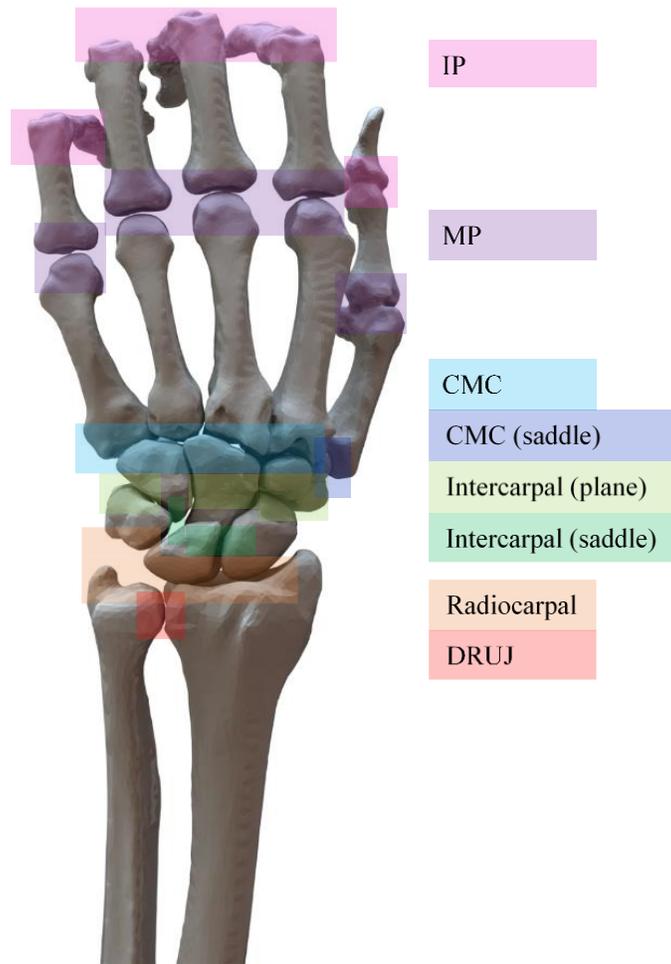
Figure 1.10: Types of joints in the wrist[5].

1.2.3 Ligamentous Anatomy

The ligaments of the hand are dense connective tissues that connect various carpals and form a complex ligamentous structure vital to the wrist's stability[1]. These ligaments act as supporting bands to statically stabilize the joint and limit range of motion[1,7]; their specific function depends on structure wherein ligaments of tightly packed bundles of collagen fibers have important mechanical function, while less structurally packed ligaments contain mechanoreceptors important for proprioception[13]. Intracapsular ligaments are those surrounded by a loose connective tissue sheath and can be either extrinsic or intrinsic; both insert within the carpus while the former originates from the distal radius or ulna and the latter originates from within the carpus[13]. Extrinsic ligaments are stiffer, with a lower yield strength, while intrinsic ligaments have a larger insertion

14

area in cartilage than bone and have fewer elastic fibers. Thus, extrinsic ligaments tend to fail by mid-substance ruptures, while intrinsic ligaments fail by avulsion (pulling or tearing at insertion).

The important ligament for the purposes of this thesis is the scapholunate interosseous ligament (SLIL). The SLIL is comprised of three elements: one volar and one dorsal component, and a proximal fibrocartilaginous membrane (Figure 1.11)[13]. The fibrocartilaginous region separates the radiocarpal and midcarpal joints by spanning the proximal edges of the scaphoid and lunate. The dorsal SLIL connects the dorsal-distal corners of the scaphoid and lunate, while the volar SLIL connects the volar-distal corners. The dorsal SLIL is the thickest and strongest and is long believed to be the most important SLIL for stability[13-16], while the volar SLIL is weaker and resists rotation[13]. The yield strengths of the three structures are: 260 N for the dorsal SLIL, 118 N for the volar SLIL, and 63 N for the fibrocartilaginous region[13]. These ligaments play a key role in wrist motion and stability.
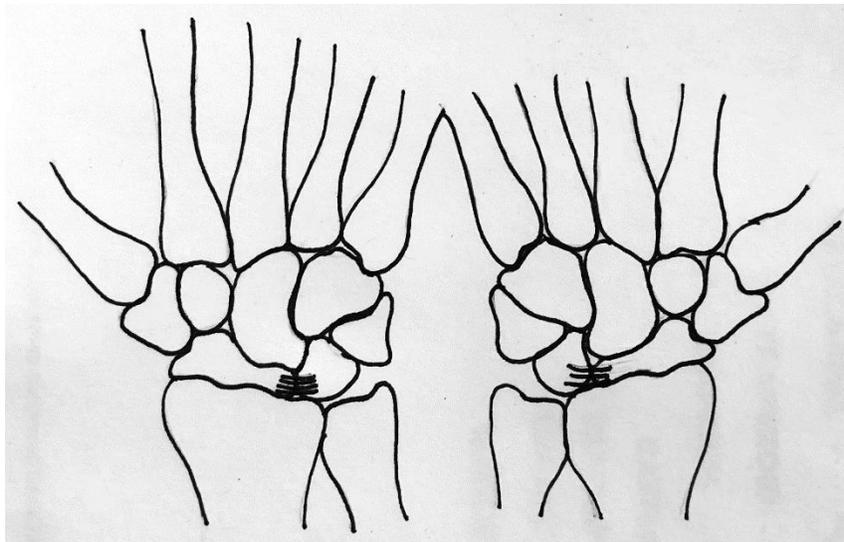
Figure 1.11: SL ligaments: dorsal (left) and volar (right). The left wrist is a view from the dorsal side (back of the hand) and the right wrist is a view from the volar side (palm of the hand).

1.2.4   Musculature

Skeletal muscles are vital tissues that work with the skeletal system to facilitate movement and act as dynamic stabilizers[1,7]. Due to the low number of static stabilizers, many dynamic stabilizers are

needed to restrict range of motion and provide a smooth motion pathway for the wrist. There are volar muscles in charge of flexing the wrist and digits, and dorsal muscles in charge of extending the wrist and digits (Figure 1.12)[1]. The superficial volar muscles include the flexor carpi radialis (FCR), palmaris longus (PL), and flexor carpi ulnaris (FCU), which all originate from the medial epicondyle of the humerus and insert at the base of the 2nd and 3rd metacarpals (FCR), the palmar aponeurosis (PL), and the pisiform, hook of the hamate, and base of the 5th metacarpal (FCU). All three muscles flex the wrist, while FCR also radially deviates the wrist, and PL and FCU ulnarly deviate the wrist. The flexor digitorum superficialis (FDS) is an intermediate volar muscle, originates at the medial epicondyle of the humerus, inserts at the base of the middle phalanx of digits 2-5, and flexes the fingers at the proximal interphalangeal joints. The deep volar muscles consist of the flexor digitorum profundus (FDP), flexor pollicis longus (FPL) and pronator quadratus (PQ). The FDP originates at the medial anterior surface of the ulna, along with the PQ, while the FPL originates at the medial aspect of the radius; FDP inserts at the base of the distal phalanx of digits 2-5, FPL inserts at the base of the distal phalanx of digit 1, and PQ originates at the lateral anterior surface of the radius. While the superficial muscles have a common function, the deep muscles do not; FDP flexes the fingers at the distal interphalangeal joints, FPL flexes the thumb, and PQ pronates the forearm.
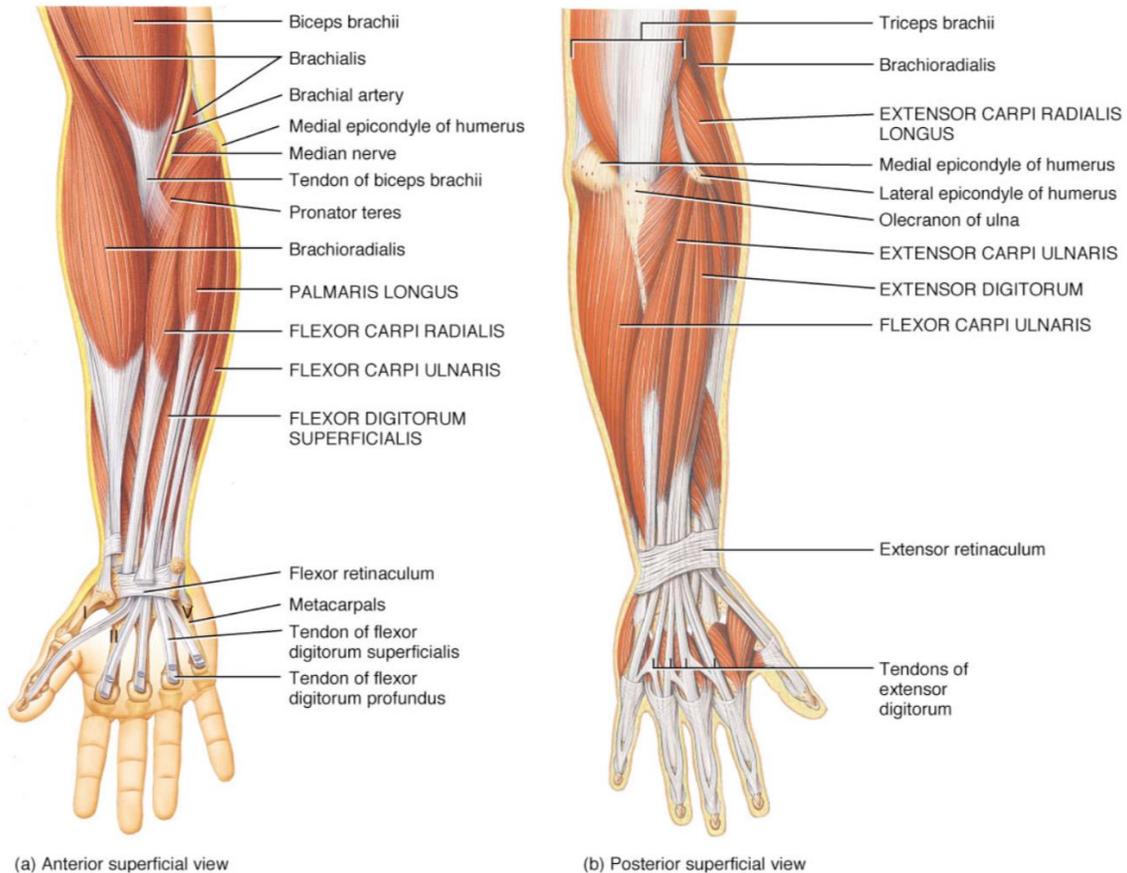
Figure 1.12: Dynamic stabilizers (muscles) of the wrist; volar view (left) and dorsal view (right)[5].

The superficial dorsal muscles all originate from the lateral epicondyle of the humerus and include: extensor carpi radialis brevis (ECRB) (inserts at the base of the 3rd metacarpal), extensor carpi radialis longus (ECRL) (inserts at the base of the 2nd metacarpal), extensor digitorum communis (EDC) (inserts at the base of the distal phalanx of digits 2-5 and the extensor hood), extensor digiti quartus (EDQ) (inserts at the base of the distal phalanx of digit 5 and the extensor hood), and extensor carpi ulnaris (ECU) (inserts at the base of the 5th metacarpal). In terms of function, ECRB, ECRL and ECU all extend the wrist and the first two radially deviate the wrist while ECU ulnarly deviates the wrist. Extension of the small finger occurs by means of EDC and EDQ, while EDC also extends all the other fingers. There are four deep dorsal muscles: abductor pollicis longus (APL), which originates at the medial aspect of the ulna and radius and inserts at the base of the 1st metacarpal; extensor pollicis longus (EPL), which originates from the posterior surface of the

17

ulna and inserts at the base of the distal phalanx of digit 1; extensor pollicis brevis (EPB), which originates at the radius and interosseus membrane and inserts at the base of the proximal phalanx of digit 1; and extensor indicis proprius (EIP), which originates from the distal third of the ulna and inserts at the base of the distal phalanx of digit 2 and the extensor hood. Thus, APL abducts and extends the thumb, EPL extends the thumb at the IP joint while EPB extends the thumb at the MCP joint, and EIP extends the index finger.

1.3   Wrist Biomechanics

The complex anatomy of the wrist allows for three primary planar motions (Figure 1.13): flexion-extension, radioulnar deviation also known as abduction-adduction, and pronation-supination also known as internal-external rotation[1]. These motions can be combined into circumduction (Figure 1.13), wherein the carpus rotates in a circle about the distal radius and ulna[1]. The wrist is also capable of many other complex motions which enable performance of functional tasks in everyday life. These bones allow for a wide range of motion in many planes, and numerous paths of motion to reach the same destination, the complexity of which makes wrist motion difficult to understand. There is no cyclic motion, such as gait cycle, that the wrist exhibits in everyday function and therefore no established standard motion by which all studies quantify their findings. Planar wrist motion (pure flexion and extension) is often used in research but rarely seen in performance and every day activities[4]; thus, coupled motions, such as Dart Thrower's Motion (DTM), are more representative of true motion[2]. The activities of daily living (ADL) analyzed vary, which make it difficult to compare results from different studies[17]. There is need of a standardized battery of tasks which encompass the total functional range of motion of the wrist and increase understanding of wrist function during day-to-day use.
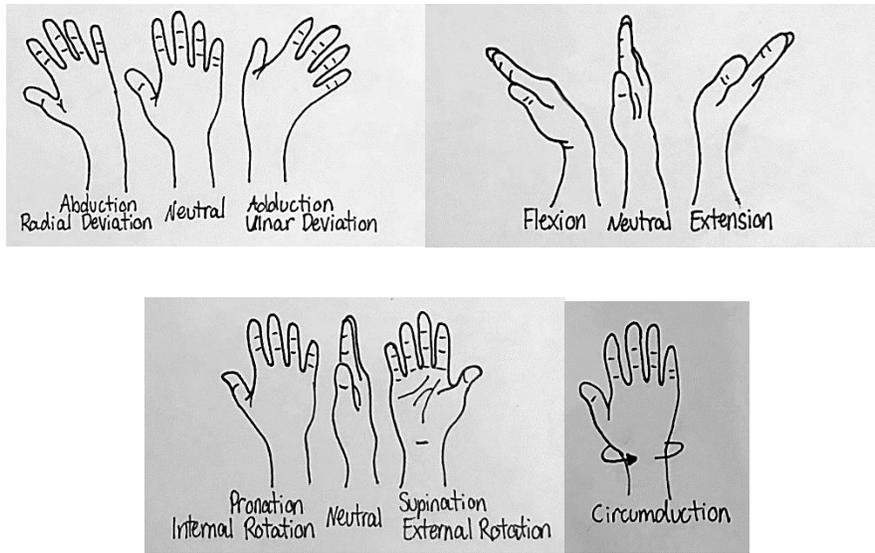
Figure 1.13: Motions of the wrist.

1.3.1 Wrist Motion Theories

There have been many theories which describe how the wrist moves. The two most basic theories are row theory and column theory[4]. Row theory, as first described by Bryce and Destot in 1896, postulates that the carpus articulates with two rows, a proximal row (lunate, triquetrum) and a distal row (trapezium, trapezoid, capitate, hamate)[18]. The proximal row is referred to as the intercalated segment because it is between two moving bones and lacks musculotendinous attachments, and its motion relies on mechanical signals from the distal row. The distal row was said to move as a rigid body, connected to the proximal row via the scaphoid, which coordinated the motion of the two rows. Motion was described as occurring at the midcarpal joint (flexion-extension) and the radioscaphoid joint (radioulnar deviation). Due to the evident oversimplification of the row theory, a column theory was proposed which grouped the carpals into radial (scaphoid, trapezium, trapezoid), central (capitate, hamate, lunate), and ulnar (triquetrum) columns[4]. Thus, flexion-extension occurs through the central column, while radioulnar deviation occurs through scaphoid and triquetrum rotation about the central column. Both of these theories have been revisited and revised several times, with different authors examining different aspects of the wrist, such joint laxity[4].

As medical imaging techniques improved and more experiments were conducted on the wrist, new theories emerged. In 1981, Lichtman proposed the Oval Ring theory, which describes the wrist as

19

a ring with two mobile links and a rigid post (classified as a row theory)[19]. Lichtman was able to explain how carpal instability sometimes occurs between rows of carpal bones, not just between columns; however, he was unable to reliably induce midcarpal instability through dividing the dorsal triquetrohamate ligaments[4]. Garcia-Elias proposed, in 1997, a combined row-column theory, which explained carpal stability through balanced moments about the lunate by means of four stabilizing bodies: the proximal row, the distal row, the midcarpals, and the radiocarpals[20,21]. While Garcia-Elias' theory is attractive for its simplicity, they were unable to treat the wrist as a whole in order to analyze the all-encompassing wrist kinematics[4]. Most recently, Sandow proposed the Central Column theory in 2013, which describes the wrist as a central column (comprised of the lunate, capitate, hamate, trapezoid, and trapezium) linking the radius to the metacarpal bases[22]. The theory is derived from 3D computer-generated models but has not been tested for all wrist motions and contradicts past established works[4]. Therefore, current literature lacks a unified theory which explains all functional motions of the wrist. Without this theory, there is not a solid basis for designing functional mechanisms to aid in wrist motion, treatment, and rehabilitation.

In order to develop a universal wrist motion theory, more information about the kinematics and mechanics of normal wrists is needed. A widely accepted phenomenon is that the functional axis of the wrist is oblique to the anatomical planes and supports DTM. Crisco et al. developed envelopes of wrist motion at maximum deflection, when relaxed, and in terms of stiffness[2]. The motion envelopes' primary axes were oblique to the anatomical planes, supporting the DTM as the functional axis of the wrist, which was later confirmed by Got et al.[23]. Other trends in the literature still require further investigation before they can be treated as universal knowledge. Tay et al. demonstrated hysteresis in carpal bones, wherein the amount a bone flexes depends on the path taken to reach the final position[24]. Gates et al. determined that wrist angles were fairly consistent between patients and between tasks when performing various ADLs, indicating high repeatability amongst ADLs[17]. ADLs requiring smaller ranges of motion elicited smaller axial forces, those with resistive forces elicited greater forces, and large compressive and out-of-plane forces can occur during physiological wrist motions and during a push-up[25].

1.4   Quantifying Wrist Kinematics

Understanding how the carpals move and interact with one another is the basis for detecting and treating carpal instabilities, among other wrist pathologies. Many previous studies have been

conducted to diagnose carpal conditions and/or increase understanding surrounding wrist function. These studies examined carpal motion in cadavers[2,23,24,26-29] or *in vivo*.

1.4.1   Direct Methods to Quantify Carpal Kinematics

Direct methods of quantifying carpal kinematics are defined as those that do not involve medical imaging. These methods include goniometry[4], physical examinations[27], motion capture (i.e., OptiTrack)[17,30], and wearable sensors (gyroscopes, accelerometers, magnetometers)[31]. Clinicians often use goniometers to measure joint angles, but these tools are limited to static measurements[4]. Physical examinations are also used in clinic for readily accessible diagnosis; however, they are subject to interpretation by the clinician, depend on clinician experience, and examine extremes of mobility, which do not always indicate abnormality[27]. Motion capture has been shown to be a valuable tool in tracking joint kinematics[4]; however, optical tracking is often limited due to line-of-sight while tracking numerous carpal bones[17] and therefore cannot capture individual carpal bone motion[4]. Manual landmark variability can be difficult and introduces a source of error to the study, as does relative motion between the markers and the participant's skin or clothing[32]. The use of wearable sensors has been used to recognize types of motion and deliver quantitative results of those motions, such as velocity of motion and displacement[31]. These methods are challenging to apply to the fine motor movements of the hand and wrist, and have only been shown to distinguish a few activities[31].

1.4.2   Two-Dimensional (2D) and Three-Dimensional (3D) Imaging

Two-dimensional and 3D imaging modalities provide further insight into carpal morphology and mechanics through visual quantification of the bones. Radiography, also known as x-ray, is a common clinical diagnostic tool that uses 2D images to describe a complex 3D pathology. Radiography is a static imaging modality and therefore can only measure carpal position and shape; common measurements include joints angles, joint space, and distance between bones[8]. In terms of diagnosing carpal instabilities, radiography is insensitive to early manifestations of the instability[33]. Another 2D imaging modality is fluoroscopy, which can be used intraoperatively to examine the bones and joints. Instabilities may not be fully recognized until weeks or months after onset when static indicators develop, at which point more invasive measures are needed to correct the instability and may not be able to fully reverse the damage[7]. Using static 2D radiographic

techniques may not reveal the extent of abnormality, can make it difficult to detect subtle bone changes (as well as detect out of plane bone deformity) due to their projection nature, and are not able to assess the dynamic nature of carpal motions[3,27,34,35].

Magnetic Resonance Imaging (MRI) is a 3D imaging modality commonly used for diagnosis due to its lack of radiation[36] and ability to image soft tissue structures[16,37-39]. Several studies will use it in place of or in addition to radiographs and physical examinations[9]. One study found 100% accuracy in determining lunate type using MRI, which has been confirmed and used in subsequent studies[9,40]. However, MRI is a static imaging modality wherein patients must remain still for one hour to eliminate any motion artifacts in the scan[37]. As such, MRI only provides information on structure and orientation, not on function[16]. Additionally, MRI is limited in its availability, with long wait times in Canada, and provides scans of low resolution when compared to other medical imaging modalities. While MRI has shown promise in differentiating some sources of chronic wrist pain, other applications, such as diagnosing SLIL tears, have been less favourable[41].

Three-dimensional computed tomography (3DCT) allows for modelling of the complex 3D bone structures and can fully characterize the effect of subtle bony changes on the surrounding joint mechanics but can only statically image the joint. Many previous studies have used 3DCT to elucidate bone kinematics and contact mechanics of the wrist in isolated quasi-static frames[34]; however, this technique is quasi-static because the 3D video is comprised of several 3D static images and therefore is not representative of true motion, nor does it incorporate the effects of active dynamic stabilizers[4,22,42]. A type of 3DCT is called micro-CT, which is CT with a micrometer resolution[43]. This resolution produces exceptionally accurate models from which to take measurements. It is imperative that the subject remain static for the duration of the scan for good volume reconstruction quality[43]. Unfortunately, due to the size of the scanner and the high radiation dose, micro-CT cannot be used to image *in vivo* human models[43]. Therefore, this measurement technique is limited to cadaveric studies on bone morphology, not motion.

1.4.3   Four-Dimensional (4D) Imaging

Information on the true kinematics of motion can be obtained using 4D (3D bone structure + time) imaging modalities. Biplane videofluoroscopy (BVF) can be 3D (2D image + time) or 4D (3D model + time); in the 3D case, x-rays are taken of the joint (2D) through motion to create a video

while in 4D, a known model of the bones of interest is fit to the 2D images to create a 3D model moving through time[44]. This method has been used to track 3D motion of the knee, hip, and shoulder, is attractive for its dynamic abilities, and overcomes many limitations of radiography (results from which are inconclusive, may not reveal the extent of abnormality, and do not reflect dynamic nature of carpals, even when a patient has pain[3,27,34,35]). However, BVF suffers from over-projection and does not provide quantitative data due to bone projection overlap, limited resolution of imaging intensifiers, and lack of normal reference values for various motions[34,45]. The measurement of intercarpal angles using videofluoroscopy is challenging and inter-examiner variability is high[7].

Another 4D imaging modality is four-dimensional computed tomography (4DCT). While 4DCT was initially used for cardiac imaging[46], it is showing increasing promise as a tool for measuring musculoskeletal bone motion. In the wrist, 3D bone scans are acquired while the bones of interest are in motion, reproducing a large spectrum of wrist motions with small changes between frames (less than 1 mm)[4,27]. There is increasing interest in current literature for the clinical applications of 4DCT in diagnosing wrist conditions and understanding the complex anatomy of the wrist[3,47]. There are numerous advantages to 4DCT over other imaging methods, including the ability to: detect dynamic instabilities and asymptomatic conditions[24,26]; capture proprioceptive and inertial influences on movement, and abnormal motions indicative of bone abnormalities[26]; capture hysteresis in movement[34]; and yield qualitative and quantitative results[34]. While 4DCT scanners emit radiation, the level is relatively low, and the wrist is an ideal place for diagnostic 4DCT because the wrist is not radiation sensitive[24]. Leng et al. used 110 mGy for the full-dose scan and 200 mGy was the skin dose, which is ten times less than the minimum threshold for skin exposure[3]. They used 18 mGy for a reduced level dose, corresponding to a 33 mGy skin dose, which yielded images three surgeons deemed effective for diagnosis.

There have been many successful studies using 4DCT. Repse et al. confidently identified their target pathology from the 4DCT scans visually and objectively[48]. Leng et al. asked three orthopaedic surgeons to use 4DCT to identify pathologies in images of healthy and unstable wrists; all three categorized the images correctly without hesitation, illustrating high inter-reader reliability[3]. While 4DCT is an excellent imaging modality, there are limitations and recommendations for effective use. The best quality scans in the study by Leng et al. were at the

beginning and end of the motions, wherein velocity was at its minimum; thus, motions must be slow and repeatable for best results and to reduce artifacts which blur the images[24,34]. However, the number of repetitions in motion should be minimized if the motion is painful for the participant[24]. Dobbe et al. recommended that "reducing the acquisition time by using a partial gantry rotation for image reconstruction is considered beneficial"[34]. To reduce error due to excessive arm movement, without restricting the participant's natural path of motion, Dobbe et al. evaluated a bone's motion relative to another bone[34]. They discovered that error due to excessive motion was greater than error in the position analysis. The temporal resolution of the CT machine limits the quality of the scans and ultimately affects the amount and reliability of information obtained from the scan[24]. Temporal resolution is affected by frame rate, which is the number of frames that can be acquired per second[32]. Another limit arises when using gated CT. Gated CT requires cyclic motion, which is difficult to replicate at the same frequency and magnitude for each trial, especially for ADLs and in individuals with pathologies[3]. Band and streak artifacts occur in scans with imperfect motion, making them difficult to read[3]. For instance, one study was unable to differentiate the contributions to motion from midcarpals and radiocarpals[2].

1.4.4   Quantifiable Outcomes from 4DCT

Wrist kinematics. Kinematics is the study of the motion of an object; thus, wrist kinematics is the study of the motion of the wrist as a whole and the wrist in terms of its individual carpals. There are a variety of measurements to quantify wrist kinematics: translation, generally of a bone's centroid measured as the weighted centre of the bone; rotation of the bone about its axes or the axes of a reference bone; and helical axes, which measure the movement of a bone's axes during motion.

Wrist arthrokinematics. In a similar way, arthrokinematics is the study of the motion of joint surfaces. Measurements of joint contact, in terms of the surface area of bone which is in contact with the other bone in a joint, can be taken throughout a range of motion to determine how bones are moving relative to one another. These findings can provide information on how far apart bones are at a given time through a range of motion and if bones are moving together (joint surface area remains consistent through motion) or if they are moving relative to one another (joint surface area changes through motion).

1.5 SLIL Tears and Their Influence on Wrist Kinematics

While this thesis focuses on the development of a 4DCT technique to measure carpal motion, the clinical use of the proposed technique was tested in a novel application: SLIL tears.

1.5.1 Types of SLIL Tears and Injury Progression

The wrist is the most susceptible to injury of all upper extremity joints, supporting the need for this research[3]. Of all musculoskeletal injuries, 28% are to the hand and wrist[7], and of those injuries, SLIL tears are the most frequent ligamentous wrist injury[14,16,37,49]. The population most affected by SLIL tears are young people of working age, who then develop wrist instability[50]. Lunate type has been shown to affect dissociative carpal instability[9], specifically those with SLIL injuries; individuals with type 2 lunates are less likely to develop dorsal intercalated segment instability (DISI)[10]. There are three types of SLIL tears: isolated volar, wherein only the volar portion of the SLIL is torn; isolated dorsal, wherein only the dorsal portion is torn; and combined, wherein the volar and dorsal segments are both torn. These injuries are painful and impair function[49], and when left untreated, lead to long-term degenerative arthritis called scapholunate advanced collapse (SLAC)[14,51-53], the most common degenerative wrist condition[52,53]. The progression of SLAC begins with degenerative changes between the tip of the radial styloid and radial distal pole of the scaphoid, followed by degeneration of the entire radioscaphoid articulation (Figure 1.14). The final stage of SLAC is described as additional degeneration of the capitolunate joint caused by proximal migration of the capitate. While the propagation of instability and degenerative arthritis are well understood in SLAC, the exact cause of joint degeneration is still unknown, as are effective methods of treatment. It is important to note that combined tears lead to SLAC, whereas the significance of isolated volar and dorsal tears are more abscure[41].
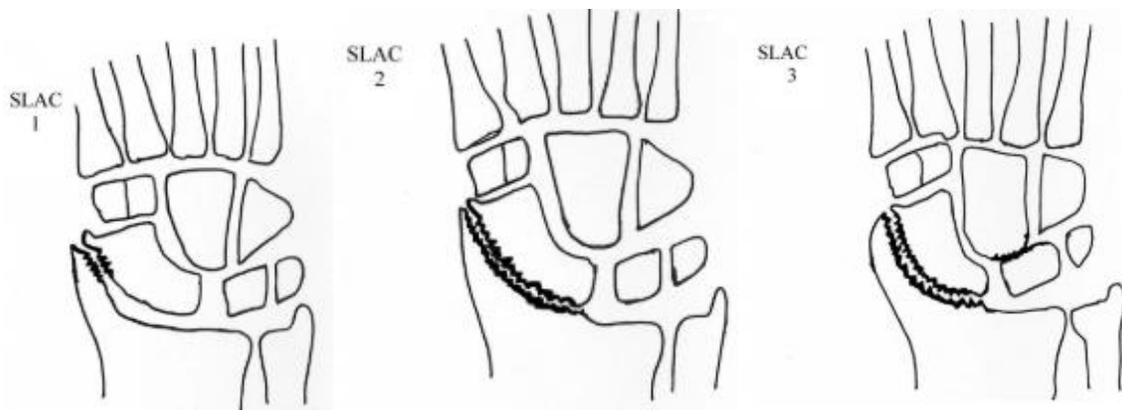
Figure 1.14: Progression of SLAC[53].

As the affected population is young working age individuals, these debilitating injuries may disable the patient from working, and severely limit function and quality of life[54]. The progression of these injuries from an SLIL tear to end-stage arthritis is harrowing due to the young age of the patients.

1.5.2   Dynamic and Static Instabilities

There are two types of instability: static and dynamic. Static instabilities present as abnormal bone positions and therefore can be detected on static radiographic examinations[3]. Dynamic instabilities, however, only present as subtle abnormal bone movement elicited during motion and/or when loaded, not abnormal bone position, and thus cannot be detected on static radiographic examinations[3]. Static instabilities are virtually irreversible and inevitably lead to degenerative arthritis[3]. However, dynamic instabilities are precursors to static instabilities, such that medical intervention at the dynamic instability stage could prevent the onset of static instability and arthritis and restore normal function[3,48,55].

1.5.3   Diagnosis and Surgical Intervention

Early diagnosis and intervention are critical because, if SLIL tears are left untreated, progression of SLAC pathology is inevitable and there is currently no effective arthroplasty for the wrist. However, early intervention to reestablish healthy carpal balance has been hindered by inadequate clinical diagnostic tools and a lack of knowledge about the spectrum of wrist instabilities[8]. New

methods of early diagnosis are vital to advancing technology in the field of upper extremity injuries and rehabilitation.

Current Diagnosis. Physical examinations are common practice in diagnosing SLIL tears. The scaphoid shift test is one such examination, wherein load is applied to the scaphoid tubercle while the wrist moves from ulnar to radial deviation[56,57]. The clinician applying the load palpates for dorsal displacement of the scaphoid's proximal pole from the scaphoid fossa on the distal radius, which sometimes produces an audible "clunk"[56,57]. However, the test is subjective and provides several qualitative findings but no measurable result[57]. To aid in diagnosis, imaging modalities (static and dynamic) are used to look inside the wrist at the bones and connective tissues and determine if there are any abnormalities in position or motion. Static methods cannot detect abnormal bone orientation nor position during motion, only abnormal static bone position, which indicates severe, end-stage instability and therefore cannot be used for early injury diagnosis[26,58]. Common static measurements obtained from planar radiographs are SL joint space, the widening of which is indicative of an SLIL tear, and SL angle, which indicates dorsal intercalated segment instability, a marker of an SLIL tear[37]. The changes in joint space and SL angle are relatively small, making diagnosis challenging[27]. There is a clear disconnect between desired intervention time (early, the markers for which are dynamic) and the best method for diagnosis (currently static radiographs, which cannot measure dynamic instability; and the scaphoid shift test, which is qualitative and subjective).

The intervention for a patient whose radiographs are normal, but who experiences pain and is suspected of having an SLIL tear, are controversial[59]. First, the patient is immobilized, and evaluations are conducted at 1 and 3 weeks. If the patient is symptomatic 4-weeks post initial evaluation, advanced imaging such as MRI may be performed. The time to intervene and heal an acute SLIL injury is limited and should happen as early as possible; thus, any advancement in the diagnosis tools and procedure is valuable.

Surgical Repair. In the case that a SLIL tear repair is viable, there are two method: arthroscopic surgery and open surgery[60]. Current arthroscopic surgery involves debridement, thermal shrinkage, and temporary pinning of the scaphoid and lunate[60]. This surgery is helpful in the case of isolated tears[41,61] but less effective for combined tears[62]. It is important to note that most of these

repairs are performed on combined SLIL tears; there is little data regarding the treatment of isolated volar and isolated dorsal tears[61]. An advantage of arthroscopy is its ability to simultaneously diagnose and treat SLIL tears, both isolated and combined[59]. Open surgical techniques include capsulodesis, tenodesis, and bone-ligament-bone reconstructions[16,60,63]; however, these require a wide dorsal approach that damages soft tissues, often resulting in mobility reduction and stiffness[60], and none have been universally adopted as the surgical treatment[62]. One technique proposed a modified arthroscopic ligamentoplasty that can repair the dorsal and volar portions of the SLIL, combining arthroscopic and open surgical techniques; however, the indications include a combined tear with no carpus malalignment[60]. Isolated volar tear repairs remain challenging because it is difficult to access the volar ligament and because they are often left undiagnosed; they have even been referred to as *predynamic instabilities* because they are such an early stage of injury[63]. Although they are not currently the focus of SLIL repairs, volar tears may affect carpal motion and may need to be repaired; thus, they require a diagnostic tool that can detect such a dynamic injury.

End Stage Treatment. As static markers of SLIL tears show up on radiographs during late-stage instability, diagnoses occur too late for repair[36]. Once SLAC has begun, there is no known way to stop its progression. As a result, recommendations to slow the progression have been made, such as reduced activity at the wrist, and solutions have been developed for end-stage arthritis when the wrist is no longer functional and is extremely painful. Treatment of end-stage wrist arthritis is complex, including salvage procedures that result in significant loss of wrist function[50]. Arthroplasty (joint replacement) or arthrodesis (complete or partial fusion of the bones) are two salvage options.

Total wrist arthroplasty (TWA) aims to improve function and reduce pain[44]. The main advantage to TWA is the maintenance of wrist range of motion and function; however, this benefit is not always realized in objective assessments[64]. Reported range of motion following TWA varies across studies and is only significantly better than preoperative values in a few studies[64]. Poor outcomes of TWA include instability, implant fracture, loosening and osteolysis, which leave surgeons feeling frustrated, and are responsible for a decline in the use of TWA[65-69]. Knee and hip arthroplasties have been optimized for biomechanical survivorship with decades of evaluation of large kinematic datasets, while progress in wrist arthroplasty development has been slow due to a

paucity of similar data[44]. The empirical nature of wrist arthroplasty evolution may contribute to implant instability and loosening[44]. Thus, there is limited knowledge on how the carpals articulate together, a change in which may alter joint mechanics[44,70]. For optimal results, TWA patients should be elderly with good bone stock, limit their wrist load during activities of daily living (ADL), and understand that a revision to a total wrist fusion may be necessary[65]. The warning of a revision surgery suggests that major complication rates are high, which has been supported by many studies wherein complication rates are as high as 9.5%[64]. As TWA can only preserve a limited amount of wrist function and tends to retain higher levels of pain compared to arthrodesis, patients tend to choose fusion.

Arthrodesis, also known as fusion, is a surgical procedure wherein several bones in the wrist are rigidly fixed in the hopes of reduced pain but also leads to extreme loss of function and mobility. This surgery can be performed as full or partial wrist fusion, wherein surgeons pin the lunate, triquetrum, capitate, and/or hamate[71]. While this surgery has been the gold standard for its reliability and success in pain reduction[64], the alteration of wrist kinematics through joint fixation can lead to further joint degeneration.

Current Problem: To effectively stop the progression of SLAC and heal SLIL tears, intervention must occur early. To intervene early, the SLIL tear must be diagnosed in its early, dynamic stage of instability. Therefore, a dynamic tool is needed that can measure bone orientation and position during motion, abnormalities in which are indicative of early SLIL tears. The noninvasive and dynamic qualities of 4DCT make it a unique modality to examine the wrist[47,54]; it may overcome the insensitivity of MRI while remaining non-invasive, unlike arthroscopy[47]. Therefore, 4DCT shows promise as a diagnostic tool to show dynamic instabilities indicative of early stages of SLIL tears.

1.6   Rationale

The wrist is a complex joint comprised of several bones, which articulate to produce a large range of complex motion in a small volume. Although many studies have sought to explain how the wrist moves, there is no unified wrist motion theory. A unified wrist motion theory can only be established once a thorough understanding of dynamic wrist motion has been established. A tool

is needed that is dynamic to measure subtle bone changes throughout motion and increase the understanding of carpal motion.

Isolated and combined SLIL tears negatively impact healthy carpal motion and often remain undiagnosed until later stages of injury when interventions can no longer prevent the progression of arthritis and are limited to salvage techniques. Differentiating between healthy dynamic carpal motion and that of SLIL tear cases would provide a provocative test situation for the aforementioned tool. The collaboration of hand surgeons, radiologists, and researchers will be needed to describe which motion is normal and which motion is abnormal.

The goal of this work is to advance biomedical engineering research through the proposal and application of 4DCT. These findings will help inform investigators of the effectiveness of 4DCT as a tool for measuring the carpus and increasing the understanding of healthy carpal motion and how it differs in injured states.

1.7   Objectives and Hypotheses

There are three main objectives for this work:

1) Employ 4DCT to measure dynamic wrist motion in a healthy cohort.

2) Validate the proposed 4DCT technique.

3) Extend the use of the 4DCT technique to measure carpal kinematics (helical axes) in healthy and injured populations.

In response to the above objectives, the hypotheses for this work are:

1) 4DCT will be a useful tool to visualize dynamic carpal motion while providing sufficient image resolution, such that noticeable differences in size and location of joint surface area between consecutive frames of motion can be seen.

2) Surface reconstruction from kinematic 4DCT scans will be valid within 0.5 mm of the gold standard.

3) 4DCT scanning will be sufficiently sensitive to detect subtle bony changes that occur due to injuries, thus differentiating between healthy and injured participants.

1.8 Thesis Overview

In Chapter 2, 4DCT is presented as a novel tool for quantifying healthy carpal kinematics. The 4DCT protocol is employed to measure osteokinematics (translation) and arthrokinematics (joint contact) of the carpals to better understand healthy wrist motion. This chapter provides further information towards to the development of a universal wrist motion theory. Chapter 3 validates the proposed 4DCT tool by comparing it to the ground truth: micro-CT. The resolution of models made from 4DCT scans in two different software are compared with models made from micro-CT scans. The 4DCT models are registered to the micro-CT models to determine the level of variation in the resolution of the models. Inter-rater reliability is also examined to determine the robustness of the surface reconstructions. Intra-rater reliability is measured to examine how consistently the surface reconstructions can be made by different raters. In Chapter 4, the 4DCT tool is used in a provocative test situation to determine its effectiveness as a clinical tool. The effects of volar SLIL tears, as well as dorsal and combined SLIL tears, on healthy carpal kinematics is discussed. Scaphoid and lunate helical axes, and intercarpal joint arthrokinematics are analyzed *in vivo* during radioulnar deviation and flexion-extension for an uninjured wrist population compared to a population with SLIL tears. The ability of 4DCT to provide quantitative differences between these two groups, and within the three types of SLIL tears, provides insight into the effectiveness of the tool and its potential applications. This chapter may also suggest that volar tears, which have historically been left unrepaired, affect normal carpal motion and may, in some cases, need to be repaired. Chapter 5 provides a summary of all studies and indicates directions for future work.

1.9 References

1.   Tortora GJ, Nielsen M. Principles of Human Anatomy. 14th ed. Danvers: Wiley; 2013. doi:10.1017/CBO9781107415324.004

2.   Crisco JJ, Heard WMR, Rich RR, Paller DJ, Wolfe SW. The mechanical axes of the wrist are oriented obliquely to the anatomical axes. J Bone Joint Surg Am. 2011;93(2):169-177. doi:10.2106/JBJS.I.01222

3.   Leng S, Zhao K, Qu M, An K-N, Berger R, McCollough CH. Dynamic CT technique for assessment of wrist joint instabilities. Med Phys. 2011;38 Suppl 1:S50. doi:10.1118/1.3577759

4.   Rainbow MJ, Wolff AL, Crisco JJ, Wolfe SW. Functional kinematics of the wrist. J Hand Surg Am. 2016;41E(1):7-21.

5.   Chambers SB. The Impact of Scaphoid Malunion on Wrist Kinematics & Kinetics : A Biomechanical Investigation. 2019.

6.   Shivdas S, Hashim MS, Ahmad TS. A three-dimensional virtual morphometry study of the sigmoid notch of the distal radius. J Orthop Surg. 2018;26(3):1-8. doi:10.1177/2309499018802504

7.   Shores JT, Demehri S, Chhabra A. Kinematic "4 Dimensional" CT Imaging in the Assessment of Wrist Biomechanics Before and After Surgical Repair. Eplasty. 2013;13:62-72. http://www.ncbi.nlm.nih.gov/pubmed/23573338%0Ahttp://www.pubmedcentral.nih.gov/articlerender.fcgi?artid=PMC3589877.

8.   Kramer A, Allon R, Wollstein R, Werner F, Lavi I, Wolf A. Distinct Wrist Patterns Founded on Measurements in Plain Radiographs. J Wrist Surg. 2018;7:366-374.

9.   Pang EQ, Douglass N, Kamal RN. Association of Lunate Morphology With Carpal Instability in Scapholunate Ligament Injury. Hand. 2018;13(4):418-422. doi:10.1177/1558944717709073

10.   Rhee PC, Moran SL, Shin AY. Association Between Lunate Morphology and Carpal Collapse in Cases of Scapholunate Dissociation. J Hand Surg Am. 2009;34(9):1633-1639. doi:10.1016/j.jhsa.2009.06.017

11.   Abe S, Moritomo H, Oka K, et al. Three-dimensional kinematics of the lunate, hamate, capitate and triquetrum with type 1 or 2 lunate morphology. J Hand Surg Eur Vol. 2018;43(4):380-386. doi:10.1177/1753193417744420

12.   Giessen M Van De, Foumani M, Streekstra GJ, et al. Statistical descriptions of scaphoid and lunate bone shapes. J Biomechanics. 2010;43(8):1463-1469. doi:10.1016/j.jbiomech.2010.02.006

13.   Wolfe SW, Hotchkiss RN, Pederson WC, Kozin SH. Green's OPERATIVE HAND SURGERY. 6th ed. (Pepper D, Sussman M, eds.). Philadelphia, PA: Elsevier; 2011.

14.   Padmore C, Stoesser H, Langohr GD, Johnson J, Suh N. Carpal Kinematics following Sequential Scapholunate Ligament Sectioning. J Wrist Surg. 2019;08(02):124-131. doi:10.1055/s-0038-1676865

15.   Andersson JK. Treatment of scapholunate ligament injury: Current concepts. EFORT Open Rev. 2017;2(9):382-393. doi:10.1302/2058-5241.2.170016

16.   Kuo CE, Wolfe SW. Scapholunate Instability: Current Concepts in Diagnosis and Management. J Hand Surg Am. 2008;33(6):998-1013. doi:10.1016/j.jhsa.2008.04.027

17.   Gates DH, Walters LS, Cowley J, Wilken JM, Resnik L. Range of Motion Requirements for Upper-Limb Activities of Daily Living. Am J Occup Ther. 2016;70(1):7001350010p1-7001350010p10. doi:10.5014/ajot.2016.015487

18.   Bryce T. Certain Points in the Anatomy and Mechanism of the Wrist-Joint Reviewed in the Light of a Series of Rontgen Ray Photographs of the Living Hand. J Anat Physiol. 1896;31:59-79.

19.   Horii E, Garcia-Elias M, An KN, et al. A kinematic study of luno-triquetral dissociations. J hand Surg (American ed). 1991;16(2):355-362. doi:10.1016/S0363-5023(10)80126-1

20.   Kamal RN, Chehata A, Rainbow MJ, Llusá M, Garcia-Elias M. The effect of the dorsal intercarpal ligament on lunate extension after distal scaphoid excision. J Hand Surg Am. 2012;37(11):2240-2245. doi:10.1016/j.jhsa.2012.07.029

21.   Kobayashi M, Garcia-Elias M, Nagy L, et al. Axial loading induces rotation of the proximal carpal row bones around unique screw-displacement axes. J Biomech. 1997;30(11/12):1165-1167.

22.   Kamal RN, Rainbow MJ, Akelman E, Crisco JJ. In Vivo Triquetrum-Hamate Kinematics Through a Simulated Hammering Task Wrist Motion. J Bone Joint Surg Am. 2012;85(1):1-7.

23.   Got C, Vopat BG, Mansuripur PK, Kane PM, Weiss APC, Crisco JJ. The effects of partial carpal fusions on wrist range of motion. J Hand Surg Eur Vol. 2014;41(5):479-483. doi:10.1177/1753193415607827

24.   Tay S-C, Primak AN, Fletcher JG, et al. Four-dimensional computed tomographic imaging in the wrist: proof of feasibility in a cadaveric model. Skeletal Radiol. 2007;36(12):1163-1169. doi:10.1007/s00256-007-0374-7

25.   Smith JM, Werner FW, Harley BJ. Forces in the Distal Radius During a Pushup or Active Wrist Motions. J Hand Surg Am. 2018;43(9):806-811. doi:10.1016/j.jhsa.2018.05.020

26.   Zhao K, Breighner R, Holmes D 3rd, Leng S, McCollough C, An K-N. A technique for quantifying wrist motion using four-dimensional computed tomography: approach and validation. J Biomech Eng. 2015;137(7). doi:10.1115/1.4030405

27.   Mat Jais IS, Tay SC. Kinematic analysis of the scaphoid using gated four-dimensional CT. Clin Radiol. 2017;72(9):794.e1-794.e9. doi:10.1016/j.crad.2017.04.005

28.   Repse SE, Koulouris G, Troupis JM. Wide field of view computed tomography and mid carpal instability: The value of the sagittal radius-lunate-capitate axis - Preliminary experience. Eur J Radiol. 2015;84(5):908-914. doi:10.1016/j.ejrad.2015.01.020

29.   Keir PJ, Wells RP. The effect of typing posture on wrist extensor muscle loading. Hum Factors. 2002;44(3):392-403. doi:10.1518/0018720024497655

30.   Murphy MA, Murphy S, Persson HC, Bergstrom U-B, Sunnerhagen KS. Kinematic Analysis Using 3D Motion Capture of Drinking Task in People With and Without Upper-extremity Impairments. J Vis Exp. 2018;(133):1-9. doi:10.3791/57228

31.   Lemmens RJM, Janssen-Potten YJM, Timmermans AAA, Smeets RJEM, Seelen HAM. Recognizing complex upper extremity activities using body worn sensors. PLoS One. 2015;10(3):e0118642. doi:10.1371/journal.pone.0118642

32.   Edirisinghe Y, Troupis JM, Patel M, Smith J, Crossett M. Dynamic motion analysis of dart throwers motion visualized through computerized tomography and calculation of the axis of rotation. J Hand Surg Eur Vol. 2014;39(4):364-372. doi:10.1177/1753193413508709

33.   Linscheid RL, Dobyns JH, Beabout JW, Bryan RS. Traumatic Instability of the Wrist. J Bone Jt Surg. 1971;54:1612-1632.

34.   Dobbe JGG, de Roo MGA, Visschers JC, Strackee SD, Streekstra GJ. Evaluation of a Quantitative Method for Carpal Motion Analysis Using Clinical 3-D and 4-D CT Protocols. IEEE Trans Med Imaging. 2019;38(4):1048-1057. doi:10.1109/TMI.2018.2877503

35.   Shakoor D, Hafezi-Nejad N, Haj-Mirzaian A, et al. Kinematic Analysis of the Distal Radioulnar Joint in Asymptomatic Wrists Using 4-Dimensional Computed Tomography-Motion Pattern and Interreader Reliability. J Comput Assist Tomogr. 2019;43(3):392-398. doi:10.1097/RCT.0000000000000839

36.   Mathoulin C, Gras M. Role of wrist arthroscopy in scapholunate dissociation. Orthop Traumatol Surg Res. 2020;106(1):S89-S99. doi:10.1016/j.otsr.2019.07.008

37.   Meister DW, Hearns KA, Carlson MG. Dorsal Scaphoid Subluxation on Sagittal Magnetic Resonance Imaging as a Marker for Scapholunate Ligament Tear. J Hand Surg Am. 2017;42(9):717-721. doi:10.1016/j.jhsa.2017.06.015

38.   Berger RA, Linscheid RL, Berquist TH. Magnetic resonance imaging of the anterior radiocarpal ligaments. J Hand Surg Am. 1994;19:295-303. doi:10.1016/0363-5023(94)90024-8

39.   Zanetti M, Saupe N, Nagy L. Role of MR imaging in chronic wrist pain. Eur Radiol. 2007;17(4):927-938. doi:10.1007/s00330-006-0365-4

40.   Malik AM, Schweitzer ME, Cuip RW, Osterman LA, Manton G. MR Imaging of the Type II Lunate Bone: Frequency, Extent, and Associated Findings. Am Roentgen Ray Soc. 1999;173:335-338.

41.   Darlis NA, Weiser RW, Sotereanos DG. Partial scapholunate ligament injuries treated with arthroscopic debridement and thermal shrinkage. J Hand Surg Am. 2005;30(5):908-914. doi:10.1016/j.jhsa.2005.05.013

42.   Kobayashi M, Berger RA, Nagy L, et al. Normal Kinematics of Carpal Bones: A Three-Dimensional Analysis of Carpal Bone Motion Relative to the Radius. J Biomchanics. 1997;30(8):787-793.

43.   Beckett RG, Conlogue GJ. Advances in Paleoimaging. Boca Raton, London, New York: CRC Press; 2020. doi:10.4324/9781315203089

44.   Akhbari B, Morton AM, Moore DC, Weiss APC, Wolfe SW, Crisco JJ. Kinematic accuracy in tracking total wrist arthroplasty with biplane videoradiography using a computed tomography-generated model. J Biomech Eng. 2019;141(4). doi:10.1115/1.4042769

45.   Ramamurthy NK, Chojnowski AJ, Toms AP. Imaging in carpal instability. J Hand Surg Eur Vol. 2016;41(1):22-34. doi:10.1177/1753193415610515

46.   Taguchi K, Chiang BS, Hein IA. Direct cone-beam cardiac reconstruction algorithm with cardiac banding artifact correction. Med Phys. 2006;33(2):521-539. doi:10.1118/1.2163247

47.   Demehri S, Hafezi-Nejad N, Morelli JN, et al. Scapholunate kinematics of asymptomatic wrists in comparison with symptomatic contralateral wrists using four-dimensional CT examinations: initial clinical experience. Skeletal Radiol. 2016;45(4):437-446. doi:10.1007/s00256-015-2308-0

48.   Repse SE, Amis B, Troupis JM. Four-dimensional computed tomography and detection of dynamic capitate subluxation. J Med Imaging Radiat Oncol. 2015;59(3):331-335. doi:10.1111/1754-9485.12260

49.   Wang P, Stepan JG, An T, Osei DA. Equivalent Clinical Outcomes Following Favored Treatments of Chronic Scapholunate Ligament Tear. HSS J. 2017;13(2):186-193. doi:10.1007/s11420-016-9525-5

50.   Messina J, Van Overstraeten L, Luchetti R, Fairplay T, Mathoulin C. The EWAS Classification of Scapholunate Tears: An Anatomical Arthroscopic Study. J Wrist Surg. 2013;02(02):105-109. doi:10.1055/s-0033-1345265

51.   Strauch RJ. Scapholunate advanced collapse and scaphoid nonunion advanced collapse arthritis - Update on evaluation and treatment. J Hand Surg Am. 2011;36(4):729-735. doi:10.1016/j.jhsa.2011.01.018

52.   Lane R, Varacallo M. Scapholunate Advanced Collapse (SLAC Wrist). StatPearls Publishing LLC.

53.   Vishwanathan K, Hearnden A, Talwalkar S, Hayton M, Murali SR, Trail IA. Reproducibility of radiographic classification of scapholunate advanced collapse (SLAC) and scaphoid nonunion advanced collapse (SNAC) wrist. J Hand Surg Eur Vol. 2013;38(7):780-787. doi:10.1177/1753193413484629

54.   Kelly PM, Hopkins JG, Furey AJ, Squire DS. Dynamic CT Scan of the Normal Scapholunate Joint in a Clenched Fist and Radial and Ulnar Deviation. Hand. 2018;13(6):666-670. doi:10.1177/1558944717726372

55.   Sikora S, Tham S, Harvey J, et al. The Twist X-Ray: A Novel Test for Dynamic Scapholunate Instability. J Wrist Surg. 2019;08(01):061-065. doi:10.1055/s-0038-1673344

56.   Wolfe SW, Gupta A, Crisco JJ. Kinematics of the scaphoid shift test. J Hand Surg Am. 1997;22(5):801-806. doi:10.1016/S0363-5023(97)80072-X

57.   Wolfe SW, Crisco JJ. Mechanical evaluation of the scaphoid shift test. J Hand Surg Am. 1994;19(5):762-768. doi:10.1016/0363-5023(94)90180-5

58.   Peymani A, Foumani M, Dobbe JGG, Strackee SD, Streekstra GJ. Four-dimensional rotational radiographic scanning of the wrist in patients after proximal row carpectomy. J Hand Surg Eur Vol. 2017;42(8):846-851. doi:10.1177/1753193417718427

59.   Geissler WB. Arthroscopic Management of Scapholunate Instability. J Wrist Surg. 2013;2(2):129-135.

60.   Corella F, Del Cerro M, Ocampos M, Larrainzar-Garijo R. Arthroscopic ligamentoplasty of the dorsal and volar portions of the scapholunate ligament. J Hand Surg Am. 2013;38(12):2466-2477. doi:10.1016/j.jhsa.2013.09.021

61.   Hirsh L, Sodha S, Bozentka D, Monaghan B, Steinberg D, Beredjiklian PK. Arthroscopic Electrothermal Collagen Shrinkage for Symptomatic Laxity of the Scapholunate Interosseous Ligament. J Hand Surg Br Eur Vol. 2005;30(6):643-647.

62.   Darlis NA, Kaufmann RA, Giannoulis F, Sotereanos DG. Arthroscopic debridement and closed pinning for chronic dynamic scapholunate instability. J Hand Surg Am. 2006;31(3):418-424. doi:10.1016/j.jhsa.2005.12.015

63.   Garcia-Elias M, Lluch AL, Stanley JK. Three-ligament tenodesis for the treatment of scapholunate dissociation: Indications and surgical technique. J Hand Surg Am. 2006;31(1):125-134. doi:10.1016/j.jhsa.2005.10.011

64.   Berber O, Garagnani L, Gidwani S. Systematic Review of Total Wrist Arthroplasty and Arthrodesis in Wrist Arthritis. J Wrist Surg. 2018;7(5):424-440.

65.   Boeckstyns MEH. My personal experience with arthroplasties in the hand and wrist over the past four decades. J Hand Surg Eur Vol. 2019;44(2):129-137. doi:10.1177/1753193418817172

66.   Adams BD, Kleinhenz BP, Guan JJ. Wrist Arthrodesis for Failed Total Wrist Arthroplasty. J Hand Surg Am. 2016;41(6):673-679. doi:10.1016/j.jhsa.2016.02.012

67.   Cobb TK, Beckenbaugh RD. Biaxial Total-Wrist Arthroplasty. J Hand Surg Am. 1996;21A:1011-1021.

68.   Nydick JA, Greenberg SM, Stone JD, Williams B, Polikandriotis JA, Hess A V. Clinical Outcomes of Total Wrist Arthroplasty. J Hand Surg Am. 2012;37A:1580-1584. doi:10.1016/j.jhsa.2012.05.016

69.   Radmer S, Andresen R, Sparmann M. Total Wrist Arthroplasty in Patients With Rheumatoid Arthritis. J Hand Surg Am. 2003;28A(5):789-794. doi:10.1053/S0363-5023(03)00307-1

70.   Lalone EA, Shannon HL, Deluce SR, Giles JW, King GJW, Johnson JA. Effect of Radial Head Implant Shape on Radiocapitellar Joint Congruency. J Hand Surg Am. 2017. doi:10.1016/j.jhsa.2017.03.009

71.   Reissner L, Hensler S, Kluge S, Marks M, Herren DB. Treatment Outcomes of 4-Corner Arthrodesis for Patients With Advanced Carpal Collapse: An Average of 4 Years' Follow-Up Comparing 2 Different Plate Types. J Hand Surg Am. 2018;43(5):487.e1-487.e6. doi:10.1016/j.jhsa.2017.10.036

Chapter 2

2 Evaluation of Four-Dimensional Computed Tomography as a Technique for Quantifying Carpal Motion

The use of four-dimensional computed tomography (4DCT) for measuring healthy carpal motion remains largely unstudied. The intent of this chapter is to present a 4DCT protocol for measuring carpal motion through the analysis of bone centroid translation and joint surface area (JSA) during radioulnar deviation in 12 healthy participants. Secondly, the responsiveness of 4DCT, that is its ability to measure small, clinically important changes, will be examined through the analysis of JSA changes between consecutive frames of motion.

A version of this work has been published in the Journal of Biomechanical Engineering, as well as presented at the 2020 Imaging Network Ontario, 2020 Western Research Forum, 2020 London Health Research Day, 2020 Canadian Orthopaedic Research Society and the 2020 Canadian Bone and Joint Conference.

2.1   Introduction

As discussed in Chapter 1, the wrist is a complex joint consisting of numerous bones and ligamentous structures that enable complex movement while ensuring wrist stability[1,2]. Due to its complexity, a unified wrist motion theory has not been established. Rainbow et. al published a review of theories from as early as 1926 describing the motion of the carpus, which range from row to column to combined theoretical frameworks with no unifying theory garnering consensus (Chapter 1, Section 1.3.1)[3]. Current techniques to measure wrist motion have many drawbacks that may contribute to this lack of understanding. Surgeons often rely on physical examinations and goniometry to assess wrist motion, but these are subject to interpretation by the clinician and limited to static positions[3]. Motion capture is a useful tool in measuring joint kinematics[3]; however, it is limited due to line-of-sight and skin marker movement[4]. Radiography is a common clinical diagnostic tool that produces 2D images of the carpals, and therefore can only measure carpal shape and orientation[5]. Imaging modalities (3D and 4D) can be used to measure carpal motion, but common methods are limited to quasi-static measurements (three-dimensional computed tomography)[3,6,7] or lack quantitative data (biplane videofluoroscopy)[8,9]. Improved imaging tools

are needed to characterize normal carpal motion, which are dynamic in nature and can therefore detect dynamic bone movements.

Four-dimensional computed tomography (4DCT) is a novel method for detecting dynamic bone movements. Quantitative measurements can be obtained through 4DCT and include osteokinematics (bone translation and rotation), and arthrokinematics (study of motion of joint surfaces)[1,10]. Studies using 4DCT to measure carpal kinematics have successfully been performed *in vivo* and *in vitro* but often have a small sample size, investigate a very specific pathology, and are often not validated[1,2,3]. Additionally, 4DCT, as it relies on continuous scanning of the x-ray tube, requires a higher dose than static 3DCT, but currently there is wide range of doses reported in the literature and is not consistently reported[11]. As a clinical tool, 4DCT is still in its infancy and as such, there are contradictions in the literature regarding which CT scanner is best for measuring wrist motion[2].

The methodology of 4DCT, while currently developed, is still in its infancy as a powerful clinical tool that may be used to detect dynamic carpal movements that are difficult to detect using x-rays or 3DCT, but yet are critical to normal wrist function. The wrist is an ideal candidate for 4D musculoskeletal imaging as it is complex in structure and yet the relative motion between carpals is not large in magnitude. For instance, it has been established that the scaphoid exhibits little motion during radioulnar deviation (RUD)[1,12]. This work presents a novel approach for measuring healthy carpal kinematics and arthrokinematics using 4DCT. The objective of this study was to employ 4DCT in a cohort of healthy individuals to examine the feasibility of this approach and to demonstrate the outcome measures that are possible using the acquired volumetric data. This technique was used to examine the motion of the scaphoid during RUD. Based on the literature, our hypothesis was that the scaphoid would extend from extreme radial deviation to extreme ulnar deviation, which would manifest as an increase in distal translation and a decrease in joint surface area (JSA) at the radioscaphoid and scapholunate joints. We then conducted a separate characterization study of a single participant to examine responsiveness of the imaging technique. We hypothesized that 4DCT has sufficient responsiveness to detect subtle bone movements between consecutive frames of motion in a kinematic 4DCT scan, which can be detected as changes in JSA. This is an important first step in providing a comprehensive understanding of

carpal mechanics to understand normal function and provide targets for treatment in the context of injury.

2.2 Methods

2.2.1 Study Protocol

Study participants were recruited from a tertiary academic upper extremity orthopaedic centre. Inclusion criteria were individuals over 18 years of age with no history of wrist injury. The study protocol was approved by the ethics review board of our institute and hospital, and complied with the Declaration of Helsinki of 1975, revised 2000.

Following recruitment, individuals (young cohort, n=6, 3 male, average age 23.7 years ± 3 years; old cohort, n=6, 3 male, average age 74.8 years ± 5 years) underwent unilateral (dominant hand only, all right-handed) CT scanning protocol, which consisted of a localizer scan (to determine wrist joint location), a neutral frame, and a kinematic scan (RUD). The dynamic motions were physically unconstrained to examine the participants' natural range and mechanics of motion. To ensure the motions were performed correctly, a video demonstration was provided prior to the day of testing. On the day of testing, a live demonstration was provided, and the CT technologist remained with the participant during the scan to coach them through the motion and count out loud to ensure the participant completed the motion in the allotted time. For the scans, participants were positioned on their stomach on the CT scanner bed (gantry) with their dominant arm outstretched above their head (180° from their torso) towards the inside of the scanner. The participants were outfitted with a body lead apron, thyroid shield, and protective eyeglasses. The participants were instructed to keep their wrist position consistent between scans relative to its position on the scanner bed.

2.2.2 4DCT Imaging Technique

A CT scanner (Revolution CT Scanner, GE Healthcare, Waukesha, Wisconsin, USA) was used to acquire kinematic scans of the distal forearm and hand using a routine wrist scan protocol (80 kV, 125 effective mA, 0.35 s rotation time, axial). The CT scanner imaged a 16 cm z-axis length, configured as 128 1.25 mm thick slices, repeatedly at 0.35 s intervals over a duration of 24.5 s for a total of 70 volumes at 2.86 Hz. The voxel size was $0.625 \times 0.625 \times 1.25$ mm. For the purposes

of this study, three passes of RUD were performed: extreme radial to extreme ulnar deviation was the first pass (bin 1, 25 volumes, 8.75 s), extreme ulnar to extreme radial deviation was the second pass (bin 2, 25 volumes, 8.75 s), and extreme radial to extreme ulnar deviation was the third pass (bin 3, 20 volumes, 7.0 s), resulting in a total time of 24.5 s per motion and 25 frames of motion per bin of data (with 20 frames of motion in bin 3). Three passes of motion were obtained to ensure the total range of motion was captured if the participant moved too slowly or if they missed the trigger to begin motion at the start of the scan; consequently, a pass of motion could carry over from one bin of data into the next. The first instance of extreme radial deviation and extreme ulnar deviation were analyzed in this study, wherein bin 2 was used to determine if the extreme ulnar deviation frame was in the first or second bin of motion. Image reconstruction was performed for 25 frames over each pass; thus, participants performed RUD at approximately 9°/s. The total exposure time for three passes per motion was 24.5 s, resulting in a dose length product (DLP) of 713.64 [mGy-cm]. Alternatively, the total skin dose was 0.067 Gy from the hand scans and the threshold for skin erythema from radiation exposure is 2 Gy[11]. Thus, the skin dose from the research study was ten times lower than the threshold.

2.2.3 3D Reconstruction

Volumetric images were rendered in 3D (output as digital imaging and communications in medicine (DICOM) files) and displayed in a cine movie loop to visualize the joint articulating surfaces in motion. For the purposes of this study, the frames of interest were the neutral frame, and the extreme radial and ulnar deviation frames. To determine which frames were those of interest, 3D-Slicer software (version 4.11.0, an open-source software platform for medical image processing available at https://www.slicer.org) was used to visualize each frame of motion and select the appropriate DICOM frames from which models of the carpals were made. To create the bone models (radius, scaphoid, and lunate) of each selected frame of interest, a semi-automatic algorithm in Mimics 22.0 software (Materialise, Belgium) was used, wherein the segmentation threshold was manually selected to visualize only the bone aspects of the CT image and then each slice could be manually edited according to the appropriate bone geometry[13]. Post-processing measures were exacted on the bone models to improve surface smoothness and bone shape. All models were wrapped and smoothed within the Mimics 22.0 software, saved as stereolithography (STL) files, remeshed in 3-Matic (Materialise, Belgium), and converted to a different file format

for ease of use in subsequent Python programs (visualization toolkit (VTK) files in Paraview (Kitware, Inc., New York, New York, www.paraview.org)). This method of reconstruction was validated previously where 3D reconstructions were created and compared to a ground truth bone digitization (average error <0.3mm)[14].

2.2.4   Characterization of CT Responsiveness.

Responsiveness, as defined in this study, is the ability of a system or instrument to measure small, clinically important changes. To determine the responsiveness of 4DCT as a dynamic imaging modality, bone models for the capitate, lunate, scaphoid, radius, ulna and third metacarpal were made for all 25 frames of motion in the first pass of RUD and flexion extension (FE, from extreme extension to extreme flexion) for one healthy participant (separate from the main cohort of n=12; female, 35 years old). This participant underwent the same unilateral (dominant wrist, right-handed) CT scanning protocol as was outlined for the cohort of 12, except there were two kinematic motions (RUD and FE) instead of one (RUD).

2.3   Data Analysis

2.3.1   Registration and Osteokinematic Transformation

Custom Python scripts were used to calculate the transformation matrices of the bones of interest and the volumetric centroids of the scaphoids. The transformation matrices were calculated using the iterative closest point (ICP) surface-based registration algorithm of the neutral bone models to the kinematic bone models (extreme radial and ulnar deviation)[15]. To improve alignment, an initial paired-point registration was performed for coarse alignment by selecting three anatomical landmarks on the bones involved in the registration. The ICP registration was applied to refine the course alignment with an end condition of surface alignment ≤ 0.001 mm root mean square or a maximum of 100 iteration (this limit was reached once out of 173 times)[13]. The accuracy of this step had been previously described and is less than 0.4 mm[13].

A custom Matlab (The MathWorks Inc., Natick, MA) script manipulated the centroids to relate their position to that of the radius in the neutral position, thus calculating the centroid translation in a standard way that could be compared across participants. The first extreme radial deviation frame and first extreme ulnar deviation frame were chosen as the two kinematic frames of interest.

Matlab was used to calculate the inverse transformation matrices of the radii in the kinematic frames. Python was used to determine the centroid of the scaphoid in each kinematic frame by calculating the geometric centre of the scaphoid model. The centroid of the scaphoid in the kinematic frame was multiplied by the transformation matrix of the scaphoid in the kinematic frame, and then the resultant was multiplied by the inverse transformation matrix of the radius in the kinematic frame. Matlab was also used to make a local coordinate system (LCS) in the radius for each participant, according to the International Society of Biomechanics (ISB) standards: the origin was in the centre of the radial surface (between the scaphoid and lunate fossae), the positive x-axis was volar, positive y-axis was proximal (towards the elbow), and positive z-axis was radial. The inverse of this transformation matrix was used to transform the bones (in Python) and the 3D coordinates of the centroids (in Matlab) to the LCS. This procedure was done for each participant's scaphoid in extreme radial deviation and extreme ulnar deviation, from which overall translation (extreme radial to extreme ulnar deviation) was calculated by subtracting the radial deviation position from the ulnar deviation position. To illustrate the translation of the scaphoids in 3D, a custom Python script used the same kinematic scaphoid transformation matrices and inverse kinematic radius transformation matrices as were used in Matlab to reposition the kinematic scaphoid bone models into the neutral radial space.

2.3.2   Joint Congruency

To illustrate overall joint congruency, inter-bone distances were calculated of the radioscaphoid and scapholunate joints in the extreme radial deviation and extreme ulnar deviation frames of motion. A previously described Python algorithm (point-to-point) was used to illustrate overall joint congruency[13]. In this study, the JSA of the subchondral bone is a CT-derived measure of joint contact area and was determined for a given level of proximity between two bones. The proximity distance which met the criteria for two bones to be considered "in contact" was selected by considering joint space and defined as regions wherein the inter-bone distances were less than or equal to 2.0 mm. This threshold was chosen because it approximately considered the whole articular surface of the scaphoid's surrounding joints and was previously used to measure articular cartilage in the scaphoid, lunate fossae, and inter-fossa ridge[16]. For visualization, the inter-bone distances were illustrated with an iso-contoured proximity map, with colors projected on the bone

that each correspond to a distance. A scale displayed all inter-bone distances less than 2 mm (0mm, red; 2mm, blue), while all distances greater than 2 mm were dark blue[13].

For the responsiveness study, the outcome measurement from these bone models was JSA and joint congruency maps; if there were qualitative differences in the joint congruency maps between consecutive frames of motion, then 4DCT was sufficiently responsive to detect subtle changes in joint mechanics because of the bone motion.

2.3.3   Statistical Analysis

A paired t-test was conducted for JSA on two joints (radioscaphoid and scapholunate) in the 12 healthy participants to compare between extreme radial and extreme ulnar deviation. A paired t-test was also done on six joints (radioscaphoid, scapholunate, radiolunate, distal radioulnar joint (DRUJ), capitolunate, and scaphocapitate) in the one healthy participant to compare between RUD and FE for all 25 frames of motion; although there was only one participant, the sample size was n=25 due to the number of frames analyzed, thus enabling a t-test. Statistical significance was defined as $p < 0.05$.

2.4   Results

2.4.1   Scaphoid Kinematics

The translation of the scaphoid from extreme radial deviation to extreme ulnar deviation was calculated in the x-axis (volar positive), y-axis (proximal positive), z-axis (radial positive), and overall (root mean square) for each participant. The average scaphoid translated 1.7 ± 1.5 mm dorsally, 5.5 ± 1.4 mm distally, 2.3 ± 0.9 mm radially (6.4 ± 1.3 mm total). Table 2.1 shows representative data of two scaphoids' positions during extreme radial and extreme ulnar deviation relative to the neutral radius. These models show that the scaphoid extends from extreme radial deviation to extreme ulnar deviation.

Table 2.1: Scaphoid centroid translation represented by one participant. Red (light) represents extreme radial deviation and blue (dark) represents extreme ulnar deviation. The centroids of the scaphoids are in white. The right column within each view includes the lunates in extreme radial deviation (red, light) and extreme ulnar deviation (blue, dark) to show how they move with the scaphoid.

	Scaphoids with centroids	Scaphoids with lunates
Frontal View (z-y axes)		
Sagittal View (x-y axes)		
Transverse View (x-z axes)		

Arthrokinematics were determined by calculating joint congruency, wherein "in contact" was defined as a joint space of less than or equal to 2 mm. Proximity maps of the radioscaphoid and scapholunate joints for the 12 healthy participants in extreme radial deviation and extreme ulnar deviation are shown in Table 2.2. These maps indicate that there was less contact in both joints in ulnar deviation than in radial deviation. The joint congruency maps and JSA show that joint contact patterns change as the wrist moves through RUD. To determine the significance of this finding, JSA was calculated from the joint congruency maps and averaged for each joint in each extreme of motion. The average JSA for extreme radial and extreme ulnar deviation in the radioscaphoid joint were 116.9 ± 58.0 mm^2 and 49.1 ± 43.0 mm^2, respectively. The average JSA for extreme radial and extreme ulnar deviation in the scapholunate joint were 41.9 ± 26.5 mm^2 and 32.6 ± 24.7 mm^2, respectively. Thus, there is less JSA in both joints in ulnar deviation than in radial deviation; these findings are statistically significant for the radioscaphoid joint ($p = 0.001$) but not for the scapholunate joint ($p = 0.252$).

Table 2.2: Joint congruency maps of the radioscaphoid (visualized on the radius) and scapholunate (visualized on the scaphoid) joints in extreme radial and ulnar deviation for 12 healthy participants. Anatomical directions are indicated on the first participant and are consistent throughout participants. The directions are as follows: volar (V)/ dorsal (D), proximal (P)/ distal (Di), and radial (R)/ ulnar (U).

0 mm			2 mm
0.5 mm High Proximity	1.0 mm Med Proximity	1.5 mm Low Proximity	2.0 mm Ultra-Low Proximity
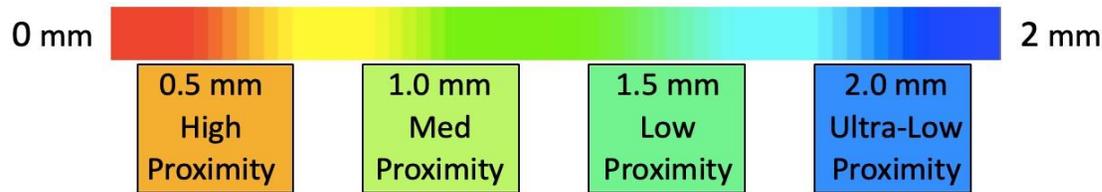
Participant Number	Radioscaphoid joint		Scapholunate joint	
	Extreme radial deviation	Extreme ulnar deviation	Extreme radial deviation	Extreme ulnar deviation
	Lunate Type 1			
1				

2				
3				
4				

8				
9				
10				

11				
12				
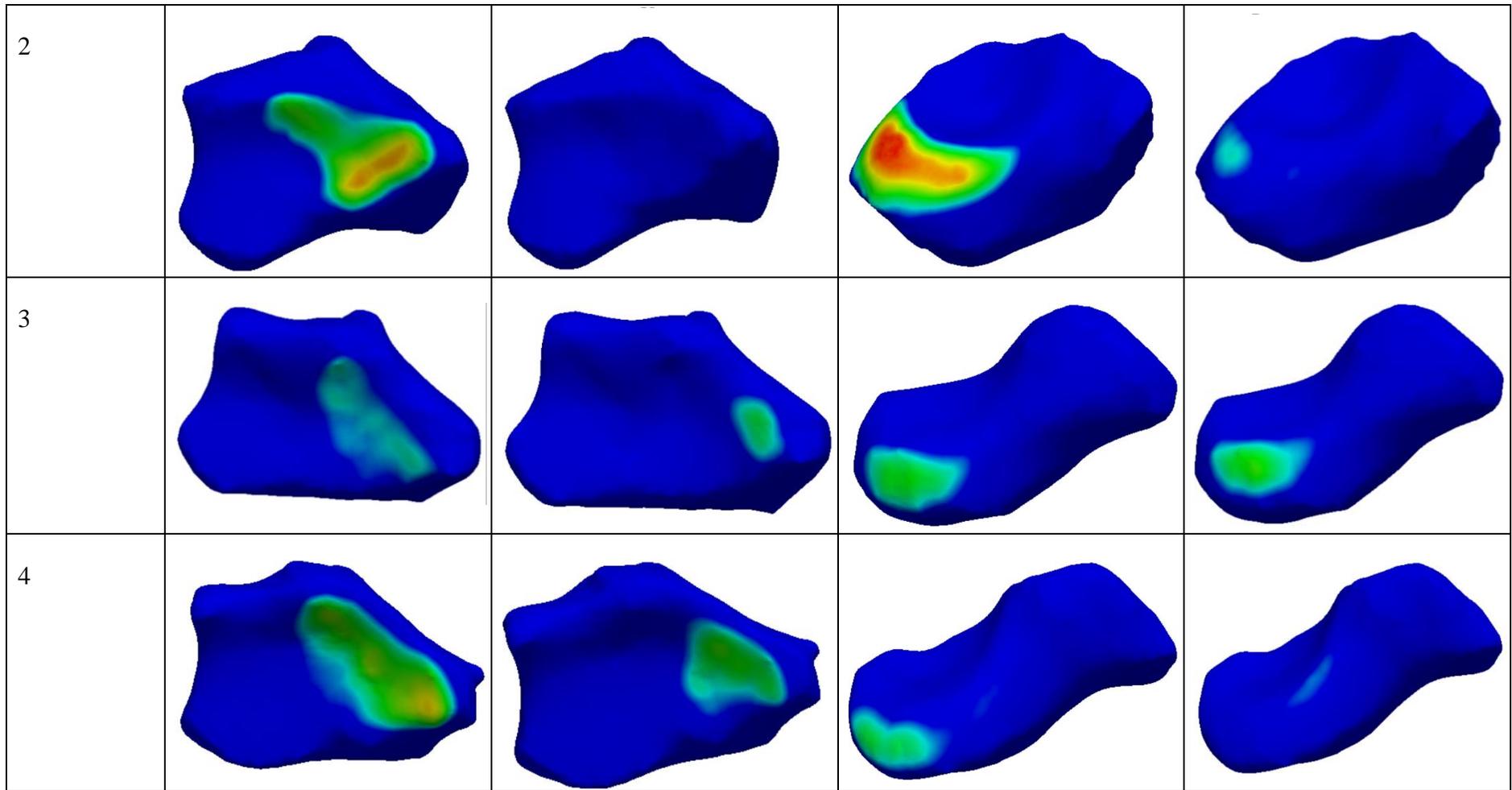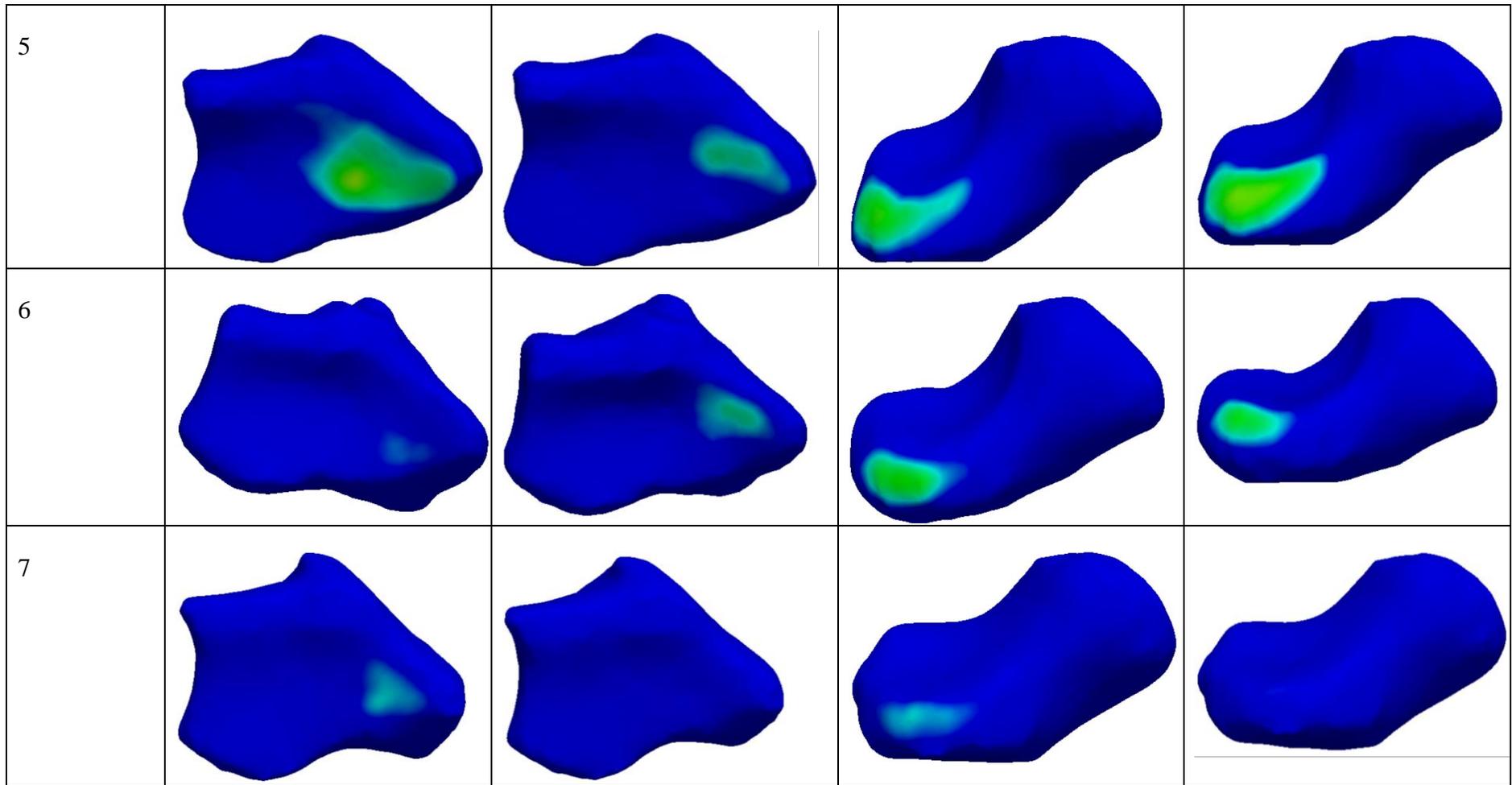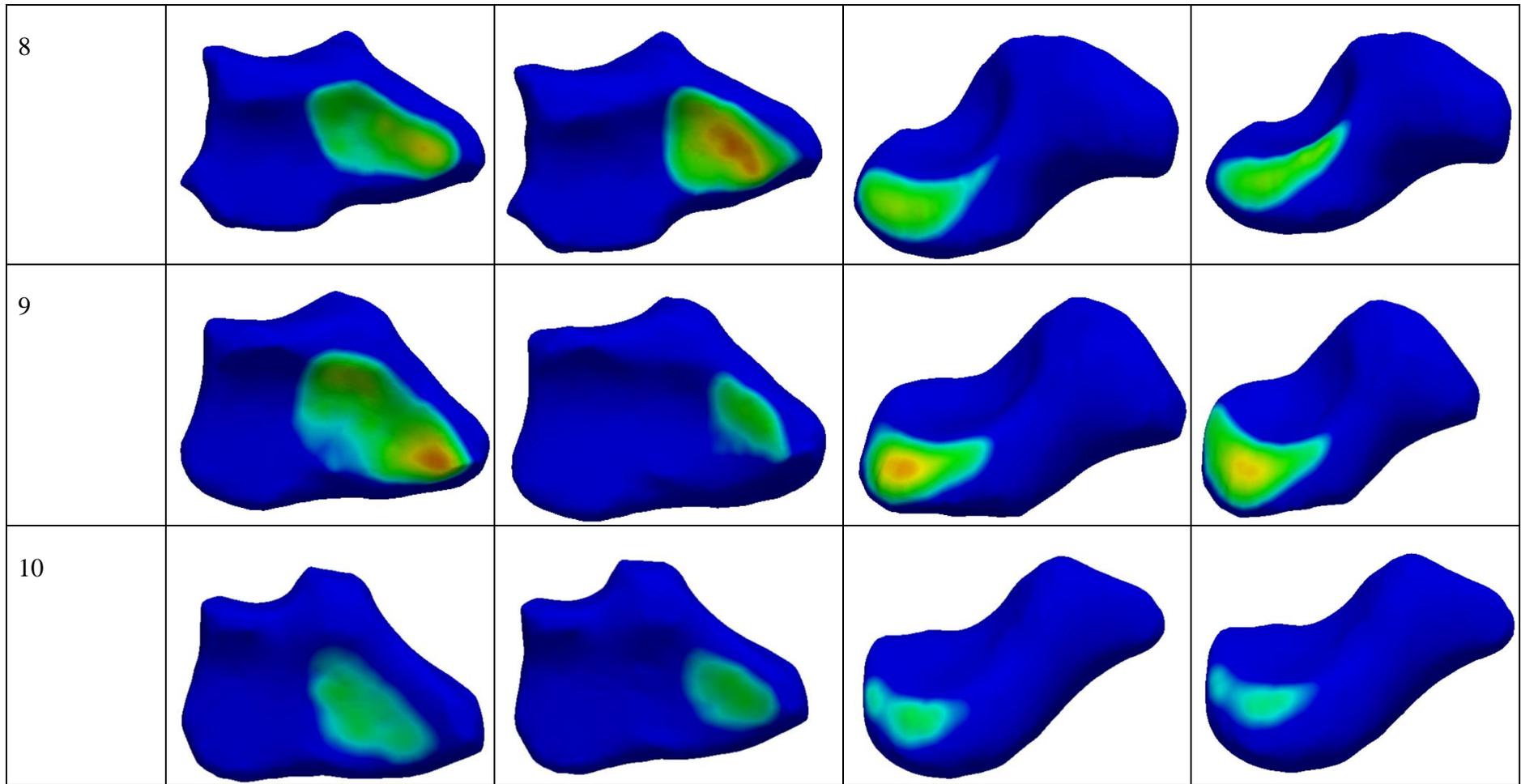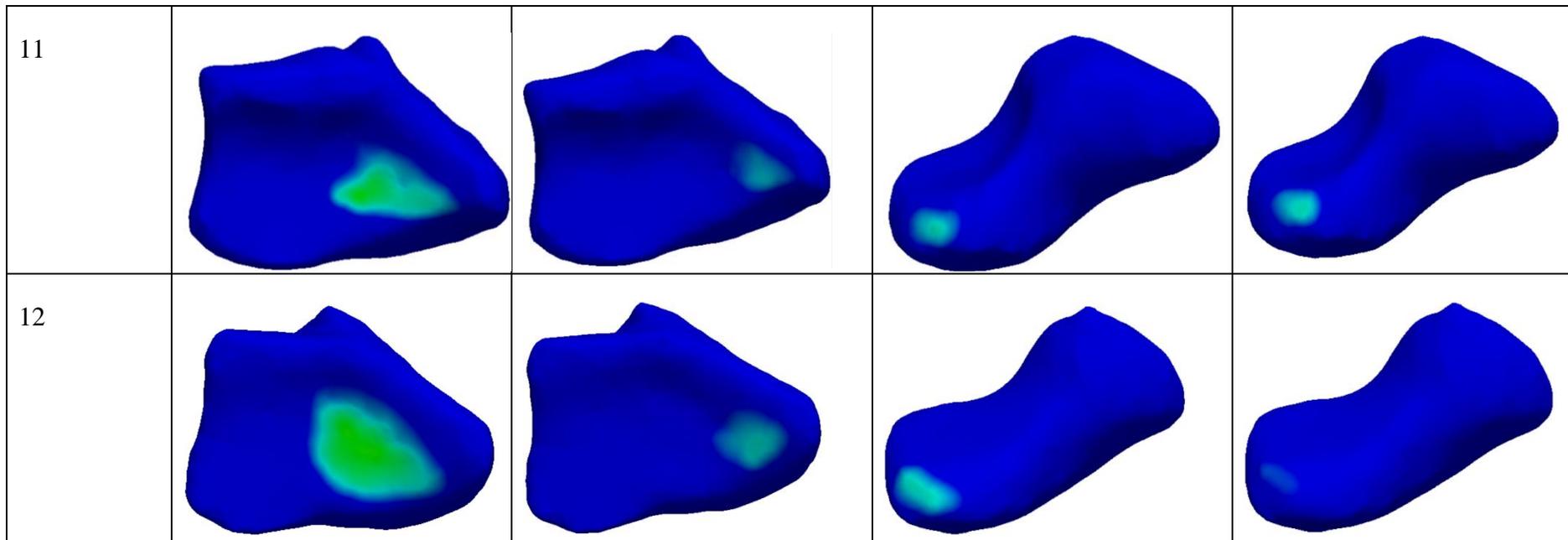
2.4.2　Characterization of CT Responsiveness

Arthrokinematics for all 25 frames of one healthy participant were analyzed for the radioscaphoid, radiolunate, scapholunate, DRUJ, capitolunate and scaphocapitate joints, wherein "in contact" was defined as inter-bone distances of less than or equal to 2 mm. Figure 2.1 shows representative data for the radioscaphoid joint during RUD and illustrates subtle changes in bone movement between each consecutive frame. In general, there was less contact in most joints in FE compared to RUD. To confirm these qualitative observations, JSA was calculated from the joint congruency maps and averaged for each joint over all 25 frames of motion to obtain quantitative measures of the difference in joint contact between RUD and FE (Figure 2.2). There is statistically significantly less JSA in FE than RUD for the scapholunate ($p = 0.001$), DRUJ ($p = 0.001$), and capitolunate joints ($p = 0.007$); although the same trend existed for the radioscaphoid joint, it was not statistically significant ($p = 0.079$). There was statistically significantly more JSA in FE than RUD for the radiolunate joint ($p = 0.001$). There was no statistically significant difference in the scaphocapitate joint between motions ($p = 0.961$). Thus, the six analyzed carpal joints changed congruency between RUD and FE. The results of the JSA calculations are visualized in Figure 2.3 (RUD) and Figure 2.4 (FE) as JSA for each frame during each motion to illustrate that joint congruency changed throughout motion and between consecutive frames of motion. Therefore, the results of this analysis indicate that the imaging tool and outcome measure reported can measure small changes throughout the range of motion.
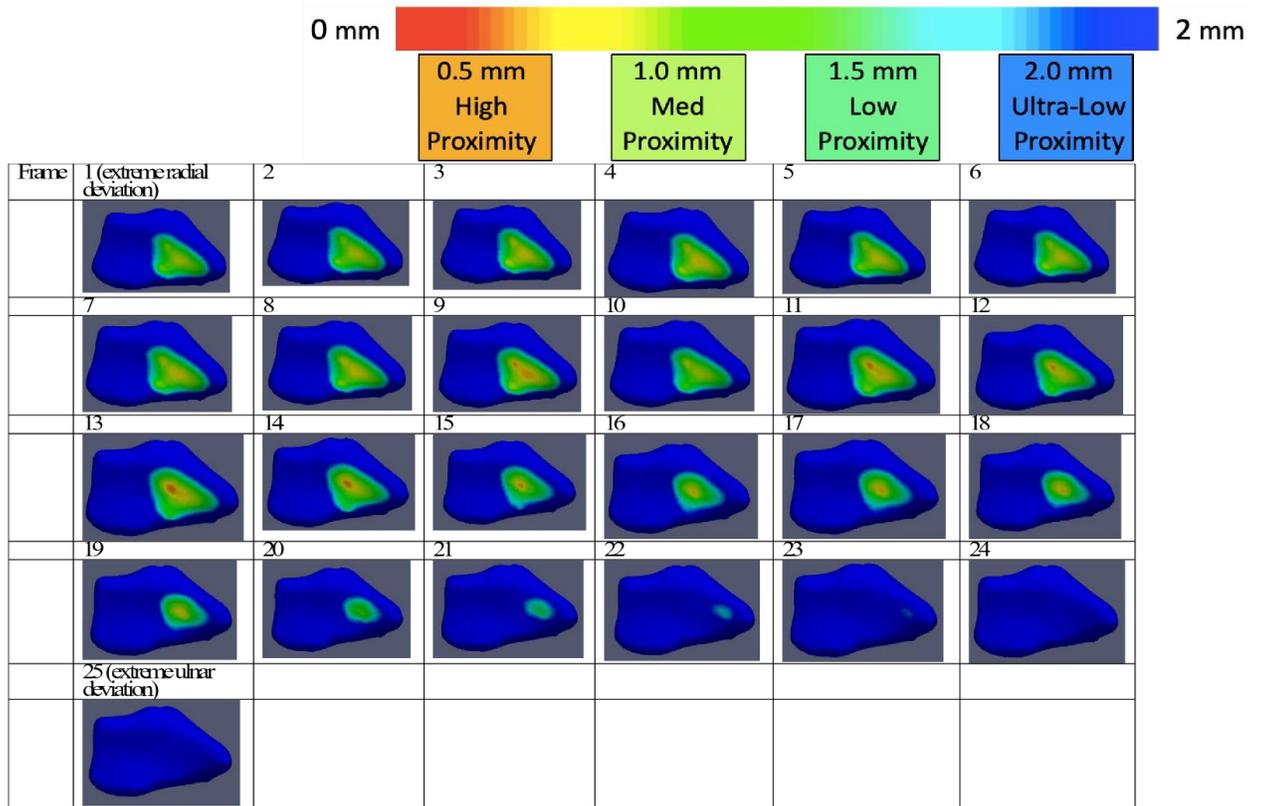
Figure 2.1. Joint congruency maps for 25 frames of one healthy participant's radioscaphoid motion during RUD to examine responsiveness.
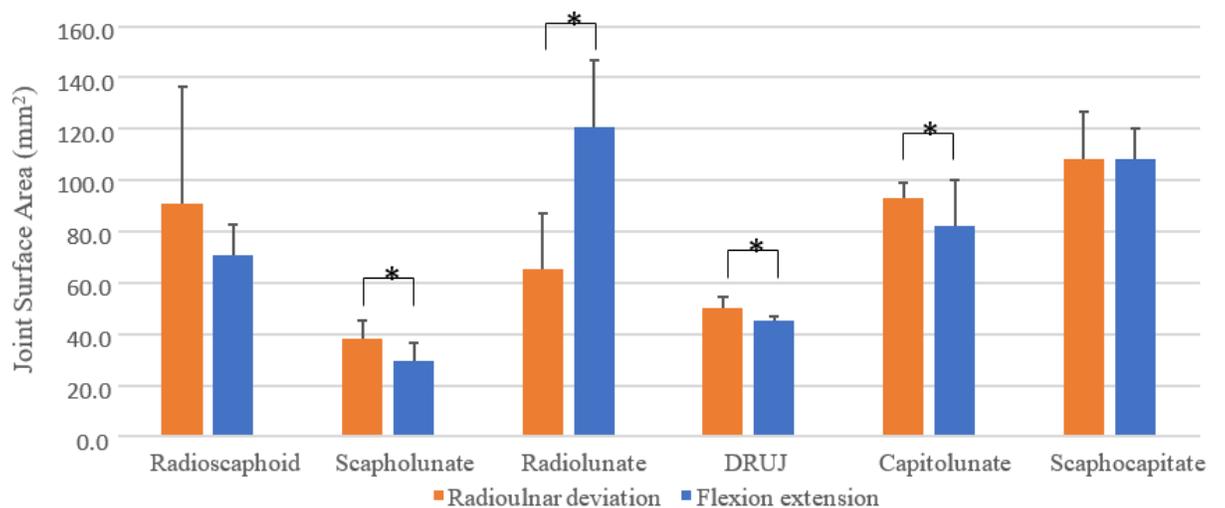
Figure 2.2. Joint surface area for one healthy participant averaged over 25 frames of motion in RUD and FE.
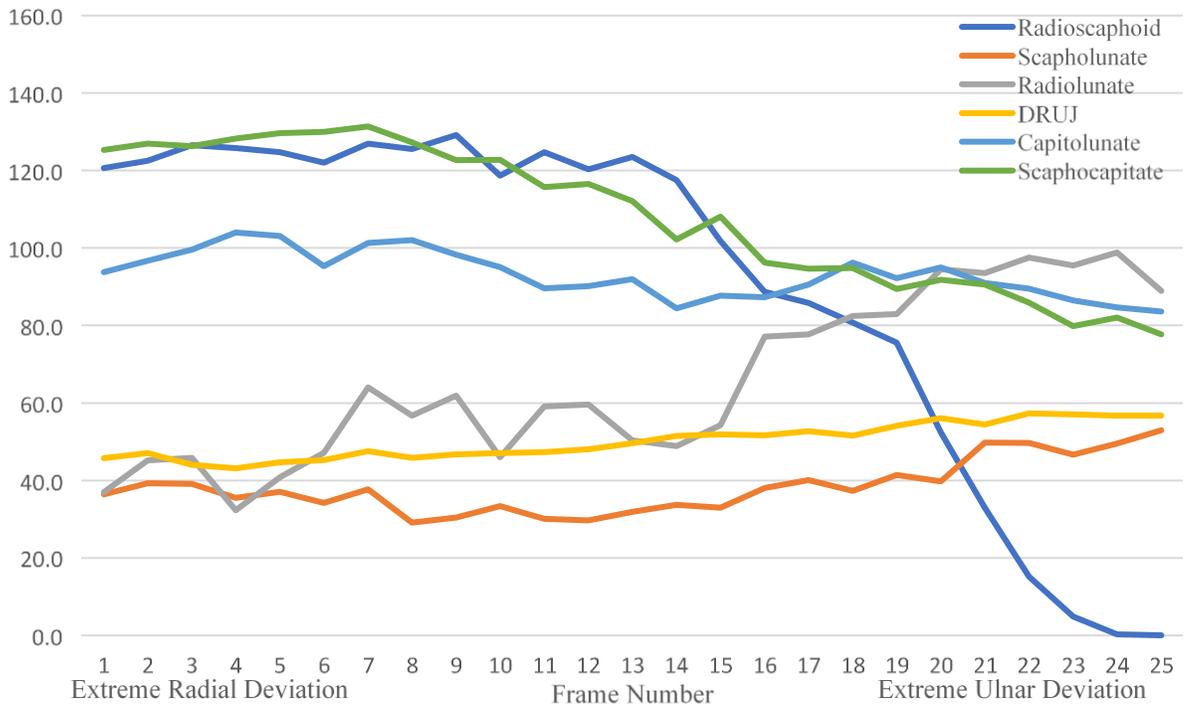
Figure 2.3. One healthy participant's joint surface areas during RUD (25 frames of motion) to illustrate responsiveness.
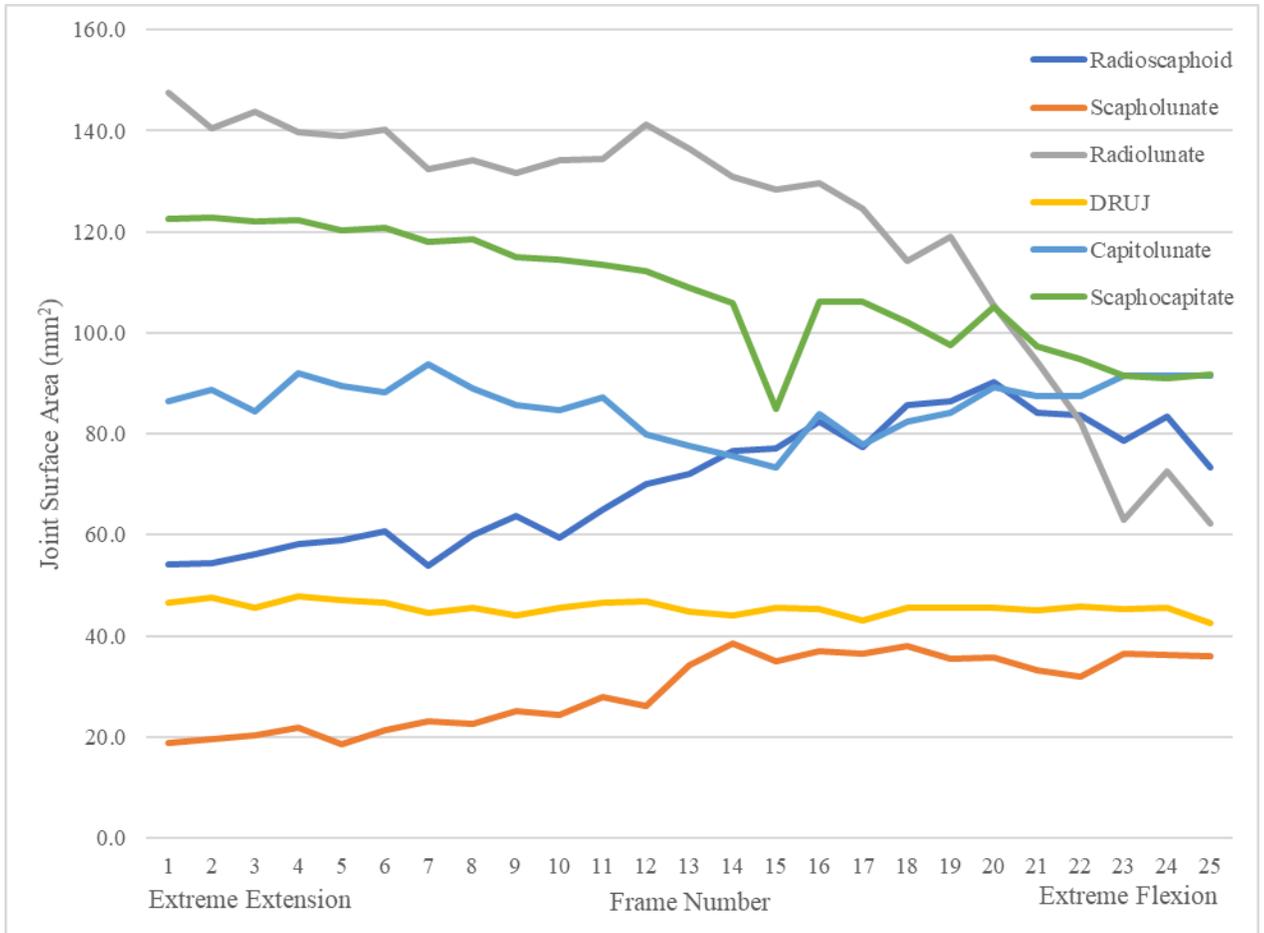
Figure 2.4. One healthy participant's joint surface areas during FE (25 frames of motion) to illustrate responsiveness.

2.5 Discussion

A universally accepted wrist motion theory has not been elucidated despite the evolution of many models to describe wrist motion which have traditionally relied on 2D radiographs, stereoradiography and 3DCT/MRI[3]. Many of these previous approaches were limited in their ability to measure 3D motion (and out of plane motion), in their ability to detect subtle bone changes due to limitations in spatial resolution, and in their ability to assess complex motions[8-11,17]. Stereoradiography required implantation of additional beads into the joint and most recently, 3D studies using CT or MRI, while inherently 3D, could not examine the full spectrum of wrist motion while undergoing a functional task or during a complex range of motion over time[3,6,7]. In recent studies, 4DCT has been shown to be

able to measure dynamic motion of the carpus in real-time[3]. In this current study, 4DCT was used to examine changes in joint congruency and kinematics throughout motion in a cohort of healthy participants, to measure responsiveness of 4DCT to small changes in JSA, and is a first step in informing current row/column theories described in the literature.

In this study, 4DCT was used to examine scaphoid translation and contact mechanics in a cohort of 12 healthy individuals during active radial and ulnar deviation. We found that as the wrist moved from radial deviation to ulnar deviation, the scaphoid translates approximately 6.4 ± 1.3 mm. Crisco et al. reported total translation of the scaphoid 7.5 ± 3.5 mm during radial ulnar deviation using quasi-static CT[12]. Zhao et al. measured resultant translation range for the scaphoid and lunate and reported a range from 2 mm to 11 mm during FE and RUD[1]. Scaphoid translation is clinically relevant because increased translation is a marker for SL injuries, thus normative data can provide a target for injury diagnosis. Additionally, previously reported scaphoid translations allowed for benchmark values, to which results of this study were compared, to show the feasibility of the proposed 4DCT protocol. Lastly, the small changes in scaphoid translation showed that 4DCT can detect subtle bone movement changes, which would be a necessary feature for detecting subtle abnormal bone motions indicative of SL injuries. Although it is beyond the scope of this work, the methodology presented provides groundwork to assess for important parameters for the early detection of early carpal instabilities, namely SL injuries.

In addition to measuring absolute translation, joint congruency can provide information on how two bones are articulating throughout a given motion. If the JSA increases or decreases from one extreme of motion to the other, it can be inferred that the bones are moving asynchronously; whereas if the JSA remains constant, the bones may be moving synchronously. In this study, the decrease in radioscaphoid joint congruency, illustrated in Table 2.2 and supported by JSA calculations, suggests that the scaphoid is in progressively less contact with the radius throughout RUD, which could be explained by scaphoid extension that was shown in this study and is supported in the literature[3]. The lack of a statistically significant change in JSA in the scapholunate joint suggests that the scaphoid and lunate move synchronously through RUD, which is illustrated in Table 2.1 and supported by Crisco et al.'s *in vivo* study[12]. Another useful insight from joint congruency

58

is that you can see how the contour maps change between frames. Based on the responsiveness data set (Figure 2.1), the difference between those frames is small at the beginning of the range of motion and increases near the end of the range of motion providing evidence that the 4DCT system is responsive to these subtle changes.

The flexion of the scaphoid in a SL injury had been documented and is known to be the beginning of degenerative arthritis, such as scapholunate advanced collapse (SLAC)[10,18]. While the progression of such a disease in relation to bone position is well documented, it is unclear what the relationship is between laxity, dynamic carpal motion, and the onset and progression of carpal instabilities[3]. Mat Jais et al. used 4DCT with cadavers which had undergone different ligament injury simulations and found the magnitude of translation relative to the neutral position in the x-, y-, and z-axes to be, on average, 0.01-1.24 mm; while translation increased with successive injury simulations, it was not drastically different than the intact state[10]. Kelly et al. measured the gap between the scaphoid and lunate in cadaveric wrists during RUD and found there to be very small gaps (< 1.20 mm), indicative of minimal scapholunate separation in normal wrists[19]. Demehri et al. measured the scapholunate interval *in vivo* in healthy wrists and calculated the interval to be < 1 mm in RUD[18]. In the review study by White et al., the range of scapholunate gaps was 0.67 mm to 1.19 mm for healthy wrists[2]. Results from this study show that the scapholunate JSA does not significantly change from extreme radial to extreme ulnar deviation indicating that the scaphoid and lunate move together through RUD. Also, the scaphoid is very constrained by neighboring bones and the surrounding ligamentous structure when compared to the elbow which, upon ligament disruption, has significantly increased laxity[10,16,20]. Shores et al. identified a gap in the literature, such that "there is clearly a need for more accurate and precise, in vivo evaluation of carpal bone kinematics in patients presenting with symptoms of instability"[21]. Thus, our future work will focus on SL injuries and how injured wrist motion differs from the healthy motion examined in this chapter; specifically, detecting different stages of SLAC will be examined by measuring scaphoid motion through FE and measuring changes in the scapholunate gap.

This study showed that dynamic measurement of carpal kinematics is integral in understanding wrist motion, and that there is noticeable change that occurs between

consecutive frames of motion, indicating that 4DCT is a responsive tool that can be used to quantify subtle, clinically important changes due to bone movement. Our results of the 25 frames of motion show a continuous motion that subtly changes at each measurement point, thus quantifying the relationships between carpals without artifact was possible with 4DCT for all 25 frames of motion (Figure 2.1, Figure 2.3, Figure 2.4). As such, 4DCT can be used to analyze time dependent or instantaneous phenomena, which would require the tool's responsiveness and the fine temporal resolution provided by all multiple frames of motion to catch the anomaly. This data is clinically important because an increase in JSA overtime could suggest joint space narrowing indicative of arthritis. Now that a sound methodology has been established, future work can focus on provocative *in vivo* tasks which provoke a symptom. Future work will test the responsiveness of 4DCT with increased speed of motion (degrees per second) to determine how speed affects motion artifacts and distinguishability of individual frames. To do so, a guiding device will be designed and implemented which standardizes speed of motion throughout a pass such that passes of different speeds can be compared. Future work will also take advantage of this responsiveness by analyzing more frames of motion.

There has been great debate in the literature about the best CT scanner for measuring wrist motion, since this is still a new application for 4DCT[2]. To minimize artifacts from inconsistences of projections from motion, a complete set (360°) of projections of the wrist must be acquired in as short a time window as possible. McCollough et al. showed that for an 'effective' x-ray exposure time of 0.5 s, motion artifacts and loss of spatial resolution were observable at movement velocity of 10 mm/s[22]. In our RUD studies, the x-ray exposure time was shorter at 0.35 s and the average velocity of motion was less at 4.5 mm/s measured at the capitate, therefore motion artifacts were minimal. Another possible source of artifact is "banding" arising from using a CT scanner with limited coverage so that a full 3D volume of the wrist must be built from multiple cycles of the RUD[23,24]. We used a 256-slice CT scanner with a coverage of up to 16 cm, therefore the banding artifact was avoided. For slower gantry rotation speed, one way to decrease the acquisition window is to use partial scan reconstruction leading to "shading" artifact[25]. In this study, because our rotation speed was fast enough to avoid motion artifacts as discussed above, we were able to use full scan reconstruction thus eliminating this source of artifact as well. Lastly, future

studies will register bone models from a high-resolution static scan to the low-resolution kinematic scans to improve the resolution of the results while maintaining acceptable levels of dose.

Dose is another consideration for 4DCT as it is significantly higher than in 3DCT because of the longer scan time. However, effective dose is relatively low in the wrist due to lack of nearby radiosensitive organs[11]. As stated in the methods, the DLP for this study was 713.64 mGy-cm and the total skin dose was 0.067 Gy, which is 30 times less than the threshold for skin erythema of 2 Gy. Due to the lead apron, neck band, and protective eyeglasses worn by the participants, the scatter radiation dose was 0.013 mSv, as measured under the lead apron. The average person receives an effective dose of 3 mSv per year from naturally occurring radioactive materials and cosmic radiation from outer space. This value is 231 times higher than the effective dose in our research study, therefore, the effects from this scatter dose were negligible. A limitation in the literature is the lack of characterization surrounding the dose from 4DCT.

Table 2.3 summarizes dose values for other studies of similar nature; there is inconsistency in which values are reported (DLP, effective dose, and/or total skin dose) and for how many scans they are reported (one scan or motion pass, or the total CT scanning protocol)[1,11,18,21,26-30]. Furthermore, DLP depends on the duration of x-ray exposure(s), the amount of radiation produced per rotation (mAs), and the range of the scan (mm). If we scale our study to the same parameters as Shores et al., the DLP of our study would be 97.65 mGy-cm, which is comparable to their 84.3 mGy-cm. Therefore, more research is needed to characterize 4DCT dose as it pertains to dynamic carpal imaging.

Table 2.3. Dose length product and effective dose values for various 4DCT wrist motion studies.

Paper	DLP [mGy-cm]	Effective Dose [mSv]	Total Skin Dose [Gy]
Threshold		3 (per year)[1]	2 (for skin erythema)
Standard CT[27]		0.03[1] Average chest CT 5.27 ± 1.68 mSy, chest radiograph 0.08 mSy[18]	
This study	713.64 total	0.013	0.067
Zhao et al.[1]	36 per scan	0.09	
Leng et al.[11]; cadaveric RUD			0.2
Garcia-Elias et al.[27]; carpal motion during DTM	33	0.79	
Troupis et al.[28]; trigger lunate syndrome	410.7 per scan, 1789.2 total	0.05 per scan, 0.18 total	
Repse et al.[26]; detection of capitate subluxation	433.7	0.04 (typical 0.134 in this institution)	
Demehri et al.[29]; pisotriquetral instability	Patient 1: 378.3	Patient 1: 3026.4	Patient 1: 0.5

	Patient 2 (right): 63.9 Patient 2 (left): 64.5	Patient 2 (right): 671.8 Patient 2 (left): 685.6	Patient 2 (right): 0.11 Patient 2 (left): 0.12
Demehri et al.[18]; scapholunate kinematics	Asymptomatic: 445.30 ± 122.04 Symptomatic: 606.46 ± 619.86	Asymptomatic: 0.06 ± 0.06 mSy Symptomatic: 0.05 ± 0.01 mSy	
Edirisinghe et al.[30]; axis of rotation for dart thrower's motion		Did not exceed 0.15 for three DTM	
Shores et al.[21]; kinematics before and after surgery	84.3	0.07	

2.6 Limitations

There were some limitations in this study. The JSA algorithm used in this study has been applied to other joints and is sensitive to the accuracy of the bone models but has yet to be validated at the wrist. Future work should look at micro-CT data of the wrist to determine the error more accurately between the bone models of the 4DCT scans and scans from the micro-CT. There were some frames on the CT scans with blurring artifacts. Future work will be done to determine why the third metacarpal is the bone with the most blurring artifact and if different motions can be done at different speeds. Only planar motions were analyzed in this study, whereas the wrist is capable of complex motions and so combined motions may be more representative of functional wrist motion[3]. Lastly, a limitation in the

literature and in this study is the small sample size, especially n=1 for the 25 frames data. Future work will be conducted on many participants with more frames of data analyzed for more reliable results.

2.7   Conclusion

Current techniques for measuring carpal motion are unable to detect subtle dynamic bone movements to fully characterize wrist motion. The use of 4DCT can mitigate these limitations, allowing for continuous measurement through motion, enabling provocative analysis of wrist motion. This work measured healthy carpal kinematics and arthrokinematics using 4DCT as a novel approach for obtaining carpal motion information. The objectives were met using 4DCT to quantify healthy scaphoid motion during RUD in terms of scaphoid translation and carpal joint congruency, which determined whether the bones were moving synchronously or asynchronously. The scaphoid extended from extreme radial deviation to extreme ulnar deviation, translating dorsal, distal, and lateral, which is supported by previous findings on scaphoid extension through RUD. The scaphoid moved relative to the lunate; however, the change in JSA was small which suggested that the bones did move synchronously. This work will lead to a comprehensive understanding of carpal mechanics, which is essential to understanding normal function and structure and to provide targets for interventions.

This study shows that 4DCT can measure centroid translation and JSA. Only extremes of motion were analyzed but because the system is responsive and changes in JSA occurred throughout motion, future studies will examine more frames of motion. In the future, 4DCT should be used to measure kinematics (bone rotation), as the next step after measuring translation. Also, the scapholunate JSA was difficult to visualize on the scaphoid due to its anatomical orientation and so future studies will visualize the JSA on the lunate. However, before these changes can be implemented, the current technique must be validated in this thesis.

2.8   References

1.   Zhao K, Breighner R, Holmes D 3rd, Leng S, McCollough C, An K-N. A technique for quantifying wrist motion using four-dimensional computed tomography: approach and validation. J Biomech Eng. 2015;137(7). doi:10.1115/1.4030405

2.   White J, Couzens G, Jeffery C. The use of 4D-CT in assessing wrist kinematics and pathology. Bone Joint J. 2019;101(B):1325-1330.

3.   Rainbow MJ, Wolff AL, Crisco JJ, Wolfe SW. Functional kinematics of the wrist. J Hand Surg Am. 2016;41E(1):7-21.

4.   Gates DH, Walters LS, Cowley J, Wilken JM, Resnik L. Range of Motion Requirements for Upper-Limb Activities of Daily Living. Am J Occup Ther. 2016;70(1):7001350010p1-7001350010p10. doi:10.5014/ajot.2016.015487

5.   Kramer A, Allon R, Wollstein R, Werner F, Lavi I, Wolf A. Distinct Wrist Patterns Founded on Measurements in Plain Radiographs. J Wrist Surg. 2018;7:366-374.

6.   Kamal RN, Rainbow MJ, Akelman E, Crisco JJ. In Vivo Triquetrum-Hamate Kinematics Through a Simulated Hammering Task Wrist Motion. J Bone Joint Surg Am. 2012;85(1):1-7.

7.   Kobayashi M, Berger RA, Nagy L, et al. Normal Kinematics of Carpal Bones: A Three-Dimensional Analysis of Carpal Bone Motion Relative to the Radius. J Biomchanics. 1997;30(8):787-793.

8.   Dobbe JGG, de Roo MGA, Visschers JC, Strackee SD, Streekstra GJ. Evaluation of a Quantitative Method for Carpal Motion Analysis Using Clinical 3-D and 4-D CT Protocols. IEEE Trans Med Imaging. 2019;38(4):1048-1057. doi:10.1109/TMI.2018.2877503

9.   Ramamurthy NK, Chojnowski AJ, Toms AP. Imaging in carpal instability. J Hand Surg Eur Vol. 2016;41(1):22-34. doi:10.1177/1753193415610515

10.   Mat Jais IS, Tay SC. Kinematic analysis of the scaphoid using gated four-dimensional CT. Clin Radiol. 2017;72(9):794.e1-794.e9. doi:10.1016/j.crad.2017.04.005

11.   Leng S, Zhao K, Qu M, An K-N, Berger R, McCollough CH. Dynamic CT technique for assessment of wrist joint instabilities. Med Phys. 2011;38 Suppl 1:S50. doi:10.1118/1.3577759

12.   Crisco JJ, Coburn JC, Moore DC, Akelman E, Weiss APC, Wolfe SW. In vivo radiocarpal kinematics and the dart thrower's motion. J Bone Jt Surg - Ser A. 2005;87(12 I):2729-2740. doi:10.2106/JBJS.D.03058

13.   Lalone EA, Mcdonald CP, Ferreira LM, Peters TM, King GW, Johnson JA. Development of an image-based technique to examine joint congruency at the elbow. Comput Methods Biomech Biomed Engin. 2013;16(3):280-290. doi:10.1080/10255842.2011.617006

14.   Lalone EA, Willing RT, Shannon HL, King GJW, Johnson JA. Accuracy assessment of 3D bone reconstructions using CT: An intro comparison. Med Eng Phys. 2015;37(8):729-738. doi:10.1016/j.medengphy.2015.04.010

15.   Besl PJ, McKay ND. A method for registration of 3-D shapes. IEEE Trans Pattern Anal Mach Intell. 1992;14(2):239-256. doi:10.1109/34.121791

16.   Pollock J, O'Toole R V., Nowicki SD, Eglseder WA. Articular cartilage thickness at the distal radius: A cadaveric study. J Hand Surg Am. 2013;38(8):1477-1481. doi:10.1016/j.jhsa.2013.04.037

17.   Shakoor D, Hafezi-Nejad N, Haj-Mirzaian A, et al. Kinematic Analysis of the Distal Radioulnar Joint in Asymptomatic Wrists Using 4-Dimensional Computed Tomography-Motion Pattern and Interreader Reliability. J Comput Assist Tomogr. 2019;43(3):392-398. doi:10.1097/RCT.0000000000000839

18.   Demehri S, Hafezi-Nejad N, Morelli JN, et al. Scapholunate kinematics of asymptomatic wrists in comparison with symptomatic contralateral wrists using four-

dimensional CT examinations: initial clinical experience. Skeletal Radiol. 2016;45(4):437-446. doi:10.1007/s00256-015-2308-0

19.   Kelly PM, Hopkins JG, Furey AJ, Squire DS. Dynamic CT Scan of the Normal Scapholunate Joint in a Clenched Fist and Radial and Ulnar Deviation. Hand. 2018;13(6):666-670. doi:10.1177/1558944717726372

20.   Pollock JW, Brownhill J, Ferreira LM, McDonald CP, Johnson JA, King GJ. Effect of the Posterior Bundle of the Medial Collateral Ligament on Elbow Stability. J Hand Surg Am. 2009;34(1):116-123. doi:10.1016/j.jhsa.2008.09.016

21.   Shores JT, Demehri S, Chhabra A. Kinematic "4 Dimensional" CT Imaging in the Assessment of Wrist Biomechanics Before and After Surgical Repair. Eplasty. 2013;13:62-72. http://www.ncbi.nlm.nih.gov/pubmed/23573338%0Ahttp://www.pubmedcentral.nih.gov/articlerender.fcgi?artid=PMC3589877.

22.   McCollough C, Bruesewitz M, Daly T, Zink F. Motion Artifacts in Subsecond Conventional CT and Electron- Beam CT : Pictorial Demonstration of Temporal Resolution. Radiographics. 2000;20:1675-1681.

23.   Taguchi K, Chiang BS, Hein IA. Direct cone-beam cardiac reconstruction algorithm with cardiac banding artifact correction. Med Phys. 2006;33(2):521-539. doi:10.1118/1.2163247

24.   Mori S, Endo M, Asakura H. Improvement in banding artefacts in four-dimensional computed tomography for radiotherapy planning. Phys Med Biol. 2006;51:5231-5244. doi:10.1088/0031-9155/51/20/010

25.   Ramirez-giraldo JC, Yu L, Kantor B, Ritman EL, McCollough CH. A strategy to decrease partial scan reconstruction artifacts in myocardial perfusion CT: Phantom and in vivo evaluation. Med Phys. 2012;39(1):214-223. doi:10.1118/1.3665767

26.   Repse SE, Amis B, Troupis JM. Four-dimensional computed tomography and detection of dynamic capitate subluxation. J Med Imaging Radiat Oncol. 2015;59(3):331-335. doi:10.1111/1754-9485.12260

27.   Garcia-Elias M, Alomar Serrallach X, Monill Serra J. Dart-throwing motion in patients with scapholunate instability: A dynamic four-dimensional computed tomography study. J Hand Surg Eur Vol. 2014;39(4):346-352. doi:10.1177/1753193413484630

28.   Troupis JM, Amis B. Four-dimensional computed tomography and trigger lunate syndrome. J Comput Assist Tomogr. 2013;37(4):639-643. doi:10.1097/RCT.0b013e31828b68ec

29.   Demehri S, Wadhwa V, Thawait GK, et al. Dynamic Evaluation of Pisotriquetral Instability Using 4-dimensional Computed Tomography. J Comput Assist Tomogr. 2014;38(4):507-512.

30.   Edirisinghe Y, Troupis JM, Patel M, Smith J, Crossett M. Dynamic motion analysis of dart throwers motion visualized through computerized tomography and calculation of the axis of rotation. J Hand Surg Eur Vol. 2014;39(4):364-372. doi:10.1177/1753193413508709

Chapter 3

3 Accuracy Assessment of 3D Bone Reconstruction Using Dynamic 4DCT

One factor that determines the accuracy with which four-dimensional computed tomography (4DCT) can measure carpal motion is dependent on the quality of the surface models that can be reconstructed from the 4DCT volumetric data. The intent of this chapter was to employ micro-computed tomography (micro-CT) as a gold standard comparison to validate the accuracy of the 3D models obtained from the 4DCT scanner. This comparison will be made using two different software packages (commercially available vs. open source). The overall error or mismatch between the two models would indicate the error in reconstructing bone models using the 4DCT scanner. The secondary objective of this study is to evaluate the inter- and intra-rater reliability of reconstructing the bone models as the process itself is semi-automatic and does require some user intervention.

3.1 Introduction

Computed tomography (CT) provides high contrast images that enable segmentation of osseous structures from surrounding soft tissue to create three-dimensional (3D) reconstructions. Four-dimensional (3D + time) CT allows for the quantification of carpal kinematics from high contrast scans conducted over time while the subject is in motion. These 4DCT scans provide novel insight into healthy carpal motion and can illuminate changes to carpal mechanics caused by wrist injuries. The validity of these measurements relies heavily on the accuracy of 3D model reconstruction, which is dependent on several factors: the resolution of the imaging modality, the software used to reconstruct the 3D models, and inter- and intra-rater reliabilities.

The accuracy of 3D reconstructions can be determined by a comparison to a ground truth measurement. A high-resolution method of 3D bone capture is micro-CT, which is defined as CT with micrometer resolution[1]. One type of micro-CT scanner, called a bench-top scanner, uses a fixed source and detector such that there is no beam collimation, and the specimen rotates on a turntable between the source and detector as the scan is acquired[1]. The digital volume is created by processing a sequence of X-ray projection images (2D

TIFFs) of the specimen. It is imperative for the quality of the volume reconstruction that the specimen remains static; motion of the specimen will result in blurring (mis-registration) artifacts in the volume[1]. An advantage of micro-CT is that it has isotropic voxels, unlike clinical 4DCT scanners whose voxels are not isotropic because they have a relatively large slice thickness. Although there are some preclinical micro-CT scanners that can scan *in vivo* small animal models[1], no micro-CT scanner is suitable for living human subjects. Therefore, while micro-CT provides high resolution scans, the applications for *in vivo* studies are limited due to specimen size restrictions and the static nature of the scan; 4DCT overcomes this limitation by enabling the measurement of dynamic movements *in vivo*. To determine if 4DCT has sufficient resolution from which to draw reliable conclusions, 4DCT scans can be compared to micro-CT scans of the same specimen and the associated error between the two models can be measured.

The reconstruction technique can also affect the accuracy of the 3D reconstruction. The first step in reconstruction is segmentation, to separate the bone from the soft tissue, which can be done manually, automatically, or semi-automatically. Manual segmentation involves the model-maker selecting each osseous structure slice-by-slice; this method is time consuming[2] and introduces significant error due to inconsistent selection[3]. Automatic segmentation is an emerging technique[2]; with advancements in technology and machine learning, this technique may become the gold-standard[3]. However, there is no current reliable automatic segmentation technique[3]. Semi-automatic segmentation incorporates elements of both former techniques; a threshold is set, and the software automatically segments the tissues according to that threshold[4,5]. Then the model-maker manually edits the segmentation to ensure all osseous structures have been included and no soft tissue structures were falsely incorporated. Several software packages offer semi-automatic segmentation capabilities. Mimics 22.0 (Materialise, Belgium) is a commercial software with many tools for segmentation, but that comes with a high cost. In contrast, 3D Slicer 4.11.0 (available at https://www.slicer.org) is an open-source software with many of the same functions as Mimics and more customizability; Slicer allows the user to incorporate custom Python code to perform functions specific to the user. While both software are able to perform the same functions, the relative accuracy between them is unknown.

The accuracy of a 3D reconstruction depends on the imaging modality and protocol, and the reconstruction technique. The objective of this study was to assess the accuracy of 3D wrist bone reconstructions completed in Slicer and Mimics from 4DCT scans through comparison with the same bones reconstructed from a micro-CT scan in Mimics. This comparison also determines the relative error between the two software. Lastly, we determined the inter- and intra-rater reliabilities of the proposed 4DCT model-making technique in Mimics. We hypothesize that the error between the micro-CT and 4DCT models will be low, less than 0.5 mm, indicating that the 4DCT kinematic models have sufficient resolution to make accurate bone models. Also, there will be negligible difference between 4DCT models made in Slicer and Mimics, indicating that these software packages can be used interchangeably to reconstruct bone models from high contrast CT images. Finally, we hypothesize that there would be high precision when model making in Mimics, supported by high inter- and intra-rater reliabilities.

3.2   Methods

3.2.1   Specimen Preparation

One cadaveric previously frozen upper extremity (n=1, left arm, male, 63 years old) was left intact (not denuded) and mounted to a wrist motion simulator (Figure 3.1). The wrist motion simulator was custom designed using plastic (acrylonitrile butadiene styrene (ABS)) such that it could be used within the 4DCT scanner (Revolution CT Scanner, GE Healthcare, Waukesha, Wisconsin, USA) without creating artifacts, since any metal in the scanner would create blurring artifacts in the scan.
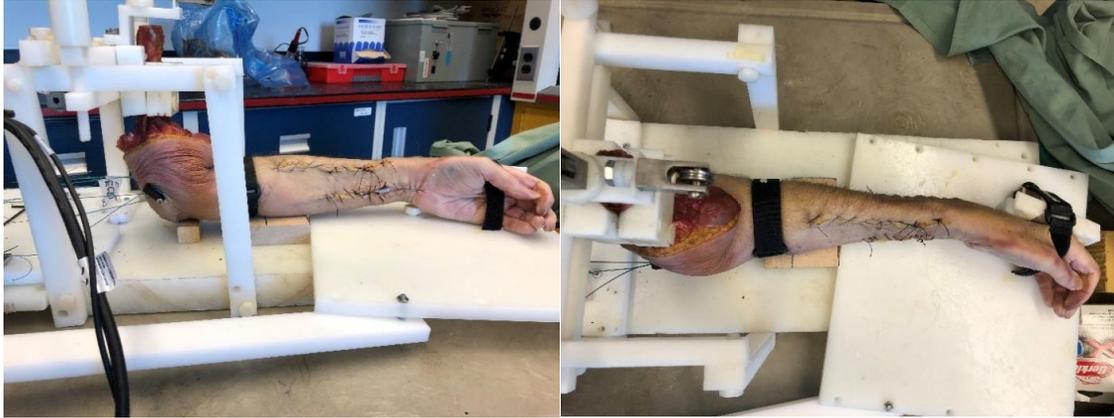
Figure 3.1. Cadaveric arm in custom wrist motion simulator.

The wrist motion simulator is comprised of four distinct parts: the vertical attachment used to secure the proximal part of the arm; a rotating base, on which the hand is secured; a servo motor and linkage which powers the rotating base; and a stationary base to which all the other components are secured. The wrist is mounted to the simulator by securing the exposed proximal end of the humerus with a plastic screw and clamp system on the vertical attachment. The proximal ends of the ulna and radius are secured onto the stationary base using a Velcro strap. The hand is secured to the rotating base with a Velcro strap around the palm/metacarpals. As the rotating base rotates, the hand strap moves the hand in unison with the rotating base while the forearm and humerus remain in fixed positions, thus simulating wrist motion.

3.2.2   Experimental Protocol

Two passes of two dynamic motions were simulated using the simulator: radioulnar deviation (RUD) beginning in radial deviation for the first pass and ulnar deviation for the second pass; and flexion-extension (FE) beginning in flexion for the first pass and extension for the second pass. Each pass of motion was six seconds long and resulted in 25 4DCT scan frames.

After 4DCT scanning was complete, the arm was refrozen and prepared for micro-CT. The arm was cut at the distal radius and ulna such that part of the distal radius and ulna, and all the carpals and metacarpals remained intact. The remaining thawed wrist was placed in a clear plastic bin and secured with insulation foam to eliminate motion during the micro-

CT scan. The wrist was brought to the Ontario Museum of Archaeology where it was micro-CT scanned for 1 hour.

3.2.3   4DCT and Micro-CT Imaging Techniques

A routine wrist scan protocol was employed using the 4DCT scanner, as outlined in Chapter 2, wherein the voxel size was $0.625 \times 0.625 \times 1.25$ mm. The micro-CT scanner (Nikon XT H 225 ST, Nikon Metrology Canada, Cambridge, Ontario, Canada) employed a routine wrist scan protocol (108 kV, 120 uA, 13.8 W, 1 s exposure). The micro-CT scanner imaged over a duration of 53 minutes for a total of 3141 projections at 150 frames per projection on a shading correction (8 min duration). The voxel size was 40 µm. The wrist was static throughout the scan. The software used to capture the scan was X-Tec Inspect-X 4.4 (Nikon Metrology Canada, Cambridge, Ontario, Canada).

3.2.4   3D Reconstruction

Volumetric images were rendered in 3D (output as DICOM files) for the micro-CT scan and the neutral frame of RUD from the 4DCT scan. To create the bone models (radius, scaphoid, lunate, capitate) of the micro-CT scan, Mimics was used; for the 4DCT scan, Mimics and Slicer were both used to make the same models. In both software, the segmentation threshold was manually selected to visualize only the bone aspects of the scan (256 Hounsfield Units (HU)) and then each slice (slice thickness 1.25 mm) was manually edited according to the appropriate bone geometry[4]. Post-processing measures were conducted to improve surface smoothness and bone shape. In Mimics, wrapping was conducted to 0.25 mm and smoothing was conducted to 0.3 mm. In Slicer, only median smoothing was performed with a kernel size of 3 mm. All models were wrapped and smoothed in their respective software, saved as STL files, remeshed in 3-Matic (Materialise, Belgium) because it is important to have a uniform mesh when conducting the interbone distances, and converted to VTK files in Paraview (Kitware, Inc., New York, New York, www.paraview.org) for ease of use in subsequent Python programs. This method of reconstruction was validated previously where 3D reconstructions were created and compared to a ground truth bone digitization (average error <0.3mm)[4].

3.3   Data Analysis

3.3.1   Registration

Custom Python scripts were used to calculate the transformation matrices of the reconstructed bones. The transformation matrices were calculated using the iterative closest point (ICP) surface-based registration algorithm of the micro-CT bone models to the 4DCT bone models[6]. To improve alignment when necessary, an initial paired-point registration was performed for coarse alignment by selecting three anatomical landmarks on the bones involved in the registration. The ICP registration was applied to refine the course alignment with an end condition of surface alignment ≤ 0.001 mm root mean square or a maximum of 100 iteration[7]. The accuracy of this step had been previously described and is less than 0.4 mm[7].

3.3.2   Model Discrepancy

To assess the accuracies of the 4DCT reconstructed bone models, inter-bone distances of the 4DCT reconstructions to the micro-CT reconstructions were calculated using a previously described Python algorithm[7]. The algorithm measured the relative difference between vertices of polygonal surfaces on the 4DCT reconstructions and those on the ground truth micro-CT reconstructions and has been previously validated[7]. Error values were positive if the micro-CT reconstructions were exterior to the 4DCT reconstructions and negative if they were interior. Absolute error values were used to calculate the mean error for each accuracy comparison and frequency plots were created to visually represent those errors.

These processes were repeated to calculate the transformation matrices and discrepancies of 4DCT bone models made in Mimics to those made in Slicer. For this comparison, a static 4DCT scan (thus, a 3DCT scan) was acquired of one participant (n=1, female, 36 years old) in 30° pronation and bone models (radius, ulna, scaphoid, lunate, capitate, third metacarpal) were made in Mimics (S.R.) and Slicer (E.N.).

3.3.3   Inter- and Intra-Rater Analysis

To calculate inter-rater reliability, one participant (n=1, female, 36 years old) was analyzed by two raters (M.R. and S.R.) following the same registration and model discrepancy processes outlined above. The motions analyzed were 20° radial deviation, neutral, and 20° ulnar deviation. Each rater made models of these positions and then the errors between the models were determined.

To calculate intra-rater reliability, the registration and model discrepancy processes were conducted on *in vivo* 4DCT scans of radioulnar deviation in two participants (n=1 male, 49 years old; and n=1 female, 19 years old). The bone models (radius, ulna, scaphoid, lunate, capitate, third metacarpal) were made in Mimics by one model-maker (M.C.) five times for the first frame of motion wherein the first model made was registered to each subsequent model made to obtain the transformation matrices and model discrepancy data. The result was four error values for each bone, which were averaged to obtain the average error and associated standard deviation.

3.4   Results

3.4.1   Micro-CT to 4DCT and Mimics and Slicer

The cadaveric 4DCT models made in Slicer and Mimics were each compared to the cadaveric micro-CT models made in Mimics. Also, 4DCT *in vivo* models made in Mimics were compared to those in Slicer. The values for the errors associated with each bone are summarized in

Table 3.1.

Table 3.1. Mean errors between micro-CT surface reconstructions and those made in Mimics and Slicer. Also includes mean errors between software (Mimics to Slicer).

Bone	Radius	Scaphoid	Lunate	Capitate
Micro-CT to Mimics error [mm]	0.4	0.4	0.3	0.4
Micro-CT to Slicer error [mm]	0.3	0.3	0.4	0.2
Mimics to Slicer error [mm]	0.2	0.2	0.3	0.2

Overall, the mean error was less than or equal to 0.4 mm for the micro-CT to 4DCT validation, and less than or equal to 0.3 mm for the Mimics to Slicer concurrent validation. Based on the average errors (

Table 3.1), frequency plots were made to visualize the errors for the micro-CT to Mimics and to Slicer (Figure 3.2). Specifically, the radius error is represented by Figure 3.2A, where 96% of the errors were within -0.5 to 0 mm for Slicer and 96% were within -1 to 0 mm for Mimics. The scaphoid error is represented by Figure 3.2B, where 97% of the errors were within -0.75 to 0.25 mm for Slicer and 95% were within -1 to 0 mm for Mimics. The lunate error is represented by Figure 3.2C, where 93% of the errors were within -0.75 to 0 mm for Slicer and 93% were within -1 to 0 mm for Mimics. The capitate error is represented by Figure 3.2D, where 95% of the errors were within -0.75 to 0.25 mm for Slicer and 98% were within -0.75 to 0 mm for Mimics.
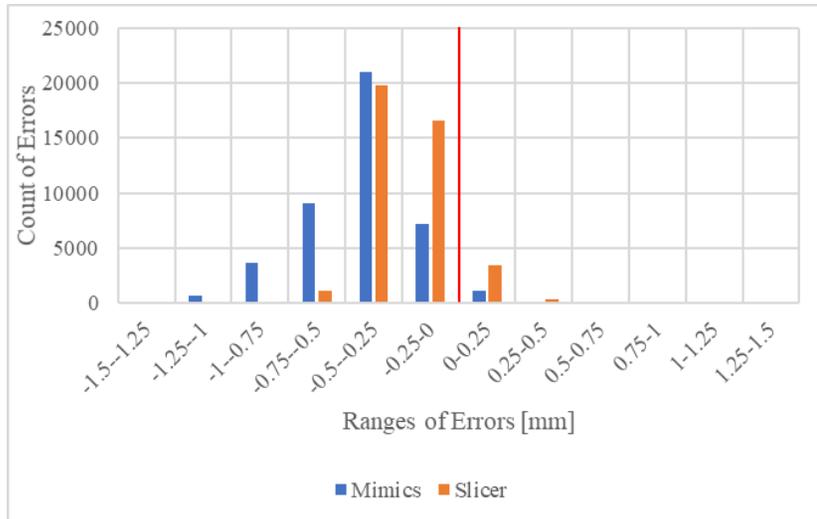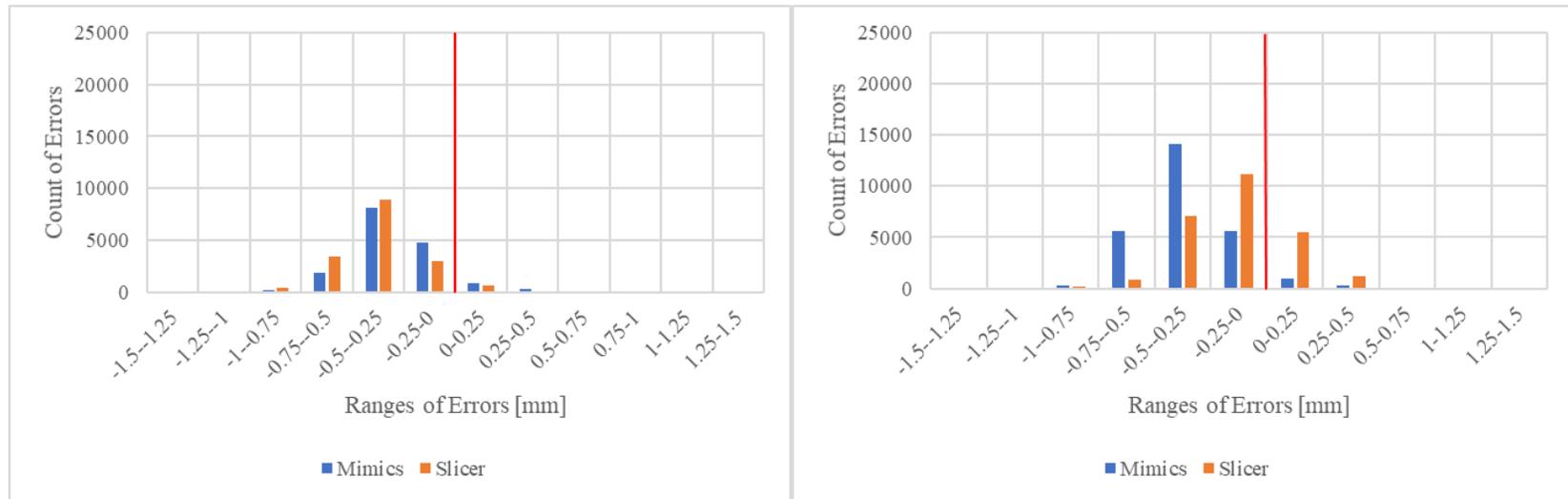
Figure 3.2. Relative error between micro-CT and both 4DCT kinematic scans made in two software: Mimics (blue) and Slicer (orange). Comparisons were made for four bones: radius (A, top left), scaphoid (B, top right), lunate (C, bottom left), and capitate (D, bottom right).

These frequency plots illustrate that the micro-CT model was always smaller than the 4DCT kinematic models (the frequency plots are skewed negative), which is reasonable due to the partial volume effect[8]. Partial volume effect is where the volume only fills a portion of the voxel; therefore, the model tends to be overestimated. In this case, the voxels are larger in the 4DCT scans compared to the micro-CT scans because they are lower resolution and so, the 4DCT models are always slightly overestimated compared to the higher resolution micro-CT models. In addition, smaller bones have less error than larger bones because larger bones have more surface area for the surface reconstruction to be altered from one model to the next.

The contour maps used to calculate the above histograms (Figure 3.2) are included in Table 3.2.

Table 3.2. Contour maps to illustrate the relative error between the micro-CT models and those made in Mimics and Slicer.

Bone	Radius	Scaphoid	Lunate	Capitate
Micro-CT to Mimics				
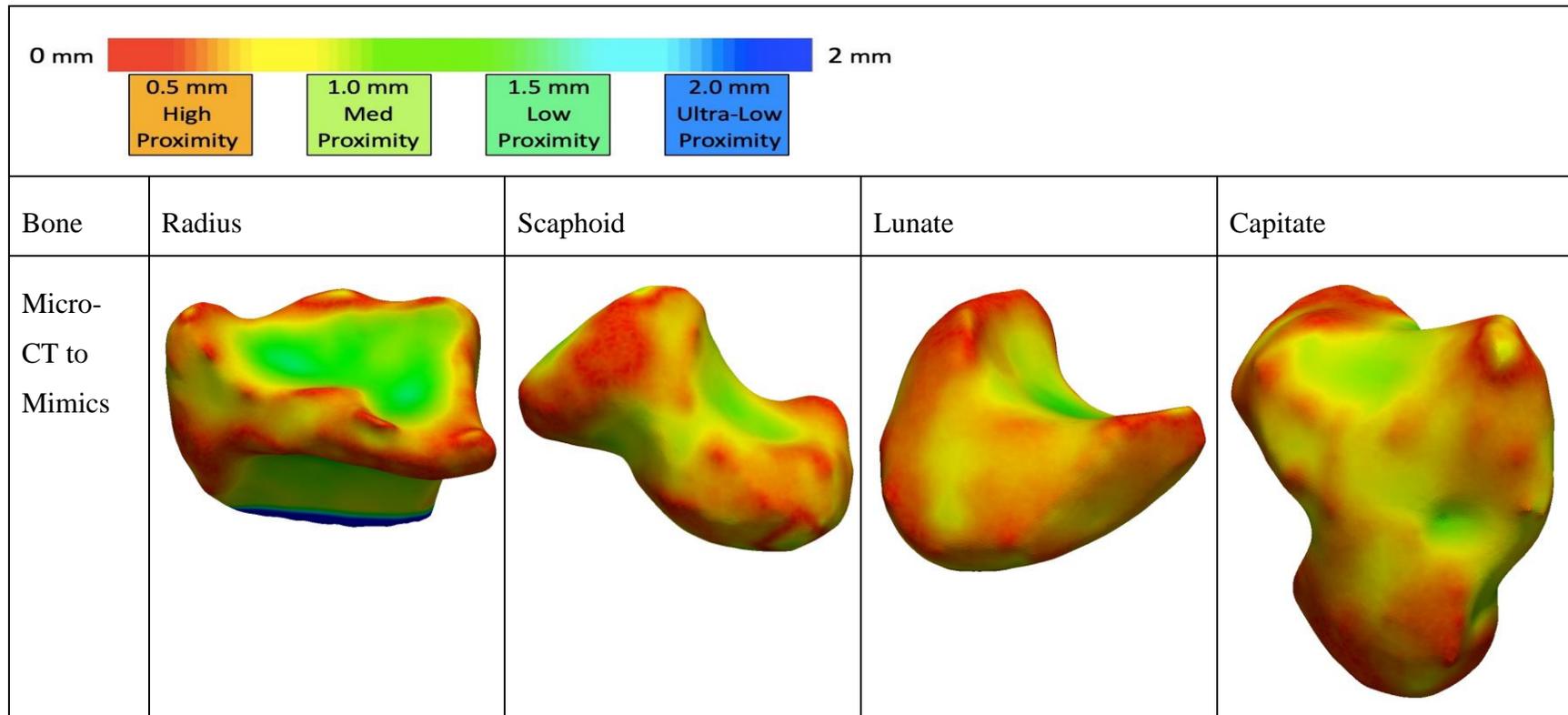
| Micro-CT to Slicer | | | | |
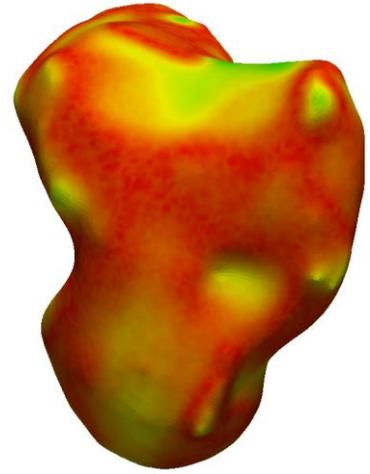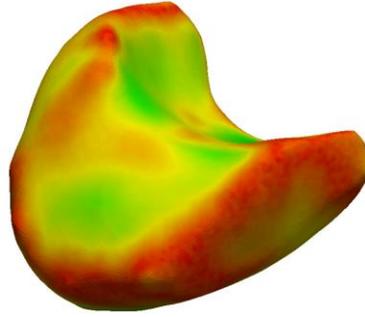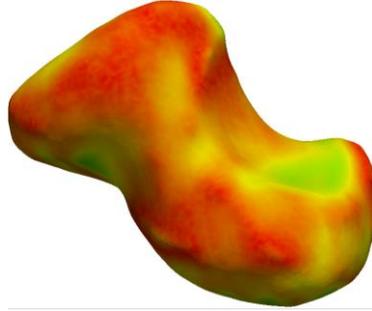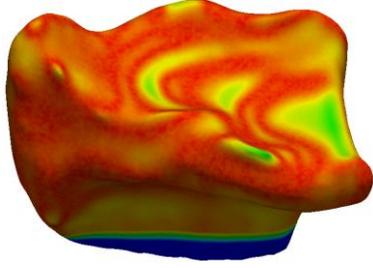
These contour maps show that there are some regional differences. In general, the largest differences (green) are in the cavities of the bones (ex. the scaphoid and lunate fossae on the radius, and the concave articular facets on the scaphoid and lunate).

3.4.2   Inter- and Intra-Rater Reliability

The errors from the inter-rater experiment are summarized in Table 3.3.

Table 3.3. Inter-rater reliability errors for four bones.

Inter-rater				
Bone	**Radius**	**Scaphoid**	**Lunate**	**Capitate**
Errors [mm ± 1 SD]	0.3± 0.01	0.3± 0.01	0.3± 0.01	0.3± 0.06

The inter-rater reliability was less than or equal to 0.36 mm. The errors from the intra-rater experiment are summarized in Table 3.4.

Table 3.4. Intra-rater reliability errors for four bones.

Intra-rater	Bone and associated error [mm ± 1 SD]			
Participant Number	**Radius**	**Scaphoid**	**Lunate**	**Capitate**
70	0.1± 0.00	0.1± 0.01	0.1± 0.01	0.1± 0.00
79	0.1± 0.03	0.1± 0.01	0.2± 0.08	0.2± 0.06

The intra-rater reliability was less than or equal to 0.26 mm.

3.5   Discussion

The accuracy of making bone models from CT scans depends on the resolution of the scan, the software used to make the models, and may be affected by inter- and intra-rater

reliabilities. Our micro-CT criterion validation confirmed our hypothesis that 4DCT kinematic scans can be reliably used to make bone models of the wrist because the error between the imaging modalities was low using two separate software (less than or equal to 0.4 mm). Comparing Mimics to Slicer proved our hypothesis that these software can be used interchangeably because there was a low error between the two (less than or equal to 0.3 mm). Lastly, Mimics is a precise software because the inter- and intra-rater reliabilities were high (error of less than or equal to 0.36 mm for inter-rater reliability and 0.26 mm for intra-rater reliability), confirming our hypothesis.

Criterion validations, wherein a new technique is validated by comparing it to a gold standard, is important in determining the accuracy of new protocols. Lalone et al. validated their CT protocol by comparing it to a ground-truth digitization protocol using optical trackers in eight cadaveric elbows[4]. They found that the overall mean error was less than 0.4 mm in the cortical region and 0.3 mm in the subchondral region. Our study focused on cortical bone and agreed closely with Lalone et al.'s findings. Zhao et al. validated a 4DCT protocol by comparing the results obtained from 4DCT to those obtained by using fiducial beads[9]. Their mean translational errors were less than or equal to 0.298 ± 0.380 mm, whereas our errors were less than or equal to 0.4 mm and thus concur with Zhao et al.'s findings. Thus, the proposed 4DCT protocol for making wrist bone models is accurate when compared to the gold-standard of micro-CT. The kinematic scans were analyzed because those are the scans that were analyzed in Chapter 2; to accurately validate those models, kinematic scans had to be used because kinematic scans have a larger slice thickness (1.25 mm) than static scans (0.625 mm) and different errors are introduced during motion. Partial volume effect is one such error that may occur due to changes in slice thickness because a larger slice thickness means the volume would only fill part of that voxel, which is why the kinematic scans were always larger than the micro-CT scans. Lastly, interscan motion blur may account for some error in the kinematic scans, which is why it is important to validate them. For more information on interscan motion blur, refer to Appendix A.

The software used to make the bone models from 4DCT scans may affect the accuracy of the models. Slicer and Mimics are two software that import DICOM files from which bone

models can be made. Virzi et al. analyzed 14 software, 12 of which were free and included 3D Slicer[10]. They concluded that 3D Slicer offered the largest number of segmentation tools and it scored high for 3D visualization. Han et al. elaborated on Virzi et al.'s work but comparing 3D modelling in Slicer to MRI fast imaging in their ability to detect the neurovascular relationship (NVR) in 40 patients with trigeminal neuralgia[11]. In Han et al.'s study, they found that 3D Slicer was significantly more accurate at detecting NVR, with a specificity and sensitivity of 100% each. Both studies show the use of 3D Slicer to be accurate, to which our findings agree. There was low mean error in this study between Slicer and Mimics (less than or equal to 0.3 mm) indicating that both software can be used interchangeable to create wrist models from 4DCT scans. In addition, the errors between the micro-CT to Slicer and the micro-CT to Mimics are comparable, therefore both software can be used interchangeably.

Inter- and intra-rater reliability is an important measure to consider for any new protocol. Mat Jais et al. found high inter- (90.3-95.4%) and intra-rater reliability (85-95.5%) in their study examining carpal hysteresis in a cadaveric wrist during radioulnar deviation using a proposed 4DCT approach[12]. Our results agree and show a low error (less than or equal to 0.36 mm for inter-rater reliability, less than or equal to 0.26 mm for intra-rater reliability), indicative of high inter- and intra-rater reliabilities and high precision in Mimics.

3.6   Conclusions

The resolution of kinematic 4DCT scans is sufficient for making wrist bone models and drawing quantitative measurements, such as centroid translation in Chapter 2. These models can be made in Slicer or Mimics software with nearly identical results. In addition, the inter- and intra-rater reliabilities of Mimics, and associated precision in model-making, are high. These findings validate the proposed 4DCT scanning protocol in Chapter 2. These findings indicate that the future work proposed in chapter 2, using 4DCT to measure wrist kinematics in injured populations, is feasible with this 4DCT wrist scanning protocol.

3.7 References

1.   Beckett RG, Conlogue GJ. Advances in Paleoimaging. Boca Raton, London, New York: CRC Press; 2020. doi:10.4324/9781315203089

2.   Anas EMA, Rasoulian A, Seitel A, et al. Automatic Segmentation of Wrist Bones in CT Using a Statistical Wrist Shape + Pose Model. IEEE Trans Med Imaging. 2016;35(8):1789-1801. doi:10.1109/TMI.2016.2529500

3.   Robinson S, Straatman L, Lee T-Y, Suh N, Lalone E. Evaluation of Four-Dimensional Computed Tomography as a Technique for Quantifying Carpal Motion. J Biomech Eng. 2021;143(6). doi: https://doi.org/10.1115/1.4050129

4.   Lalone EA, Willing RT, Shannon HL, King GJW, Johnson JA. Accuracy assessment of 3D bone reconstructions using CT: An intro comparison. Med Eng Phys. 2015;37(8):729-738. doi:10.1016/j.medengphy.2015.04.010

5.   Dobbe JGG, de Roo MGA, Visschers JC, Strackee SD, Streekstra GJ. Evaluation of a Quantitative Method for Carpal Motion Analysis Using Clinical 3-D and 4-D CT Protocols. IEEE Trans Med Imaging. 2019;38(4):1048-1057. doi:10.1109/TMI.2018.2877503

6.   Besl PJ, McKay ND. A method for registration of 3-D shapes. IEEE Trans Pattern Anal Mach Intell. 1992;14(2):239-256. doi:10.1109/34.121791

7.   Lalone EA, Mcdonald CP, Ferreira LM, Peters TM, King GW, Johnson JA. Development of an image-based technique to examine joint congruency at the elbow. Comput Methods Biomech Biomed Engin. 2013;16(3):280-290. doi:10.1080/10255842.2011.617006

8.   Liu Y, Wang L, Su Y, et al. CTXA hip: the effect of partial volume correction on volumetric bone mineral density data for cortical and trabecular bone. Arch Osteoporos. 2020;15(1). doi:10.1007/s11657-020-00721-8

9.   Zhao K, Breighner R, Holmes D 3rd, Leng S, McCollough C, An K-N. A technique for quantifying wrist motion using four-dimensional computed tomography: approach and validation. J Biomech Eng. 2015;137(7). doi:10.1115/1.4030405

10.   Virzì A, Muller CO, Marret JB, et al. Comprehensive Review of 3D Segmentation Software Tools for MRI Usable for Pelvic Surgery Planning. J Digit Imaging. 2020;33(1):99-110. doi:10.1007/s10278-019-00239-7

11.   Han K wei, Zhang D feng, Chen J gang, Hou L jun. Presurgical visualization of the neurovascular relationship in trigeminal neuralgia with 3D modeling using free Slicer software. Acta Neurochir (Wien). 2016;158(11):2195-2201. doi:10.1007/s00701-016-2936-8

12.   Mat Jais IS, Liu X, An KN, Tay SC. A method for carpal motion hysteresis quantification in 4-dimensional imaging of the wrist. Med Eng Phys. 2014;36(12):1699-1703. doi:10.1016/j.medengphy.2014.08.011

Chapter 4

4 The Effects of SLIL Volar Tears on Carpal Kinematics

The application of four-dimensional computed tomography (4DCT) to measure in vivo carpal kinematics in individuals with scapholunate interosseous ligament (SLIL) tears has yet to be explored. The intent of this chapter was to employ 4DCT as a tool for detecting subtle bone movement differences due to three types of SLIL tears: volar, dorsal, and combined. To do this, 4DCT was used to measure carpal rotation about the helical axes and joint surface area. The secondary objective of this study was to determine if volar tears, which are currently underrepresented clinically and in the literature, warrant further investigation.

4.1 Introduction

Scapholunate interosseous ligament (SLIL) tears are the most frequent ligamentous wrist injury and the most common etiology of wrist instability[1-4]. These injuries cause pain and impaired function[2], leading to altered wrist mechanics. These tears affect working age individuals (39 years old on average) and time from injury to surgery is 19 months, on average[5]. If untreated, scapholunate advanced collapse (SLAC) and a predictable pattern of degenerative arthritis throughout the carpus frequently occurs[1,6-8]. The intrinsic part of the SLIL has volar, dorsal, and central components, wherein the dorsal part is thickest, strongest, and considered most important biomechanically[1,4,9,10], and the volar part is considerably thinner, contributing to rotational stability of the scapholunate joint[4,10]. Any one of these components can be injured in isolation or in combination. There are several recommended surgical approaches to repair isolated dorsal tears (DT) and combined tears (VDT)[4,10,11]; however, isolated volar tears (VT) are largely ignored in SLIL studies and have no recommended surgical technique[1,4,10,12]. Even in a study that proposed a method for repairing VTs, the indication for the technique was a VDT[12]. Despite different tear types leading to different treatments, the effects caused by each type of SLIL tear on *in vivo* carpal mechanics are not known.

Quasi-static measurements of carpal motion can be obtained from three-dimensional (3D) computed tomography, wherein 3D videos are made by extrapolating motion between static positions[13]; however, the quasi-static nature of this modality renders it unable to measure true dynamic carpal motion. Four-dimensional computed tomography (4DCT; 3D + time) is a novel method for detecting subtle abnormal bone movements, whereby 3D bone scans are acquired while the bones are in continuous motion, resulting in 3D kinematic frames of motion as well as 4D movies of the bones in motion[14]. Thus, 4DCT can increase our understanding of carpal motion and determine how wrist injuries affect said motion[15].

The objective of this pilot study was to employ a novel 4DCT technique to examine the differences in carpal kinematics and arthrokinematics between uninjured individuals and those with SLIL tears, specifically a VT, a DT, and a VDT. This technique was used to examine the motion of the scaphoid and lunate during FE and RUD. Based on the literature, we hypothesized that there are biomechanical differences in the VT from the uninjured case and from the other tears. In the presence of a VT, the strength of the dorsal ligament may alter the position of the scaphoid and lunate and may cause abnormal carpal motion. We hypothesized that larger effects on carpal motion would result from a VDT; with no piece of the SLIL intact, the scaphoid and lunate would separate from one another, which would have negative effects on carpal motion. This work is important for informing the management of SLIL tears and resulting patient outcomes, thus providing insight into which tears may require surgical repair. In addition, this pilot study will determine if 4DCT is an appropriate tool for analyzing injured wrist motion and whether VTs are worth investigating.

4.2   Materials and Methods

4.2.1   Study Protocol

Participants were recruited from a tertiary academic upper extremity orthopaedic centre. Inclusion criteria were participants over 18 years of age either with no history of wrist injury or with MRI proven SLIL tears. Those with MRI proven SLIL tears had no other

ligamentous injuries. The study protocol was approved by the ethics review board of our institute and hospital, and complied with the Declaration of Helsinki of 1975, revised 2000.

Following recruitment, participants (uninjured cohort, n=3, 2 male, average age 28 years ± 7 years; injured cohort, n=3, 2 male, average age 38.7 years ± 23 years) underwent unilateral CT scanning of the dominant hand (n=5 right-handed, n=1 left-handed), which consisted of a localizer scan (to determine wrist joint location), a neutral frame, and two kinematic scans (FE and RUD). This protocol has been previously described[16] but will be described here in short. The participants were positioned on their stomach on the CT scanner bed with their dominant arm outstretched and asked to perform unconstrained FE and RUD. Video demonstrations of these motions were provided prior to testing to standardize angular speed. During testing, participants wore protective equipment, which included a body lead apron, thyroid shield, and protective eyeglasses.

4.2.2   4DCT Imaging Technique

A CT scanner (Revolution CT Scanner, GE Healthcare, Waukesha, Wisconsin, USA) was used to acquire kinematic scans of the distal forearm and hand using a previously described routine wrist scan protocol (80 kV, 125 effective mA, 0.35 s rotation time, axial)[16]. For the purposes of this study, one pass of each motion was performed: FE began in extreme extension and moved to extreme flexion, while RUD began in extreme radial deviation and moved to extreme ulnar deviation. The total scan time was 24.5 s and participants performed 2-3 complete passes of motion; the data was automatically separated into bins of data comprised of 25 frames and 8.75 s of motion. The angular speed of RUD was 9 ± 4°/s and FE was approximately 13 ± 2°/s.

4.2.3   3D Reconstruction

Volumetric images were rendered in 3D (output as digital imaging and communications in medicine (DICOM) files) and displayed in a cine movie loop to visualize the joint articulating surfaces in motion. For the purposes of this study, the frames of interest were every 10° in a range of 50° extension to 50° flexion for FE (11 frames total) and a range of 20° of radial deviation to 20° of ulnar deviation for RUD (5 frames total). To determine which frames were those of interest, 3D-Slicer software (version 4.11.0, an open-source

software platform for medical image processing available at https://www.slicer.org) was used to visualize each frame of motion. To create the bone models (radius, scaphoid, lunate, and capitate) of each frame of interest, a semi-automatic algorithm (Mimics 22.0 software, Materialise, Belgium; 3D-Slicer 4.11.0) was used as previously described[16]. Briefly, the segmentation threshold was manually selected and then each slice was manually edited according to the appropriate bone geometry[17]. Post-processing measures were exacted on the bone models to improve surface smoothness and bone shape, as previously described[16]. This method of reconstruction was validated previously (Chapter 3) where 3D reconstructions were created and compared to a ground truth micro-CT (average error <0.4 mm).

4.2.4　Participant Demographics

The mechanism of injury for each injured participant was recorded. Each participant completed the Patient Rated Wrist Evaluation (PRWE), a patient reported outcome that measures pain and disability following wrist injury[19]. Planar radiographs were used to calculate the Kellgren and Lawrence (KL) score for the injured cohort, as a measure of the severity of degenerative changes in the wrist indicative of arthritis[18]. Ranges of motion were determined from goniometric measurements. The radiographs of the SLIL tear participants were also used to measure the scapholunate (SL) gap and SL angle; measurements were taken by an orthopaedic surgeon (N.S.). Coronal views from the uninjured CT scans (neutral position) were used to measure their SL gaps. The uninjured participants did not have radiographs and as such, no SL angles could be measured. These measures were used to report demographic information of our participants and to provide an indication of wrist function and pain.

4.3　Data Analysis

4.3.1　Scaphoid and Lunate Rotation

The transformation matrices of the bones and frames of interest were calculated using the iterative closest point (ICP) surface-based registration algorithm of the neutral bone models (0° FE and 0° RUD) to the kinematic bone models (3D-Slicer; Python)[20]. To improve alignment, an initial paired-point registration was performed if initial ICP registration was

insufficient[16]. The accuracy of the ICP registration algorithm, with an end condition of surface alignment ≤ 0.001 mm root mean square or a maximum of 100 iterations, had been previously described and is less than 0.4 mm[17].

A custom Matlab (The MathWorks Inc., Natick, MA) script calculated the helical axes of the scaphoid, lunate and capitate relative to the neutral radius. Firstly, we computed the local coordinate system (LCS) in the radius for each participant according to the International Society of Biomechanics (ISB) standards (Figure 1).
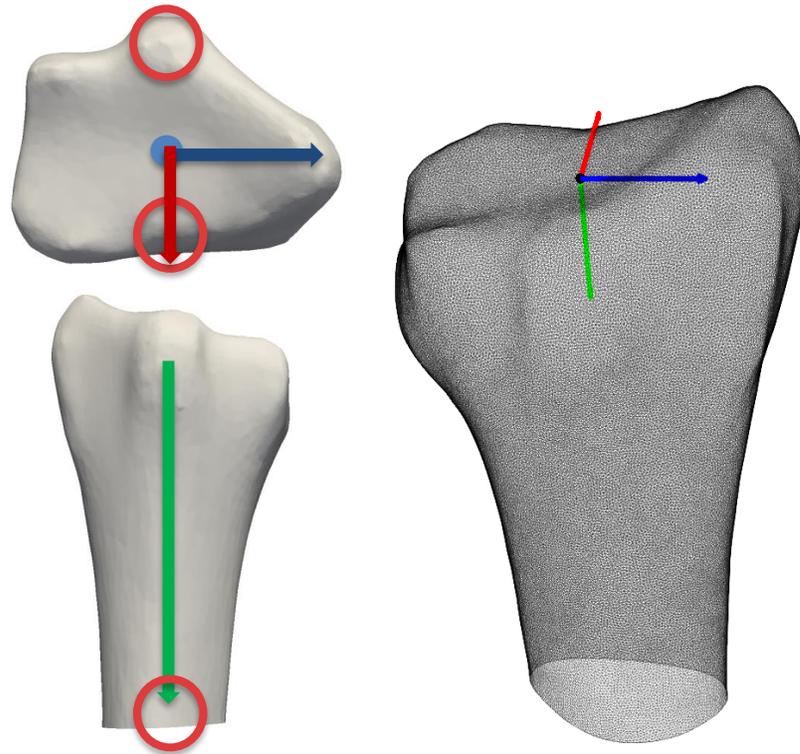
Figure 4.1: Local coordinate system (LCS) in the radius. The axes (+/-) are as follows: x-axis (red, volar/dorsal), y-axis (green, proximal/distal), and z-axis (blue, radial/ulnar). On the left, the red circles represent the anatomical points used to create the LCS (from top to bottom: dorsal point, volar point, proximal point). The blue dot is the origin of the LCS.

The anatomical landmarks used to create the LCS were a volar and distal point on the ridge between the radioscaphoid and SL fossae, and a proximal point on the radial shaft in line

with the dorsal point. These landmarks were selected for their distinct morphological shapes that lead to high repeatability in selection across participants. In the LCS, the x-axis described radioulnar deviation and pointed volar, the y-axis described pronation-supination and pointed proximal, and the z-axis described flexion-extension and pointed radial. The origin of the LCS was at the centre of the radial surface between the scaphoid and lunate fossae. Rigid body transformations described the motion of each carpal bone relative to the neutral radius in the LCS, which standardized measurements across participants. The following transformation matrix math describes the calculations performed for the scaphoid, lunate, and capitate to obtain a transformation matrix from neutral (pose 1) to all other kinematic poses (pose 2); the transformation matrix describes the subscript relative to the superscript, wherein "kin" stands for "kinematic".

Equation 4.1. Matrix math to obtain the transformation matrix of the kinematic bone (scaphoid, lunate, or capitate) relative to the kinematic radius

$$T_{kin}^{radius\ kin} = inv(T_{radius\ kin}^{static}) \times T_{kin}^{static}$$

Equation 4.2. Matrix math to obtain the transformation matrix of the kinematic bone (scaphoid, lunate, or capitate) relative to the LCS.

$$T_{kin}^{LCS} = inv(T_{LCS}^{radius\ kin}) \times T_{kin}^{radius\ kin}$$

Equation 4.3. Matrix math to obtain the transformation matrix of the kinematic bone (scaphoid, lunate, or capitate) in the kinematic position relative to the same bone in the neutral position.

$$T_{pose2}^{pose1} = T_{kin\ pose2}^{LCS} \times inv(T_{kin\ pose1}^{LCS})$$

Then, helical axes were calculated (from the transformation matrix from pose 1 to pose 2) that describe 3D motion as the rotation and translation of a rigid body about and along a single axis[13]. The rotation of each bone about the helical axis was used to describe carpal rotation. Motion between the third metacarpal and capitate is considered negligible and as such, radiocapitate motion was used to represent global wrist motion[13]. The rotation (°) of the three uninjured participants were used to determine a range of normal scaphoid and

lunate rotation during FE and RUD; the uninjured range was defined as the 95% confidence interval (with an alpha of 0.05) about the uninjured average. To determine the 95% confidence interval, the standard deviation of the three uninjured individuals was used in the Microsoft Excel formula for a normal distribution of the confidence interval. The rotations from the injured participants were compared to these ranges.

4.3.2   Joint Surface Area

To illustrate overall joint congruency, interbone distances were calculated of the radioscaphoid and SL joints for all frames of interest in FE and RUD using a previously described Python algorithm to illustrate overall joint congruency[17]. The joint surface area (JSA) of the subchondral bone is a CT-derived measure of joint contact area and was determined for a proximity of less than or equal to 2.0 mm, as previously described[16]. This threshold was chosen because it approximately considered the whole articular surface of the scaphoid's surrounding joints and was previously used in the scaphoid, lunate fossae, and interfossal ridge[21]. For visualization, the JSAs were visualized on an iso-contoured proximity map, with colors corresponding to a distance; a scale from red (0 mm) to blue (2 mm) illustrated the JSA while all distances greater than 2 mm were dark blue[17]. To compare between participants, the JSA (in mm^2) was normalized by dividing it by the participant's total articular surface to get JSA as a percent; the articular surface of the radioscaphoid joint was the area of the scaphoid fossa on the radius, and that of the SL joint was the semilunar facet on the lunate. The JSAs (%) of the three uninjured participants were used to determine a range of normal joint contact during FE and RUD; the uninjured range was defined as the 95% confidence interval (with an alpha of 0.05) about the uninjured average calculated in Excel. The JSAs from the injured participants were compared to these ranges.

4.3.3   Validation and Reliability

To determine the concurrent validity of the proposed helical axes technique to measure bone rotation, it was compared to a well-established method: Euler angles. The same transformation matrix calculated by Equation 4.3 was used in the helical axes and Euler angle methods. The data used to compare these methods were the rotations from the three uninjured participants in both motions, FE and RUD. The error between the measurements

was defined as the average and standard deviation of the difference between the Euler angle and the helical axis angle for each uninjured participant in each position (excluding neutral; thus, 30 data points for FE and 12 for RUD).

In addition, inter- and intra-rater reliabilities were calculated. Inter-rater reliability was determined by comparing rotation results in two positions (20° of radial deviation and 20° of ulnar deviation) from models made by two raters. Intra-rater reliability was determined by comparing rotation results in those two positions from models made twice by the same rater. High reliability would indicate high precision in the helical axes technique due to high precision in model making and registration.

4.4   Results

4.4.1   Participant Demographics

The mechanisms of injury for all participants include a traumatic event associated with a fall (Table 1). Although injured participants had ranges of motion comparable to those of the uninjured cohort, the injured cohort all had a PRWE score greater than 15[22,23]. The VDT had a KL score of 2, indicating a presence of osteophytes and narrowing joint space. The VT's SL gap was the same as those of the uninjured participants, while that of the DT and VDT show SL joint widening indicative of an SLIL tear. The radiographic SL angles were greater than the established normal range (30° to 60°)[4] in the DT and VDT, but not in the VT.

Table 4.1: Participant demographics.

Participant	Age	Sex	Injury	PRWE	KL Score	Range of Motion [°]	SL gap [mm]	SL angle [°]
1	27	Male	Healthy	2	N/A	135 FE, 55 RUD	2	N/A
2	22	Male	Healthy	0	N/A	117 FE, 60 RUD	2	N/A
3	36	Female	Healthy	0	N/A	162 FE, 77 RUD	2	N/A
4	17	Male	Isolated volar SLIL tear having suffered a distal radius fracture two years previously.	34.5	0	163 FE, 90 RUD	2	40

			Patient does exhibit midcarpal clunk during RUD.					
5	37	Female	MRI dorsal SLIL tear, sprained volar SLIL band. Patient suffered an injury to wrist several years ago and then suffered a slip and fall that exacerbated pain that is aggravated with motion.	34	0	162 FE, 94 RUD	3	80
6	62	Male	Combined tear of the volar and dorsal SLIL band. Patient suffered injury one year ago and now present with debilitating pain.	38.5	2	115 FE, 63 RUD	6.5	68

4.4.2   Scaphoid and Lunate Rotation

For FE (Figure 2), the scaphoid of each tear case rotated similarly to, if not within, the uninjured range, while the lunate showed more abnormal rotation. The DT and VDT lunates followed the uninjured range in flexion but were more flexed in extension. Conversely, the VT lunate followed the uninjured range in extension but flexed more in flexion.
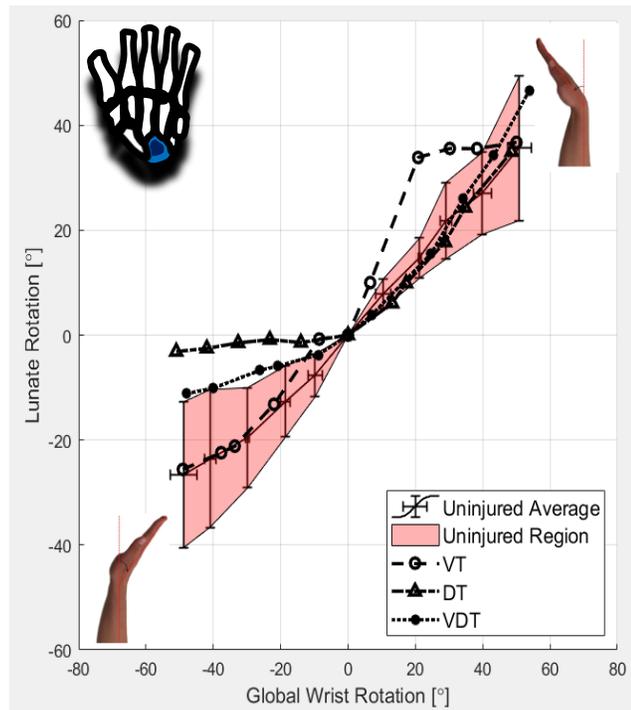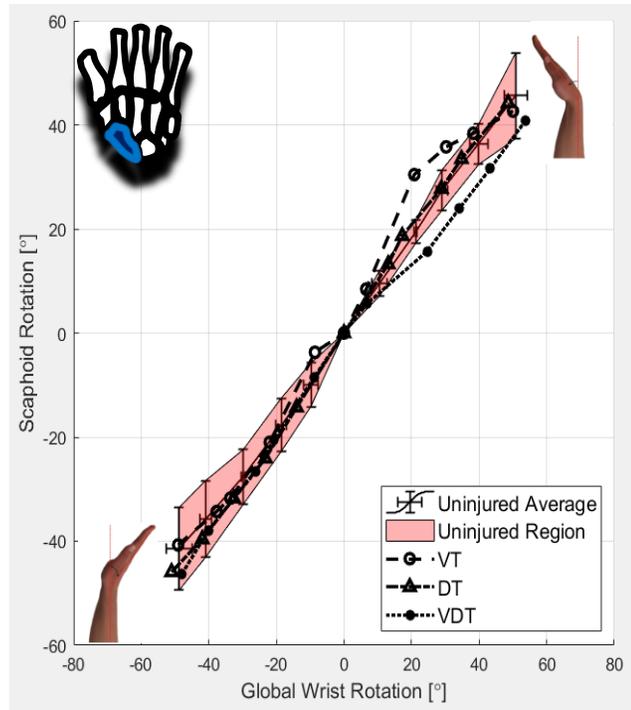
Figure 4.2: Helical axes angles of scaphoid (A) and lunate (B) during FE; the hands are right wrists, radial views. Global wrist angle is the angle of the capitate relative to the radius. The shaded region is the 95% confidence interval of the healthy data.

Any points outside of this range indicate abnormal rotation. Injured participants include the volar tear (VT), dorsal tear (DT) and combined tear (VDT).

For the scaphoid in RUD (Figure 3A), the DT and VDT closely followed the uninjured trend, except the DT flexed more in 20° of radial deviation. The VT scaphoid, however, was more extended in ulnar deviation. The lunate (Figure 3B) exhibited less overall rotation in the DT and VDT in RUD. The VT lunate rotation was the most abnormal, extending more in 20° ulnar deviation and all of radial deviation.
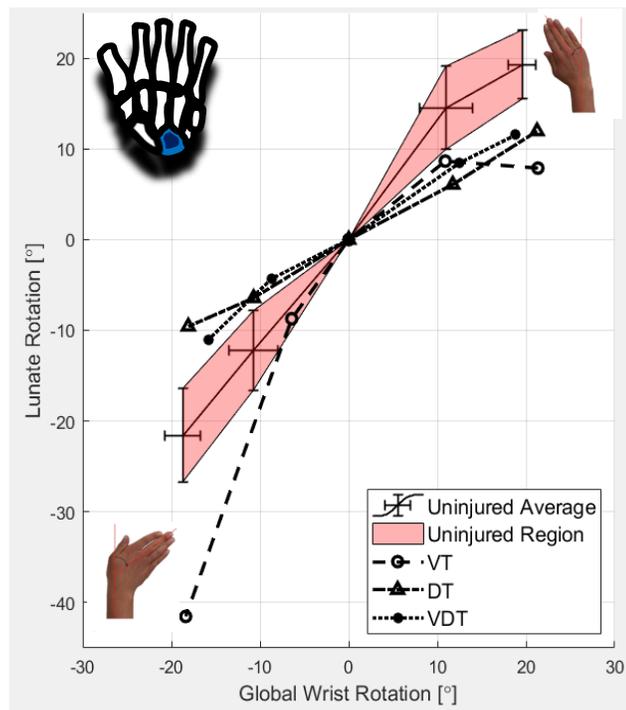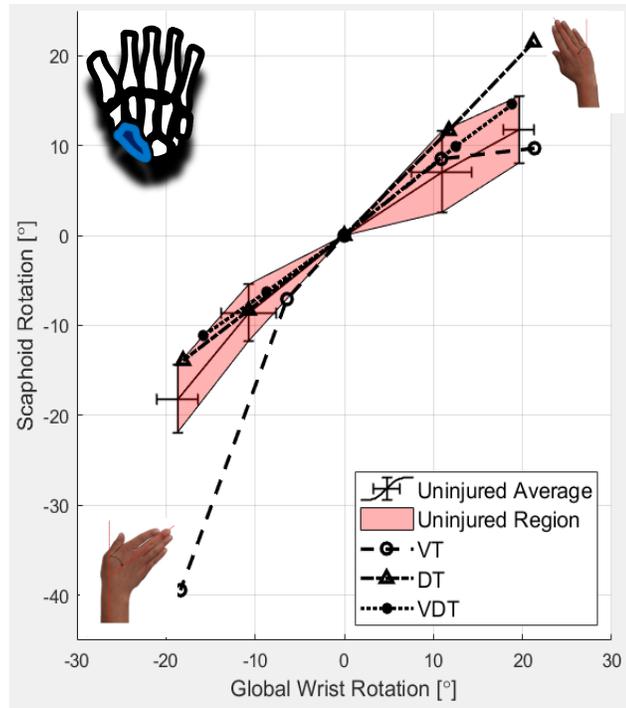
Figure 4.3: Helical axes angles of scaphoid (A) and lunate (B) during RUD; the hands are right wrists, dorsal views. Global wrist angle is the angle of the capitate relative to the radius. The shaded region is the 95% confidence interval of the

healthy data. Any points outside of this range indicate abnormal rotation. Injured participants include the volar tear (VT), dorsal tear (DT) and combined tear (VDT).

Overall, the lunate exhibited more abnormal rotation in each tear case in both motions compared to the scaphoid. The VDT and DT participants' rotations were similar to one another and tended to follow the uninjured range trends. The VT rotation was not similar to the other two tears, nor did it follow the uninjured trends (except for the scaphoid in FE).

4.4.3   Joint Surface Area

Representative proximity maps of the radioscaphoid and SL joints for the participants in 20° of radial deviation (Figure 4, left and right columns respectively) illustrate that JSA was altered with each SLIL tear. The normalized JSAs (Figures 5 and 6) show that JSA changed as the wrist moved through FE and RUD.
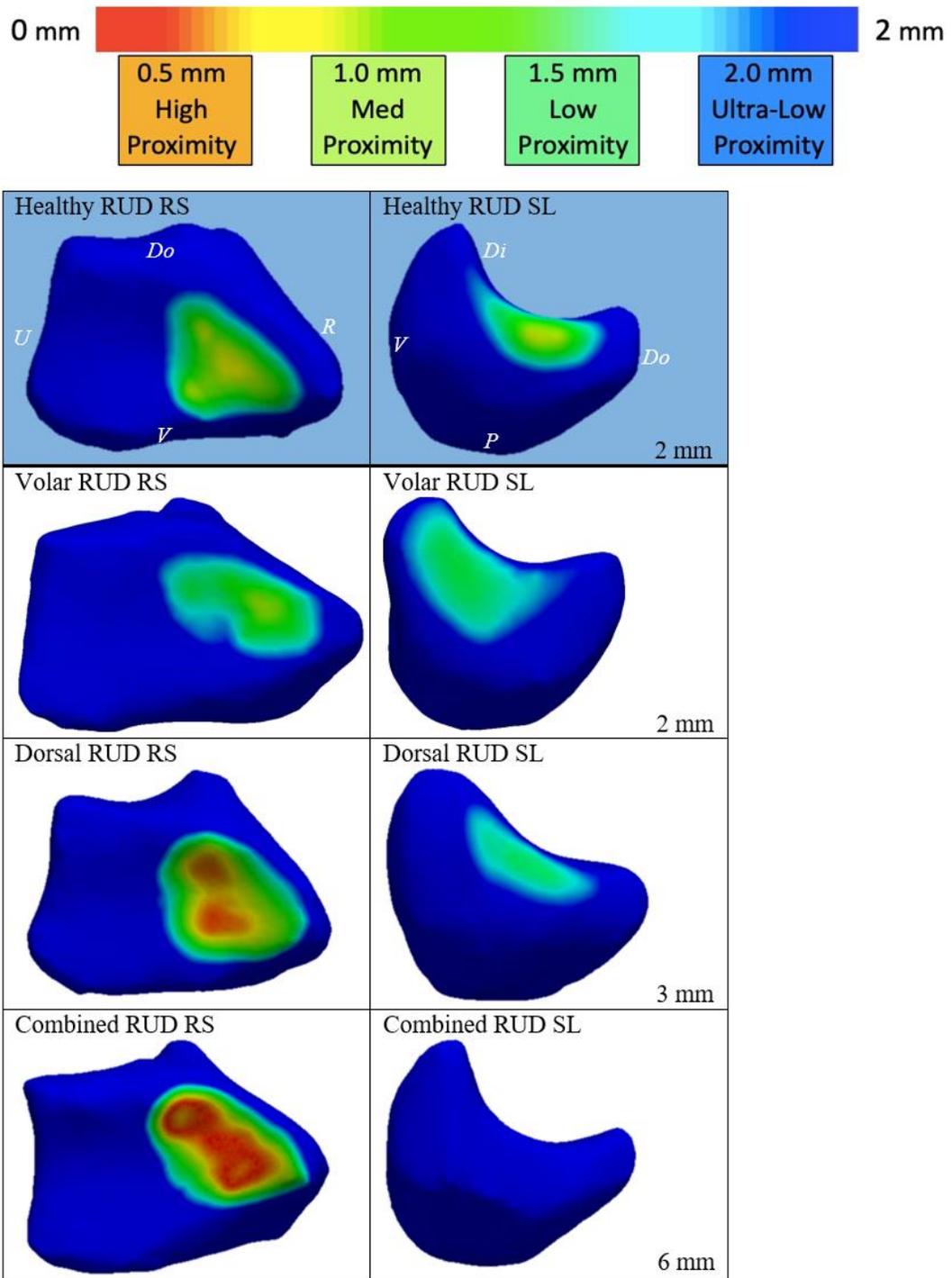
Figure 4.4: JSA colour maps in the RS and SL joints (left and right columns respectively) in 20° radial deviation. Representative data from one participant was used to represent the healthy data. Anatomical directions are labelled as follows:

dorsal (Do)/volar (V), proximal (P)/distal (Di), ulnar (U)/radial (R). SL gap is shown in the bottom right corner of the SL joint column.

In FE, Figure 5A shows the JSA in the radioscaphoid joint increased from extension to neutral and then decreased with increasing flexion; the VT and VDT JSAs generally followed this trend. Conversely, the DT JSA changed less between consecutive positions and was often greater than the uninjured range. In the SL joint (Figure 5B), the JSA increased with increasing flexion; the DT also followed this trend in flexion. However, the VT did not follow the same trend and showed greater JSA in extension, neutral and 10° of flexion. The VDT had 0% JSA throughout motion.
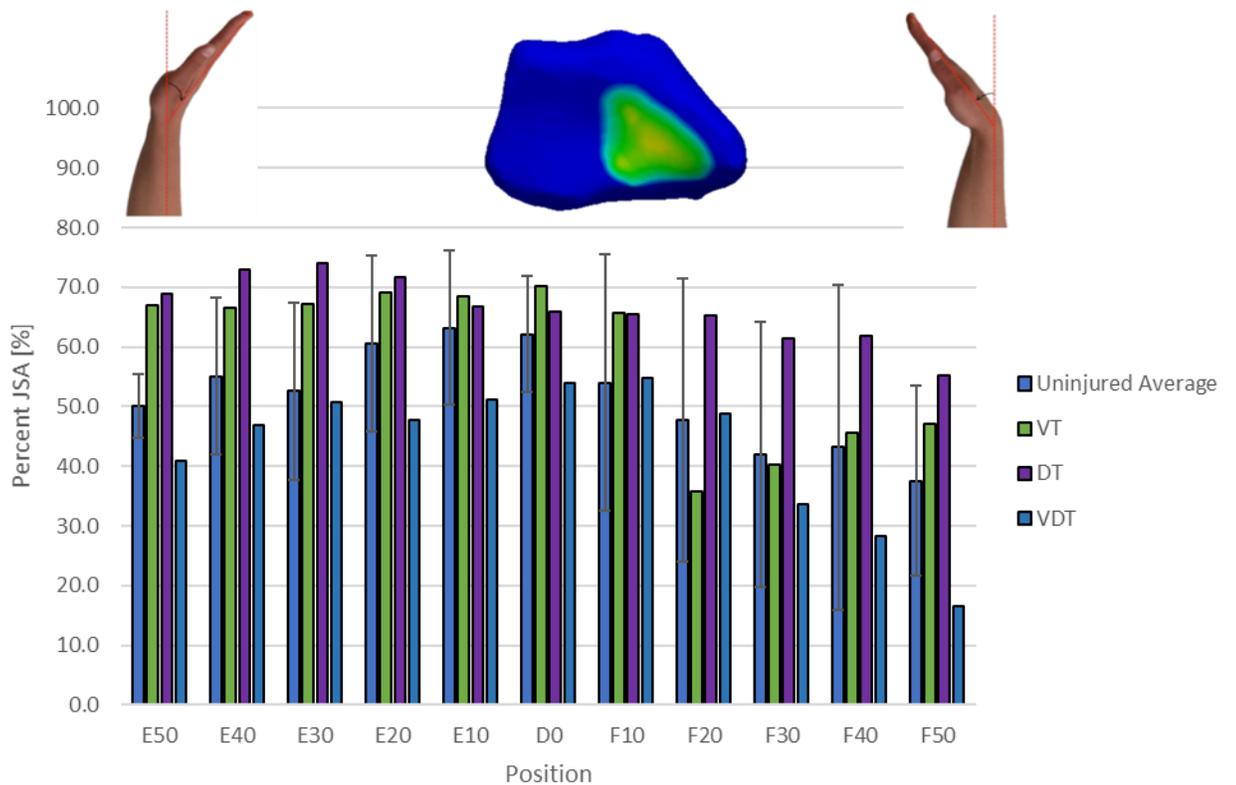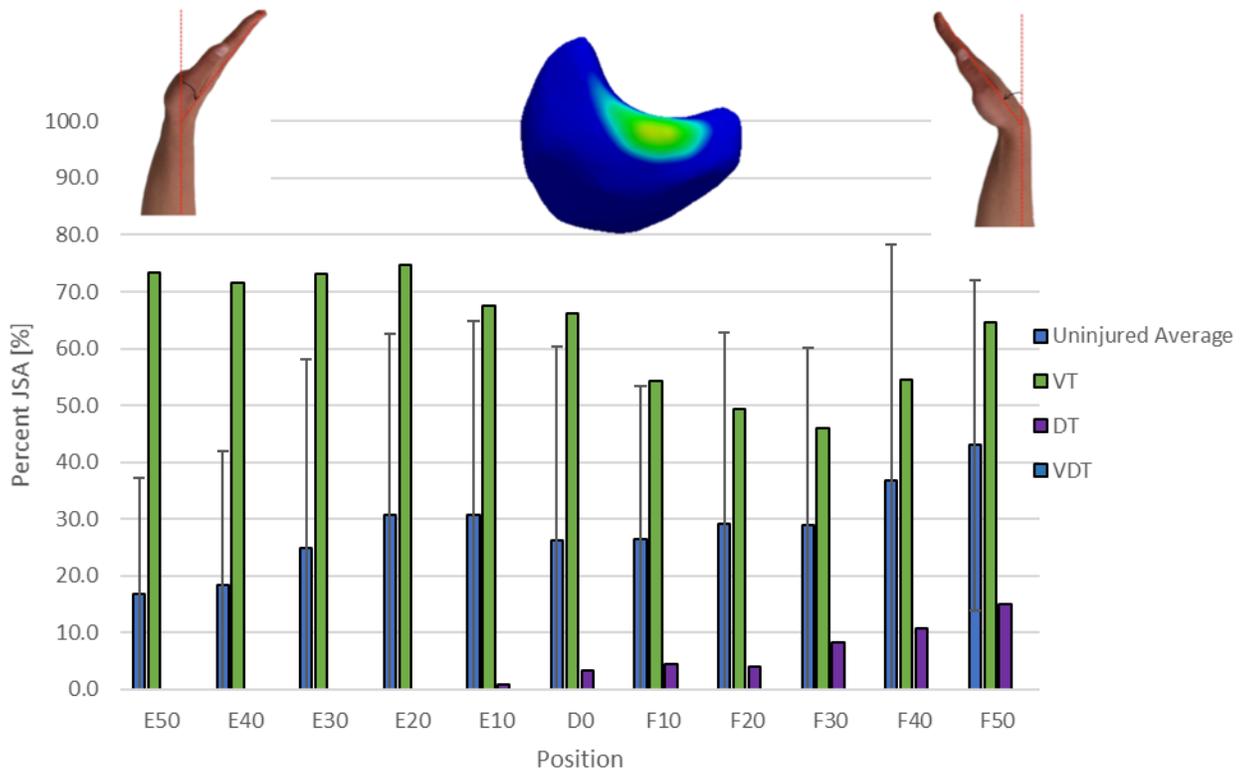
Figure 4.5: Percent JSA of the radioscaphoid (A) and scapholunate (B) joints during FE; the hands are right wrists, radial views. Positions are named E (extension) or F (flexion) followed by the degree value (ex. E50 is 50° of extension). The error bars of the healthy average data represent the 95% confidence interval. Any bars outside of this range indicate abnormal JSA. Injured participants include the volar tear (VT), dorsal tear (DT) and combined tear (VDT).

Figure 6A shows that the JSA at the radioscaphoid joint decreased with increasing ulnar deviation. This trend was consistent for the DT and VDT, even though their JSAs were larger in some positions. However, the JSA for the VT was outside the uninjured range at all positions of RUD (except for 10° of ulnar deviation) and showed an increase in JSA in ulnar deviation, contradicting the uninjured trend. At the SL joint (Figure 6B), the JSA for the DT was consistently below the uninjured range (except in 10° of radial deviation) while the VT followed the uninjured trend. The VDT had 0% JSA throughout the entire range of motion.
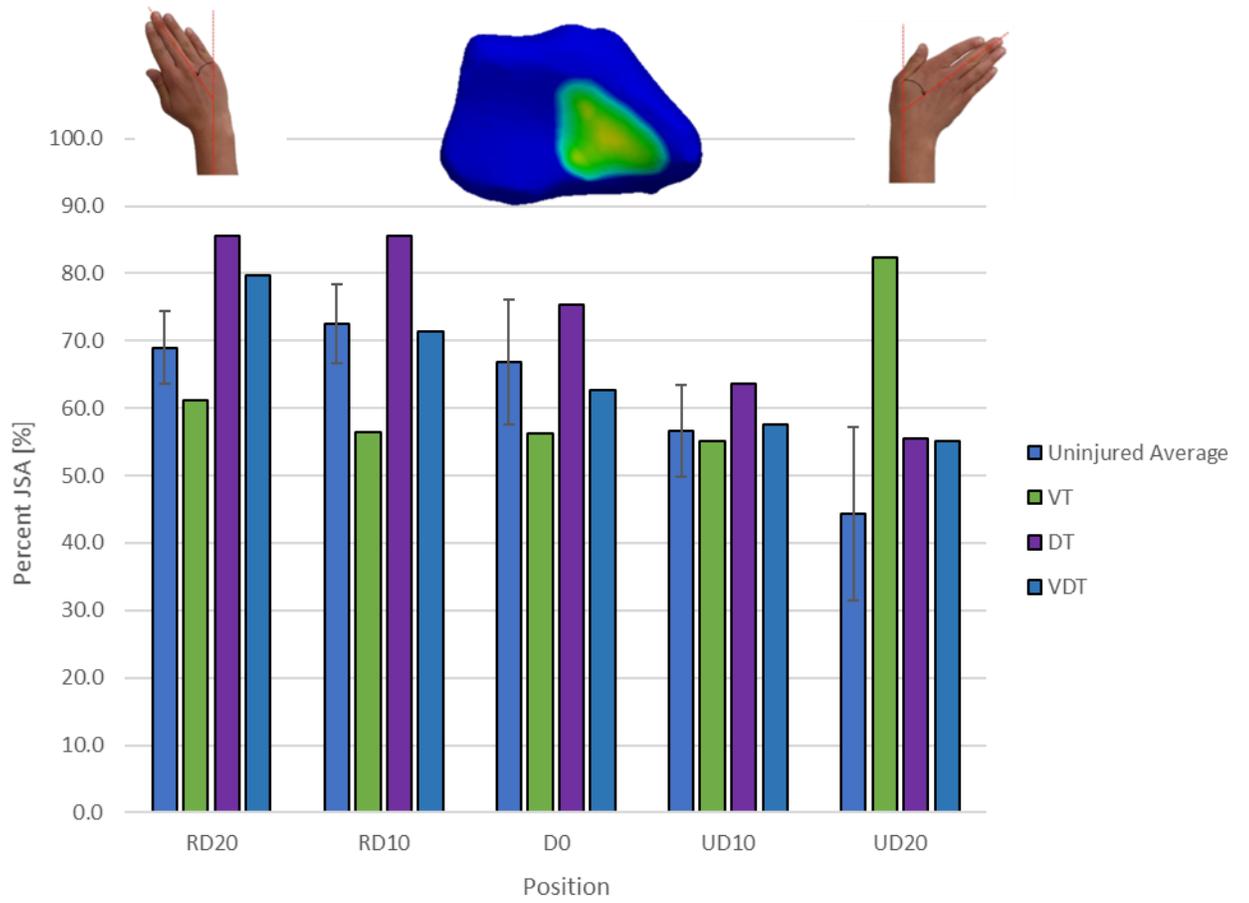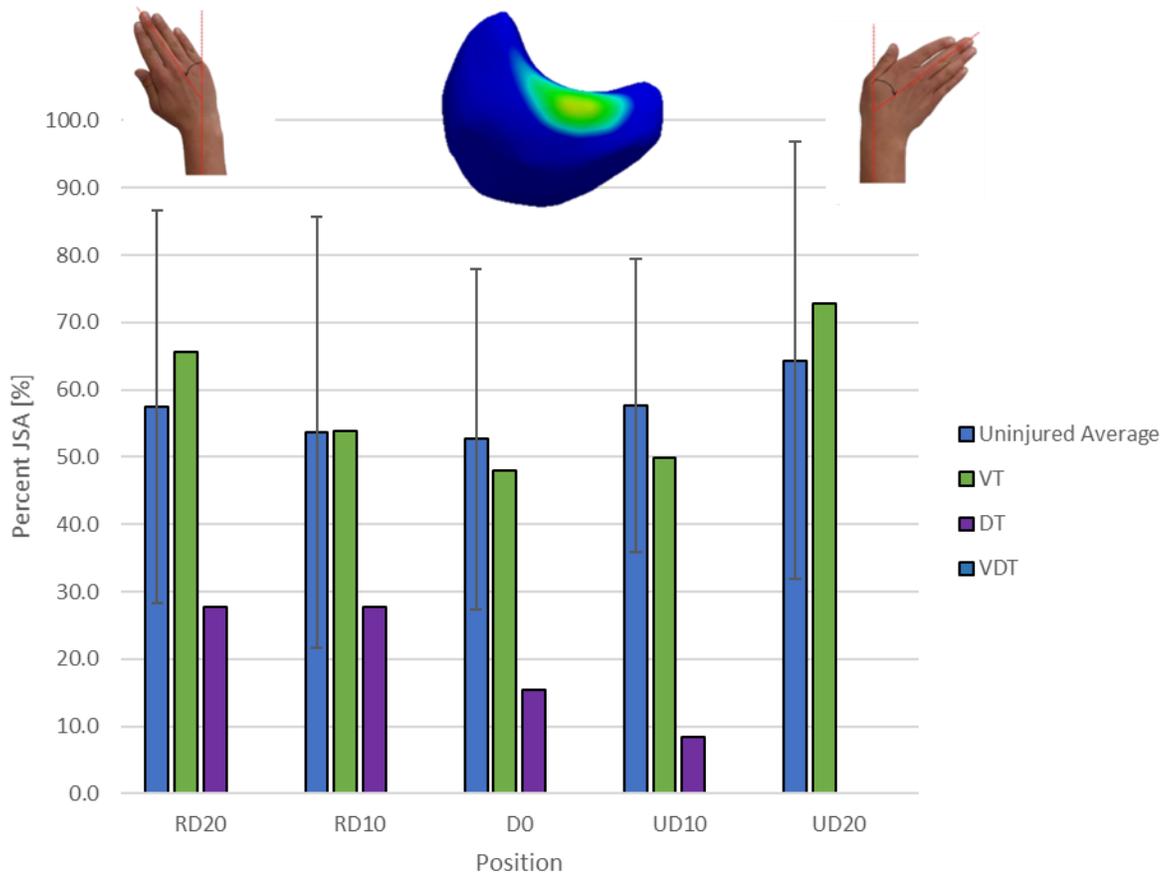
Figure 4.6: Percent JSA of the radioscaphoid (A) and scapholunate (B) joints during RUD; the hands are right wrists, dorsal views. Positions are named RD (radial deviation) or UD (ulnar deviation) followed by the degree value (ex. RD20 is 20° of radial deviation). The error bars of the healthy average data represent the 95% confidence interval. Any bars outside of this range indicate abnormal JSA. Injured participants include the volar tear (VT), dorsal tear (DT) and combined tear (VDT).

4.4.4   Validation and Reliability

The error in the helical axes angles when compared to Euler angles was less than 0.6° (Table 2). The rotational difference between consecutive frames of motion in a kinematic 4DCT scan is on the order of magnitude of 5° and as such, the error from the helical axes calculation is inconsequential.

Table 4.2: Differences between Euler angles and helical axes angles for three uninjured participants during both FE and RUD.

Motion	Scaphoid Difference [° ± SD]	Lunate Difference [° ± SD]	Capitate Difference [° ± SD]
FE	0.2 ± 0.3	0.1 ± 0.1	0.1 ± 0.5
RUD	0.1 ± 0.1	0.2 ± 0.1	0.04 ± 0.03

The inter- and intra-rater reliabilities were also determined as the relative difference between two angles; for inter-rater reliability, it is between the rotation from the same model made by two raters and for intra-rater reliability, it is between the rotation from the same model made twice by the same rater (Table 3).

Table 4.3: Inter- and intra-rater reliabilities for one participant in two positions, 20° of radial deviation and 20° of ulnar deviation.

Reliability	Scaphoid Difference [° ± SD]	Lunate Difference [° ± SD]	Capitate Difference [° ± SD]
Inter	0.5 ± 0.3	0.4 ± 0.1	0.5 ± 0.1
Intra	0.2 ± 0.1	0.2 ± 0.1	0.2 ± 0.1

The inter-rater reliability is higher (less than 0.8°) than the intra-rater reliability (less than 0.3°), but both are less than the rotational difference between consecutive frames of motion and are thus inconsequential.

4.5   Discussion

In this study, we proposed a 4DCT scanning protocol to detect subtle changes in bone movement between uninjured and SLIL tear participants during dynamic wrist motion. Our findings show abnormal carpal motion in the injured participants, which may explain their pain with otherwise normal ranges of wrist motion (Table 1). We confirmed our hypothesis

that 4DCT could detect subtle changes in bone movement to distinguish between uninjured and SLIL participants. We showed that SLIL lunate and scaphoid rotation as well as radioscaphoid and SL JSA were often outside of the defined uninjured range, indicating abnormal carpal motion when compared to uninjured. Our hypothesis that a VDT would have the largest effect on carpal motion was both true and false; while the VDT had 0% JSA in the SL joint during both motions, the largest deviation from uninjured in this joint and motion, the radioscaphoid JSA closely followed the uninjured trends in both motions. Also, the scaphoid and lunate rotation in the VDT were often within the uninjured range. We showed that VTs do alter wrist biomechanics in several ways, and in ways that differ from those caused by other types of tears, confirming our second hypothesis. The VT showed abnormal scaphoid and lunate rotation about the helical axis in both RUD and FE. A reason for this could be due to the thickness and strength of the dorsal SLIL ligament[1,4]; without the volar ligament to balance the joint, the dorsal ligament pulls the scaphoid and lunate into abnormal positions causing abnormal rotation. The VT JSA was abnormal in all instances except one; the SL joint in RUD. A cause for this could be that the VT SL gap was the same as all uninjured participants' SL gap. These findings indicate that further investigation should be conducted into the impact of VTs on carpal motion and whether VT repairs can restore wrist motion.

Scapholunate gaps and angles are common measurements to help diagnose SLIL tears[3], thus it is important to establish an uninjured baseline to which diagnostic values can be compared. Kelly et al. measured the gap between the scaphoid and lunate in cadaveric wrists during RUD and found there to be very small gaps (< 1.20 mm), indicative of minimal SL separation in normal wrists[24]. Demehri et al. measured the SL interval *in vivo* in uninjured wrists and calculated the interval to be < 1 mm in RUD[25]. Although our uninjured SL gaps were approximately twice as large as previous findings (2 mm), they are consistent with accepted values for uninjured wrists (less than or equal to 3 mm)[3,4]. An increase in the SL gap is a marker for SLIL injury[3]. Meister et al. retrospectively examined 36 MRIs: 18 from participants with VDTs and 18 from participants with ulnar-sided wrist pain but no tear[3]. They found that the SL angles and gaps were significantly greater in the SLIL tear cohort (3.9 mm) than in the uninjured cohort (1.6 mm). Although we looked at radiographs and CT images, our findings agree such that the SL gaps of the DT (3 mm)

and VDT (6.5 mm) were greater than those of the uninjured participants. However, the VT SL gap was the same as those for the uninjured cohort. This could be because the dorsal ligament is strongest and still intact in the VT, thereby keeping the SL joint close to normal. This theory is supported by the SL angles, which was smallest in the VT and larger for the DT and VDT.

Abnormal rotation of the carpals can be an effect of wrist injury; dynamic measurements of carpal motion can illuminate how different SLIL tears affect carpal motion. Padmore et al. examined FE in eight uninjured cadavers, whose carpal ligaments were sequentially sectioned to simulate different injuries, two of which were DTs and VDTs[1]. They found that the lunate extended more in the DT and VDT compared to intact, while the scaphoid flexed more. However, our findings show that the lunate flexes more in the VT in flexion, and in the DT and VDT in extension. The scaphoid of the VDT extended more in flexion, which also disagrees with Padmore et al.; however, the scaphoid flexed more in the VT, which follows the trends Padmore et al. saw but in a different type of SLIL tear than they tested. The discrepancy in results could be due to the differences in methodology: Padmore et al. examined cadavers while we examined *in vivo* motion, and they used optical tracking with bone markers while we used 4DCT. Although the specific trends disagree, both studies show that different types of SLIL tears affect normal carpal motion. Mat Jais et al., another cadaveric study, also examined rotation of the scaphoid, and similarly to this study, they used 4DCT to analyze RUD[14]. They found that the centroid of the scaphoid flexed more in the VDT compared to uninjured. Our findings agree for the DT and VDT in 20° of ulnar deviation and just the DT in 20° of radial deviation; however, the VT scaphoid extended more in ulnar deviation. These findings show that VTs act differently than DTs or VDTs; future studies will focus on VTs to build a stronger understanding how VTs affect carpal motion differently than other SLIL tears.

In addition to kinematics, SLIL tears affect the JSA of the radioscaphoid and SL joints. Reduced radioscaphoid JSA and widening of the SL joint are known elements in the progression of SLAC[7]. Studies have shown that scaphoid malunions, a common result of scaphoid fractures and a condition which also leads to arthritis, lead to an increase in radioscaphoid JSA[26]. Similarly, our findings show an increase in radioscaphoid JSA in the

SLIL tear cohort compared to the uninjured cohort (except in the VT in radial deviation and neutral, and the VDT in 50° extension and 50° flexion). These results also show that SL gap increases in the DT and VDT, which, when coupled with increased radioscaphoid JSA, points to SLAC progression in all SLIL tear cases. In addition, our findings show differences between the VT and the other two tears, indicating that the VT is biomechanically impactful and may need to be repaired, which should be examined further in future studies. Lastly, SLAC has a known progression, the stages of which can be seen in the SLIL cohort.

The efficacy of using 4DCT to measure abnormal carpal kinematics is contingent on its ability to successfully measure uninjured carpal kinematics. Wolfe et al. examined *in vivo* scaphoid and lunate rotation about the helical axes during FE and found that the lunate rotated less than the scaphoid[13]. Crisco et al. also showed that lunate rotation was always less than scaphoid rotation in uninjured subjects in various positions of Dart Thrower's Motion (DTM)[27]. Our findings show that the lunate rotated less than the scaphoid during FE by an average of 7.4° ± 4.3°; however, the lunate rotated more in RUD by an average of 5.5° ± 2.3°. Discrepancies in these findings could be due to the types of motions analyzed. Joint synchronicity is an interesting outcome measure from 4DCT. Crisco showed that the SL joint moves synchronously while the radioscaphoid joint does not in DTM[27]. Findings from our uninjured cohort show that radioscaphoid JSA changes throughout RUD and FE (decreasing from extension to flexion and radial deviation to ulnar deviation) while SL JSA does not change either motion; suggesting, the radioscaphoid joint is potentially an asynchronous joint while the SL joint is potentially a synchronous joint. Future work will explore the synchronicity of carpal joints in more detail.

A major limitation of this study was the n=1 sample size for each injured case. These preliminary findings support the hypothesis that 4DCT is an effective tool to measure injured wrist motion and that VTs are worth investigating; however, a larger sample size is required to determine if these patterns hold true. While 4DCT is a dynamic imaging modality with many strengths, such as non-invasiveness and quantitative measures[28], there are inherent limitations. The incidence of MRI proven VTs is unknown, thereby limiting the number of participants recruited. Due to the lack of SL widening, VTs are rarely

diagnosed from planar radiographs. There is a significant amount of data collected from 4DCT scans and surface reconstructions are a labour-intensive, time-consuming process. This process also limits the number of participants that can be included. For the best results, motions should be performed slowly to reduce blurring artifacts[28,29], which limits the applicability of these motions as true motion is often performed quickly (median angular velocity for a wrist was 30°/s, when measured in female operators in an industrial workplace[30]). Loaded and/or complex motions are more relevant to the types of motions people perform in daily living. As such, unloaded, planar motions are not as representative of true human motion. However, we suspect that if the motions were performed loaded, the findings from this study would be even more apparent as loading the joints would exaggerate the negative effects of the SLIL tears. Contralateral kinematic scans were not performed due to the significant increase in radiation dose; instead, three separate healthy wrists were compared to the injured participants. Future work needs to examine hand dominance to determine if contralateral kinematics would be an accurate comparison. Although these limitations impact the applications of 4DCT, its ability to provide quantitative measurements of dynamic wrist motion has been tested and it shows promise in this area[14].

4.6 Conclusions

Four-dimensional CT shows promise as a tool with which to quantify abnormal carpal kinematics due to different types of SLIL tears. The results of this study provide a basis to show that 4DCT can distinguish between the motion of different SLIL tears and may indicate that VTs negatively impact carpal motion such that they may need to be repaired. The SLIL tear participants in this study had pain but a good range of motion; 4DCT is a sensitive, dynamic imaging modality that can detect subtle changes in carpal kinematics indicative of an SLIL tear and which may explain the presence of wrist pain. This study suggests that VTs may not be fully appreciated and therefore, further consideration into the impacts of VTs is warranted.

4.7 References

1.   Padmore C, Stoesser H, Langohr GD, Johnson J, Suh N. Carpal Kinematics following Sequential Scapholunate Ligament Sectioning. J Wrist Surg. 2019;08(02):124-131. doi:10.1055/s-0038-1676865

2.   Wang P, Stepan JG, An T, Osei DA. Equivalent Clinical Outcomes Following Favored Treatments of Chronic Scapholunate Ligament Tear. HSS J. 2017;13(2):186-193. doi:10.1007/s11420-016-9525-5

3.   Meister DW, Hearns KA, Carlson MG. Dorsal Scaphoid Subluxation on Sagittal Magnetic Resonance Imaging as a Marker for Scapholunate Ligament Tear. J Hand Surg Am. 2017;42(9):717-721. doi:10.1016/j.jhsa.2017.06.015

4.   Kuo CE, Wolfe SW. Scapholunate Instability: Current Concepts in Diagnosis and Management. J Hand Surg Am. 2008;33(6):998-1013. doi:10.1016/j.jhsa.2008.04.027

5.   Montgomery SJ, Rollick NJ, Kubik JF, Meldrum AR, White NJ. Surgical outcomes of chronic isolated scapholunate interosseous ligament injuries: a systematic review of 805 wrists. Can J Surg. 2019;62(3):199-210. doi:10.1503/cjs.006918

6.   Strauch RJ. Scapholunate advanced collapse and scaphoid nonunion advanced collapse arthritis - Update on evaluation and treatment. J Hand Surg Am. 2011;36(4):729-735. doi:10.1016/j.jhsa.2011.01.018

7.   Lane R, Varacallo M. Scapholunate Advanced Collapse (SLAC Wrist). StatPearls Publishing LLC.

8.   Vishwanathan K, Hearnden A, Talwalkar S, Hayton M, Murali SR, Trail IA. Reproducibility of radiographic classification of scapholunate advanced collapse (SLAC) and scaphoid nonunion advanced collapse (SNAC) wrist. J Hand Surg Eur Vol. 2013;38(7):780-787. doi:10.1177/1753193413484629

9.   Mathoulin C, Gras M. Role of wrist arthroscopy in scapholunate dissociation. Orthop Traumatol Surg Res. 2020;106(1):S89-S99. doi:10.1016/j.otsr.2019.07.008

10.   Andersson JK. Treatment of scapholunate ligament injury: Current concepts. EFORT Open Rev. 2017;2(9):382-393. doi:10.1302/2058-5241.2.170016

11.   Jakubietz MG, Zahn R, Gruenert JG, Waschke J, Meffert RH, Jakubietz RG. Kirschner wire fixations for scapholunate dissociation: a cadaveric, biomechanical study. J Orthop Surg (Hong Kong). 2012;20(2):224-229. doi:10.1177/230949901202000218

12.   Corella F, Del Cerro M, Ocampos M, Larrainzar-Garijo R. Arthroscopic ligamentoplasty of the dorsal and volar portions of the scapholunate ligament. J Hand Surg Am. 2013;38(12):2466-2477. doi:10.1016/j.jhsa.2013.09.021

13.   Wolfe SW, Neu C, Crisco JJ. In vivo scaphoid, lunate, and capitate kinematics in flexion and in extension. J Hand Surg Am. 2000;25:860-869. doi:10.1053/jhsu.2000.9423

14.   Mat Jais IS, Tay SC. Kinematic analysis of the scaphoid using gated four-dimensional CT. Clin Radiol. 2017;72(9):794.e1-794.e9. doi:10.1016/j.crad.2017.04.005

15.   Linscheid RL, Dobyns JH. Dynamic carpal stability. Keio J Med. 2002;51(3):140-147. doi:10.2302/kjm.51.140

16.   Robinson S, Straatman L, Lee T-Y, Suh N, Lalone E. Evaluation of Four-Dimensional Computed Tomography as a Technique for Quantifying Carpal Motion. J Biomech Eng. 2021;143(6). doi: https://doi.org/10.1115/1.4050129

17.   Lalone EA, Mcdonald CP, Ferreira LM, Peters TM, King GW, Johnson JA. Development of an image-based technique to examine joint congruency at the elbow. Comput Methods Biomech Biomed Engin. 2013;16(3):280-290. doi:10.1080/10255842.2011.617006

18.   Struwe C, Bornemann R, Schildberg FA, Wirtz DC, Pflugmacher R, Rommelspacher Y. The Kellgren and Lawrence Score as a helpful tool for the indication for total disc replacement at the cervical spine. Technol Heal Care. 2019;27(3):317-326. doi:10.3233/THC-191614

19.   Macdermid JC. The PRWE / PRWHE update. J Hand Ther. 2019;32(2):292-294. doi:10.1016/j.jht.2019.01.001

20.   Besl PJ, McKay ND. A method for registration of 3-D shapes. IEEE Trans Pattern Anal Mach Intell. 1992;14(2):239-256. doi:10.1109/34.121791

21.   Pollock J, O'Toole R V., Nowicki SD, Eglseder WA. Articular cartilage thickness at the distal radius: A cadaveric study. J Hand Surg Am. 2013;38(8):1477-1481. doi:10.1016/j.jhsa.2013.04.037

22.   Sorensen A, Howard D, Tan WH, Ketchersid J, Calfee R. Minimal Clinically Important Differences of Three Patient-Rated Outcomes Instruments. J Hand Surg Am. 2013;38(4):641-649. doi:10.1016/j.jhsa.2012.12.032.Minimal

23.   Walenkamp MMJ, de Muinck Keizer RJ, Goslings JC, Vos LM, Rosenwasser MP, Schep NWL. The Minimum Clinically Important Difference of the Patient-rated Wrist Evaluation Score for Patients With Distal Radius Fractures. Clin Orthop Relat Res. 2015;473(10):3235-3241. doi:10.1007/s11999-015-4376-9

24.   Kelly PM, Hopkins JG, Furey AJ, Squire DS. Dynamic CT Scan of the Normal Scapholunate Joint in a Clenched Fist and Radial and Ulnar Deviation. Hand. 2018;13(6):666-670. doi:10.1177/1558944717726372

25.   Demehri S, Hafezi-Nejad N, Morelli JN, et al. Scapholunate kinematics of asymptomatic wrists in comparison with symptomatic contralateral wrists using four-dimensional CT examinations: initial clinical experience. Skeletal Radiol. 2016;45(4):437-446. doi:10.1007/s00256-015-2308-0

26.   Chambers SB, Padmore CE, Grewal R, Suh N. The Impact of Scaphoid Malunion on Radioscaphoid Joint Contact: A Computational Analysis. J Hand Surg Am. 2020;45(7):610-618.e1. doi:10.1016/j.jhsa.2020.01.009

27.   Crisco JJ, Coburn JC, Moore DC, Akelman E, Weiss APC, Wolfe SW. In vivo radiocarpal kinematics and the dart thrower's motion. J Bone Jt Surg - Ser A. 2005;87(12 I):2729-2740. doi:10.2106/JBJS.D.03058

28.   Dobbe JGG, de Roo MGA, Visschers JC, Strackee SD, Streekstra GJ. Evaluation of a Quantitative Method for Carpal Motion Analysis Using Clinical 3-D and 4-D CT Protocols. IEEE Trans Med Imaging. 2019;38(4):1048-1057. doi:10.1109/TMI.2018.2877503

29.   Tay S-C, Primak AN, Fletcher JG, et al. Four-dimensional computed tomographic imaging in the wrist: proof of feasibility in a cadaveric model. Skeletal Radiol. 2007;36(12):1163-1169. doi:10.1007/s00256-007-0374-7

30.   Arvidsson I, Åkesson I, Hansson GÅ. Wrist movements among females in a repetitive, non-forceful work. Appl Ergon. 2003. doi:10.1016/S0003-6870(03)00042-5

Chapter 5

5 General Discussion and Conclusions

This chapter summarizes the objectives and hypotheses as well as the work performed to complete these objectives and hypotheses. The strengths and limitations are discussed, and this chapter concludes with an outline of future work that will stem from this thesis.

5.1 Summary and Conclusions

The wrist is one of the most complex and functionally important joints in the upper extremity[1]. Due to its large range of motion in a small volume, the wrist is a provocative location to test medical imaging modalities and there remains no unified wrist motion theory to describe wrist motion. Current tools for measuring carpal morphology and motion range from static methods (radiographs, goniometers, MRI, etc.), which can at most measure carpal morphology and orientation in static positions, to dynamic methods (4DCT, BVF), which can measure carpal morphology and orientation throughout motion. In particular, 4DCT has evolved from primary use in the heart to applications in MSK systems; it has shown promise as a useful clinical tool for measuring dynamic bone motion. As such, this thesis sought to examine the application of 4DCT to imaging dynamic wrist motion, validate the method, and test 4DCT as a useful clinical tool by using it to differentiate between healthy carpal motion and that in an SLIL tear population.

The first objective of this work was to employ 4DCT to measure dynamic wrist motion in a healthy cohort, specifically measuring the translation of the centroid of the scaphoid and the JSA of the radioscaphoid and scapholunate joints during radioulnar deviation. The hypothesis was that 4DCT will be a useful tool to visualize dynamic carpal motion while providing sufficient image resolution. Chapter 2 describes the use of 4DCT in a healthy cohort (n=12) wherein each participant underwent unilateral 4DCT scanning of the wrist during radioulnar deviation. Bone models were made for the extremes of motion, from which scaphoid centroid translation and JSA were calculated. The objective was achieved, and the hypothesis was confirmed; 4DCT successfully measured scaphoid translation and JSA changes between extremes of motion. In addition, one participant was scanned during

radioulnar deviation and flexion-extension, and all 25 frames of motion were made for the first pass of each motion. This data showed that 4DCT is a responsive system because there were qualitative and quantitative changes in JSA between consecutive frames of motion. These findings led to three decisions: (1) due to the responsiveness of 4DCT and the changes in translation and JSA that occur throughout motion, more frames of motion should be made in subsequent studies; (2) translation was successfully calculated and so the natural extension of that measurement would be to measure carpal kinematics (rotation) in future studies; lastly, (3) the scapholunate JSA was difficult to visualize on the scaphoid and so future studies will visualize it on the lunate. The current workflow and pipeline for data analysis requires a 3D surface reconstruction of each carpal bone for each frame of motion. Transformation matrices are created by performing a surface-based registration. Additionally, joint surface area measures can be obtained and used to examine joint contact mechanics. All of these steps require an accurate depiction of the underlying bony structure. Before these next studies could be performed, the accuracy of the surface models obtained from the 4DCT needed to be determined and validated using a gold standard micro-CT scanner. This was the focus of Chapter 3.

In this study, a validation of the surface reconstruction was performed. The hypothesis was that surface reconstructions from kinematic 4DCT scans would be valid within 0.5 mm of the gold standard (micro-CT). This hypothesis was based on a similar validation study conducted at the elbow, wherein the associated error was 0.3 mm compared to the gold standard[2]. In this current study, the gold standard was micro-CT, which is computed tomography with a micrometer resolution, and the surface reconstructions were of the radius, scaphoid, lunate, and capitate. There were three aims of this study: (1) validate the proposed 4DCT technique by comparing surface reconstructions made from kinematic 4DCT scans, in two software, to those made from a micro-CT scan; (2) measure the inter-rater and (3) intra-rater reliability of the proposed 4DCT technique. One cadaver was scanned during motion (radioulnar deviation and flexion-extension) using a custom-made wrist motion simulator in the 4DCT scanner. It was then scanned in a micro-CT scanner. Mimics was used to create surface reconstructions from one 4DCT kinematic frame and the micro-CT scan, and Slicer was used to create the same 4DCT surface reconstruction. The error in the 4DCT scans relative to the ground truth was less than or equal to 0.4 mm,

while it was less than or equal to 0.3 mm between software; this confirmed the hypothesis and achieved objective (1). Surface reconstructions were made in Mimics of one *in vivo* scan by two raters to calculate inter-rater reliability. The error was less than or equal to 0.36 mm, which achieved objective (2). Lastly, intra-rater reliability was calculated from surface reconstructions of two *in vivo* participants: one rater made one scan five times for each participant. The resulting error was less than or equal to 0.26 mm. Since the 4DCT technique was validated and is comparable to past validations at the elbow, it was now important to extend the use of this tool to determine its sensitivity at distinguishing between healthy and abnormal kinematics that result from injury to the wrist.

The third and final objective of this thesis was to extend the use of the 4DCT technique to measure carpal kinematics in healthy and injured populations, specifically those with SLIL tears. It was hypothesized that 4DCT scanning will be sufficiently sensitive to detect subtle bone changes that occur due to injuries, thus differentiating between healthy and SLIL tear cases. The SLIL tear cohort consisted of three participants, one with each type of SLIL tear: one isolated volar tear, one isolated dorsal tear, and one combined tear. Clinically, dorsal and combined tears are the focus of reconstructive surgeries, and all SLIL tears are difficult to diagnose because early markers are dynamic and therefore cannot be detected by static radiographs. However, this work sought to confirm the hypothesis that volar tears affect carpal motion, and 4DCT will be able to detect differences between each tear case. These objectives were achieved by measuring the rotation of the scaphoid and lunate, as well as the JSA of the radioscaphoid and scapholunate joints. To measure rotation, the helical axes were calculated for each bone relative to the neutral radius; the helical axis is the axis about which a bone rotates, and the axis moves during motion. Three healthy (n=3) and three SLIL tear (n=3) participants underwent unilateral 4DCT scanning of their wrist during radioulnar deviation and flexion extension. Surface reconstructions of the radius, scaphoid, lunate, and capitate were made for every 10° of motion, from 50° extension to 50° flexion (11 frames of motion) and from 20° radial deviation to 20° ulnar deviation (5 frames of motion). The rotations of the scaphoid and lunate showed abnormal rotation in each tear case. Interestingly, the dorsal and combined tear cases behaved most similar to one another, while the volar case rotated abnormally relative to healthy and the other two tear cases. The rotation data confirmed the hypothesis that the isolated volar SLIL tear

affected healthy carpal kinematics. A concurrent validation was performed by comparing the helical axes method to another method for measuring rotation: Euler angles. The average difference between the angles calculated from helical axes and those calculated from Euler angles were less than 0.6° during FE and less than 0.3° for RUD; these extremely low differences show that helical axes were a valid method of measuring carpal rotation. This work focused on a single rotation about the helical axis; future work will split the helical axis rotation into three rotations, one about each anatomical axis: radioulnar deviation, pronation supination, and flexion extension. JSA data also confirmed the hypothesis that volar tears affect healthy carpal motion, especially in the amount of translation of the JSA centroid in each joint; the volar tear case always translated the most out of the three tears. Therefore, the use of 4DCT was extended to injured populations and could detect subtle differences in carpal kinematics and arthrokinematics that allowed for the differentiation between the tear cases and between the healthy and injured cohorts.

5.2   Strengths and Limitations

While the findings from these studies are promising, the studies themselves are not void of limitations. In terms of 4DCT as an imaging modality, it has significant radiation. This is because there is continuous exposure to radiation as the scan is taking place, and the scan often lasts for several seconds. In this work, each motion was 24.5 seconds in duration and the participant performed multiple motions. However, the wrist is an excellent location for 4DCT scanning due to the lack of radiation sensitive organs; thus, there is less risk radiating the wrist than there would be the head or torso. The total skin dose was 0.2 Gy for each participant, whereas the threshold for skin erythema from radiation exposure is 2 Gy. Thus, the skin dose from these studies was ten times less than the threshold, indicating a safe level of radiation. Protective equipment (lead apron, thyroid collar shield, leaded eye goggles) was also worn to mitigate the risks associated with radiation. The scatter radiation dose measured under the apron was 0.04 mSv, which is 75 times lower than the effective dose a person receives per year from naturally occurring radioactive material and cosmic radiation from outer space (3 mSv).

In terms of procedure, a limitation of this work was small sample sizes. In Chapter 2, the sample size had sufficient power at n=12. However, there were six males and six females,

and six older participants and six young participants; unfortunately, the groups of six did not have sufficient power to make conclusive comparisons between the groups. In chapter 3, the micro-CT validation was performed on n=1 participant; this is in part due to the cost associated with cadaveric specimens and micro-CT testing, as well as the considerable time to perform such scans. However, this is a gold standard method for 3D bone visualization and as such, it was not thought that an increased sample size would drastically affect validity. For inter-rater reliability, there were two raters for one scan. The results of this test were close to those of the micro-CT validation and therefore not the limiting factor, thus one scan provided sufficient information. The intra-rater reliability test had a good sample size (each frame was made five times, for two different participants) and so more data was not thought to affect results. Lastly, Chapter 4 had three healthy participants to age and sex match to the three SLIL tear participants. Furthermore, there were only one participant for each type of tear. However, the objective of this chapter was to show the potential applications of the proposed 4DCT tool, not to define the exact motion patterns from different types of SLIL tears in order to make clinical recommendations. The small sample size was sufficient to confirm the hypothesis that 4DCT can differentiate between healthy and injured cases. In addition, MRI confirmed volar SLIL tears are difficult to find, which explains how only one type of each SLIL tear were recruited. Volar tears do not often result in an increased SL gap, as seen in chapter 4, and therefore they are often missed in standard radiographs. To remain consistent, only one participant of each type of tear was chosen until more volar tear participants could be recruited. Small sample sizes were also necessary in order to disseminate findings in a timely fashion because surface reconstructions are immensely time consuming to compute. Creating one bone model can take an hour, depending on the level of arthritis in the joints and how consistent their angular velocity was throughout motion, as this was not constrained. Therefore, up to 20 hours are needed per participant in order to make five frames of motion (as was made for RUD in Chapter 4); in total for Chapter 4, 16 frames (5 RUD, 11 FE) were made per participant for six participants, which equals 384 hours of manual segmentation. Clearly, an automatic segmentation algorithm would benefit the field of medical imaging segmentation, enabling researchers to examine more data in a timelier manner.

There were also limitations regarding the analyzed motions. This work focused on planar motions; however, the wrist is capable of complex and combined motions and rarely performs purely planar motions during tasks of daily living. Although planar motion is not directly representative of functional wrist motion, this work sought to test the use of 4DCT in measuring carpal motion, which was accomplished by analyzing planar motion. The wrist is also capable of moving quicker than was analyzed in this work; studies have estimated the wrist rotates at angular velocities of 30°/s, whereas this chapter analyzed angular velocities of 10-20°/s [3]. As outlined in Appendix A, increased angular velocity is accompanied with interscan blurring and as such, lower angular velocities were examined in this work to reduce said blurring. More information on this relationship and how it was investigated can be found in Appendix A. In addition, during the *in vivo* experiments in chapters 2 and 4, the motions were unconstrained and so, each participant moved their wrist in a way that was natural to them. While leaving the wrist unconstrained meant that the motion was close to natural, a resulting drawback was that participants exhibited inconsistent angular velocity. The author sought to mitigate these risks by providing participants with instructional videos and coaching through the motion; however, the angular velocity varied between participants and was not consistent throughout motion within a given participant. Future studies will rectify this limitation with guiding devices that assist the participants in achieving the target angular speed consistently throughout motion. Lastly, loading the wrist joint may affect carpal motion; this phenomenon was not examined in this work and so future work should incorporate loading tasks.

A limitation of measuring JSA in this work was that cartilage effects were largely ignored, thus JSA was only an approximation of the actual joint contact area. Previous work has been done in the laboratory to validate this measurement technique and while it was largely successful, but it was performed at the elbow, not the wrist[4]. This work used JSA to measure changes in bone movement throughout motion using 4DCT to show the usefulness of 4DCT in this context; thus, while cartilage effects were a limitation, they did not invalidate the aims of this work.

Despite these limitations, there were numerous strengths to the presented work. Primarily, 4DCT itself is non-invasive; this allows for the easy application to *in vivo* testing on human

participants. The non-invasive nature is also an attractive quality for other 4DCT applications, such as a diagnostic tool for injuries (Chapter 4). This imaging modality is also dynamic, providing real-time measurements, which is a large improvement to current static imaging modalities, like radiography and MRI. Dynamic imaging modalities enable accurate measurement of carpal motion that is otherwise missed by static imaging modalities, therefore providing further insight into true carpal motion.

Surface reconstructions, as validated in Chapter 3, are associated with another strength of this work: high repeatability. All raters involved in making the surface reconstructions used in this work were trained by experienced raters, had access to informative step-by-step documents, and had their work sporadically monitored by experienced raters. These measures ensured there was high repeatability in the model-making process, as shown by the low errors in the intra- and inter-rater reliability tests in Chapter 3.

The *in vivo* experiments in this work are a huge strength. The carpal motions analyzed in Chapters 2 and 4 were very close to natural; the participants' passive and active stabilizers were engaged, and any healing response to injuries in Chapter 4 were elucidated by the injured cohort. As mentioned before, the motions were unconstrained, which adds to the realistic nature of these motions. For these reasons, the proposed 4DCT tool measured true, dynamic carpal motion in this work.

5.3   Current and Future Directions

There are extensive opportunities for further development of the proposed 4DCT technique to measure healthy and injured carpal kinematics. As mentioned, current motions suffer from angular speed variability within and between patients. Future work should aim to standardize angular speed, which would result in more consistent comparisons between participants. The 4DCT tool would benefit from a standardization solution that keeps participants motion at a constant angular speed that is the same across participants. Additionally, this work examined planar motion even though the wrist is capable of complex motions; future work should incorporate the analysis of complex and combined motions, such as the dart thrower's motion[5].

The current method of analyzing the 4DCT scans involves significant amounts of manual segmentation. This process is labour intensive and time consuming (approximately 400 hours for the one study conducted in Chapter 4), which limits the number of scans that can be analyzed for any given project, resulting in lower sample sizes or lower numbers of analyzed frames. The segmentation process would benefit from an automatic technique, trained on the extensive number of surface reconstructions already made by the lab, that is sufficiently robust to segment all bones in the wrist regardless of age and health status. This would greatly decrease analysis time and would enable increased sample sizes, thus allowing for greater power in studies and more statistically reliable comparisons between groups.

While Chapter 4 tested the applications of the 4DCT technique by comparing injured and healthy cohorts, there is opportunity to expand this endeavor. More SLIL tear participants of each type (volar, dorsal, and combined) would allow for a statistically sound comparison of the motion trends between these groups. There are other wrist injury groups wherein 4DCT may be an effective measurement and potential diagnostic tool. Distal radius fractures are a common wrist injury and may provide a provocative test case for this proposed tool to measure changes in carpal motion[6]. These applications may confirm the proposal of 4DCT as a useful measurement and diagnostic tool, testing the limitations of this technique as well as potentially providing clinical recommendations.

5.4   Conclusions

Despite the high prevalence of SLIL tears, little is known about their effects on healthy carpal motion, nor how their effects differ with different types of SLIL tears. Furthermore, there is no unified wrist motion theory to which injured carpal kinematics can be compared. This lack of understanding healthy and injured carpal motion has hindered early diagnosis and effective medical intervention. The 4DCT tool described and validated in this thesis enables the examination of true dynamic carpal motion in healthy and injured populations. This research increases our understanding of effective applications of 4DCT as well as resultant healthy and injured wrist kinematics. The techniques developed in this thesis, namely 4DCT and helical axes, have already been used by other members in our laboratory to elucidate the effects of hysteresis on carpal motion, as well as contributions to wrist

motion from the radiocarpal and midcarpal joints. These techniques can be applied to other joints, as evidence by the extension into shoulder kinematics analyses in this laboratory. Clinically, this technique may prove useful as a diagnostic tool because it can differentiate between injured and healthy populations. Healthy target values could be measured using 4DCT and then injured patients could undergo 4DCT scanning to determine how their carpal kinematics compare to the healthy targets. Clinical recommendations could be established this way, which outline the kinematic values that correlate to different injuries and what to do at each stage. Diagnosing injuries at their dynamic instability phase would allow for better surgical intervention and ultimately, better patient outcomes. In conclusion, the techniques proposed in this work contribute to improved understanding of 4DCT as a biomechanical measurement tool, and of healthy and injured carpal motion.

5.5   References

1.   Wolfe SW, Hotchkiss RN, Pederson WC, Kozin SH. Green's OPERATIVE HAND SURGERY. 6th ed. (Pepper D, Sussman M, eds.). Philadelphia, PA: Elsevier; 2011.

2.   Lalone EA, Willing RT, Shannon HL, King GJW, Johnson JA. Accuracy assessment of 3D bone reconstructions using CT: An intro comparison. Med Eng Phys. 2015;37(8):729-738. doi:10.1016/j.medengphy.2015.04.010

3.   Arvidsson I, Åkesson I, Hansson GÅ. Wrist movements among females in a repetitive, non-forceful work. Appl Ergon. 2003. doi:10.1016/S0003-6870(03)00042-5

4.   Lalone EA, Mcdonald CP, Ferreira LM, Peters TM, King GW, Johnson JA. Development of an image-based technique to examine joint congruency at the elbow. Comput Methods Biomech Biomed Engin. 2013;16(3):280-290. doi:10.1080/10255842.2011.617006

5.   Crisco JJ, Coburn JC, Moore DC, Akelman E, Weiss APC, Wolfe SW. In vivo radiocarpal kinematics and the dart thrower's motion. J Bone Jt Surg - Ser A. 2005;87(12 I):2729-2740. doi:10.2106/JBJS.D.03058

6.   Ferreira LM, Greeley GS, Johnson JA, King GJW. Load Transfer at the Distal Ulna Following Simulated Distal Radius Fracture Malalignment. J Hand Surg Am. 2015;40(2):217-223. doi:10.1016/j.jhsa.2014.10.012

Appendices

Appendix A: Motion Blur

A.1 Introduction

The quality of 4DCT reconstruction depends on the quality of the scan, which can be impaired by blurring artifacts that distort the image. One cause of blurring artifacts is patient motion during scan acquisition[1]; thus, reducing the scan acquisition time reduces the risk of artifacts. McCollough et al. showed that motion artifacts and loss of spatial resolution were observable at movement velocity of 10mm/s for an 'effective' x-ray exposure time of 0.5 s[1]. However, a previous ergonomic study has shown that median angular velocity for a wrist was 30°/s, when measured in female operators in an industrial workplace[2]. Therefore, there is a disconnect between wrist angular velocity in real life and that which can be achieved during 4DCT scans. Rotation must also be considered because structures furthest from the centre of rotation (COR) will move quickest while those near the COR will move slowest; thus, objects closer to the COR will exhibit fewer artifacts[1]. In addition, numerous changes can be made to the scanning protocol that can affect scan acquisition quality; scanning the complete volume can avoid "banding" artifacts[3,4], and using full scan reconstruction can avoid "shading" artifacts[5]. The objective of this appendix was to characterize the blurring artifacts that occur in 4DCT scans due to rotation speed and scanning protocol. We hypothesized that a slower scan acquisition time will reduce blurring artifacts and using a cardiac protocol that implements partial volume acquisition will also reduce blurring artifacts.

A.2 Methods

For the speed characterization experiment, the cadaver was left intact (n=1, left arm, male, 61 years old). The same 4DCT scanning protocol was used as described in Chapter 2 (2.2.2 4DCT Imaging Technique). Three passes of two dynamic motions were simulated using the simulator: radioulnar deviation (RUD) beginning in radial deviation for the first and third passes and ulnar deviation for the second pass; and flexion-extension (FE) beginning in flexion for the first and third passes and extension for the second pass. Each pass of

motion resulted in 25 4DCT scan frames but varied in duration: 2 s, 4 s, and 8 s, where 8 s was the control and the duration used in the experiments in Chapters 2-4 of this thesis. During RUD, these scan durations corresponded to angular velocities of 36°/s, 18°/s, and 9°/s respectively while in FE, the angular velocities were 88°/s, 44°/s, and 22°/s. The CT gantry rotation speed was fixed at 0.35 s/revolution. To determine the amount of blur at each speed, an experienced rater examined each frame of data in all three passes and determined the number of frames that could not be used to make surface reconstructions due to the level of blur. In addition, peak-to-peak ratios were calculated by calculating the profile from a DICOM image of one slice of the CT scan. This profile was exported to excel, and the ratio of the peaks was measured; a ratio close to one indicates no blur.

For the protocol characterization experiment, the cadaver was left intact (n=1, left arm, male, 63 years old). A new 4DCT protocol (100 kV, 99 effective mA, 0.28 s rotation time), employing the prospective ECG gated cardiac scanning mode on the Revolution CT scanner, was used to accommodate faster wrist angular velocity. The scanner was triggered with an internally generated ECG signal that simulates a 30 beats/min heartbeat to acquire continuous projection data for 6s with a gantry rotation speed of 0.28 s/revolution, compared to the previous 0.35s/revolution. Subsequently, images are reconstructed using an acquisition window of 0.19(0.21) s at intervals of 12 ms using partial scan reconstruction (270° instead of full scan 360°) at 30° increments of cardiac phase. If the previous 0.35 s acquisition window was able to scan 9°/s of RUD without intrascan motion blurring, and the acquisition window scale is assumed to be inversely proportional to wrist velocity, then the wrist angular velocity could increase to 16.8°/s with the new protocol, 1.86 times more than before. Two passes of two dynamic motions were simulated using the simulator: radioulnar deviation (RUD) beginning in radial deviation for the first pass and ulnar deviation for the second pass; and flexion-extension (FE) beginning in flexion for the first pass and extension for the second pass. Each pass of motion was six seconds long (angular velocities of 13.5°/s for RUD and 33°/s for FE) and resulted in 39 4DCT scan frames per pass of motion, 78 frames total.

A.3 Results

The number of blurry frames for each scan acquisition time were counted (Table A.1). These frames were considered blurry if there was enough artifact that bone models could not be successfully made of the third metacarpal; the third metacarpal is the bone on the periphery of motion and therefore, it experienced the most blurring artifacts.

Table A.1: Number of blurry frames in each motion in each duration of scan

	Number of blurred frames (out of 25 total)		
Motion	**8 s**	**4 s**	**2 s**
Flexion - extension	1 ± 1	11 ± 2	11 ± 2
Radioulnar deviation	3 ± 2	12 ± 2	11 ± 3

These results show that there were similar levels of blurring in the four second and two second scans, whereas the eight second scan had considerably less blurring. Therefore, an eight second duration was the quickest scan time allowable for this thesis. The unconstrained motion of the *in vivo* studies meant that participants did not move at a constant speed and as such, a conservative scan time should be chosen. There was no noticeable difference between the number of blurry frames during RUD and those during FE.

These findings are supported by the peak-to-peak ratios. Figure A.1 shows the metacarpal bones at the same phase of motion of the wrist for the three scans.
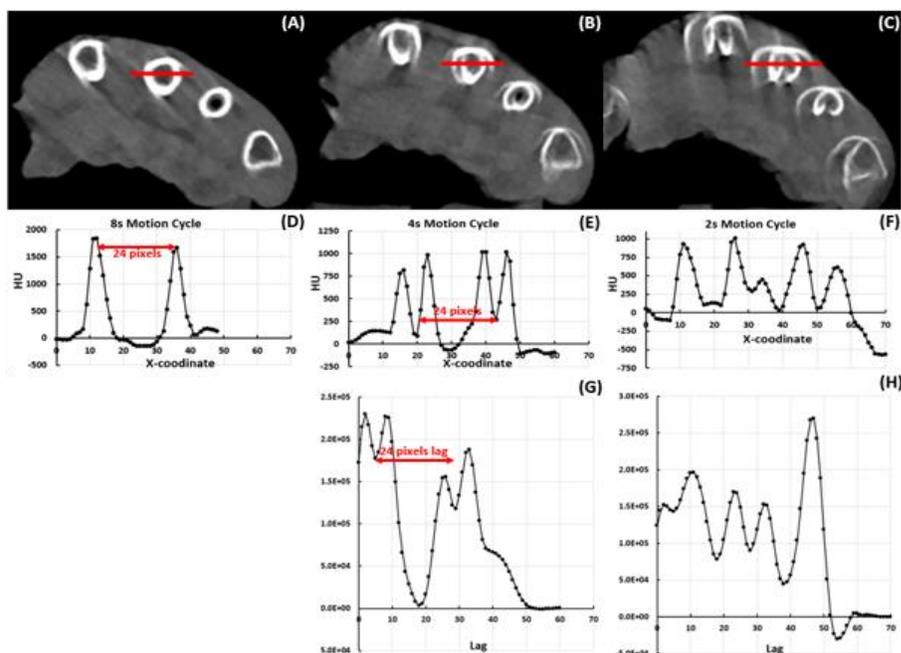
Figure A.1: (A) to (C) cadaveric wrist image at 8, 4, 2s motion cycle corresponding to angular velocity of 9°, 18° and 36°/s during radioulnar deviation. (D) to (E) profile along red line across the 2nd metacarpal bone in (A) to (C). As shown in (D) the two cortical bone edges can be seen in (B, E) and (C, F). The cross-correlation of profile (E) and (H) with reference profile (D) are shown in (G) and (H).

There is 'ghosting' at the cortical edges of the metacarpals caused by intrascan motion blurring. Ghosting was seen at wrist angular rotation velocities of 18°/s and 36°/s but did not appear at 9°/s for RUD; in FE, only an angular rotation velocity of 22°/s did not have ghosting. To semi-quantitatively measure motion blur, profile (E) and (F) was cross correlated with profile (D) to create cross-correlation plots (G) and (H) respectively. Two 'clean' peaks in the cross-correlation plot would indicate no motion blur. Slight indentations in the peaks, as seen in Figure A.1 (G), would indicate some motion blur; the magnitude of indentation relative to the average of the peaks on either side is proportional to level of motion blur. If the motion blur is too severe to reliably create surface reconstructions of the carpal bones, the cross-correlation plots do not show the expected 'clean' peaks (Figure A.1 (H)). This evaluation of motion blur is dependent on a profile void of blur (Figure A.1 (D)). These calculations show that 4DCT scans with a gantry rotation speed of 0.35s/revolution could be used to make surface reconstructions of the

wrist bones if the angular velocities were 9°/s for RUD and 22°/s for FE. As wrist motion frequently occurs at velocities of 30°/s, future studies should aim to improve the 4DCT scanning protocol such that quicker motions can be reliably scanned.

The results from the new and old protocol comparison were calculated as errors between reconstructions, as peak-to-peak ratios, and qualitatively. Examples of blurring artifacts can be seen in Figure A.2.
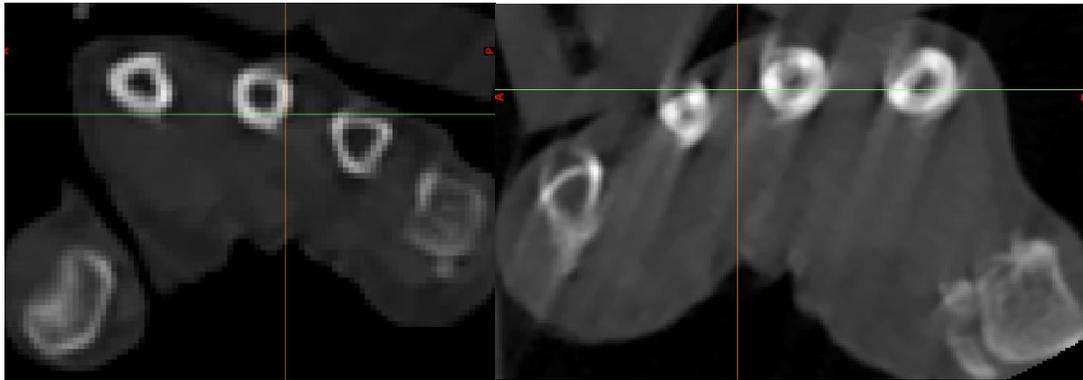

Figure A.2: New protocol (left) and old protocol (right). The old protocol shows considerably more blurring artifacts.

Clearly, the new protocol has no blurring artifacts qualitatively. The errors were calculated from the surface reconstructions of the old and new protocols. The histograms of the individual errors are shown in Figure A.3 while the errors between the two protocols are summarized in Table A.2.

Table A.2: Errors [mm] when comparing surface reconstructions made using the old and new protocols.

Bone	Radius	Scaphoid	Lunate	Capitate
New protocol [mm]	0.4	0.3	0.2	0.3
Old protocol [mm]	0.4	0.4	0.3	0.4
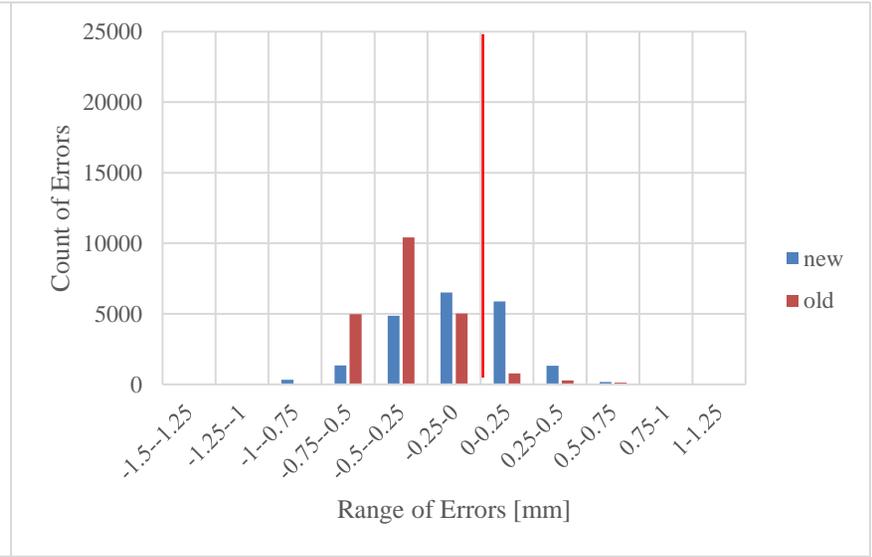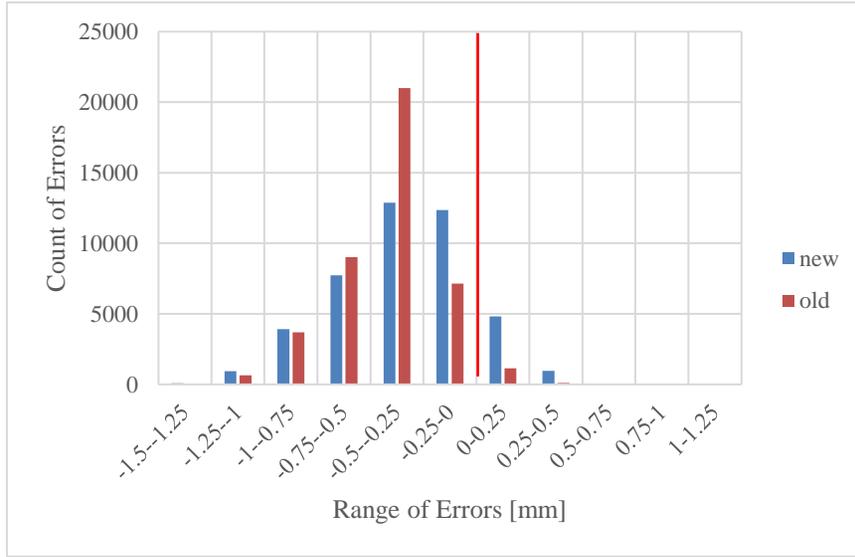
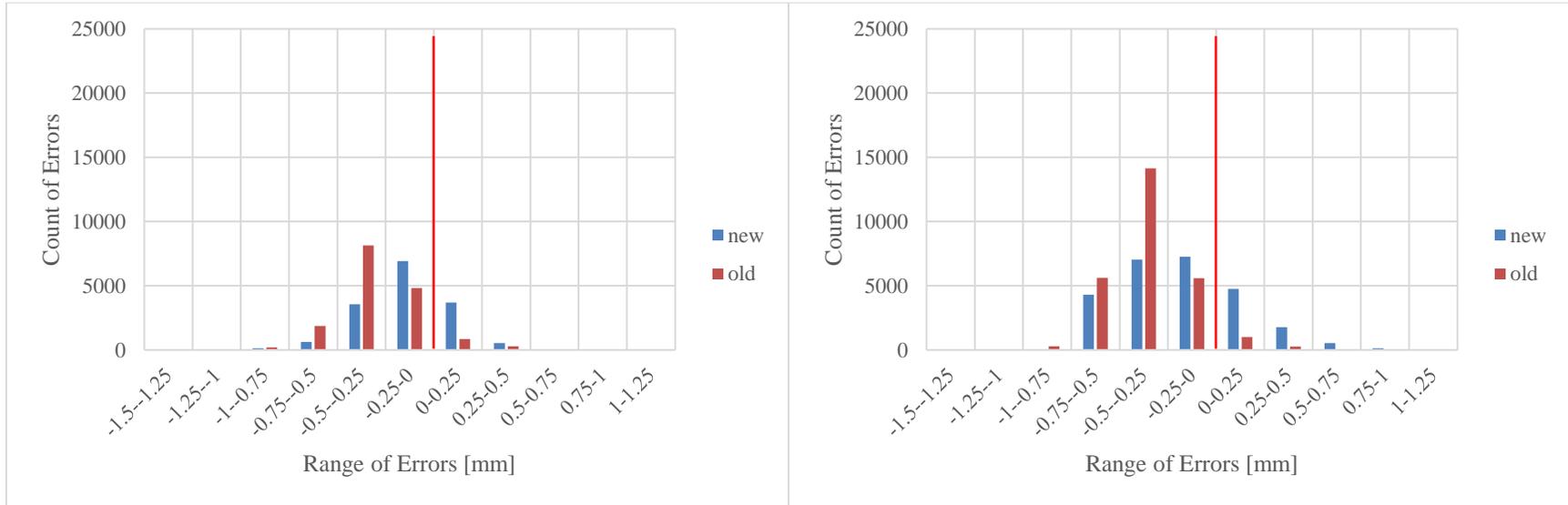**Figure A.3: Histograms of surface reconstruction error of the old and new protocols for the radius (top left), scaphoid (top right), lunate (bottom left), and capitate (bottom right). A red line indicates the zero axis.**

The new protocol had less error in all bones except the radius, where the error was the same as that of the old protocol. The histograms showed similar results. In addition, the histograms highlight how the data is skewed negative in all cases but more so in the old protocol. This indicates that the kinematic models are always smaller than the static models, and that there is a larger size difference between those in the old protocol. In addition, the error in the histograms decreased as the size of the bone decreased, which is reasonable as the larger bones have more surface area where error could occur. While the new protocol is advantageous, the decrease in error is 0-0.1 mm from the old protocol to the new one, which is a very low difference. These are smaller than the errors found in Chapter 3 when comparing 4DCT to the gold standard, comparing between programs, and comparing inter- and intra-rater reliabilities. Thus, an appropriate scan acquisition time is more impactful for blurring artifacts than the change in protocol.

A.4 References

1.   McCollough C, Bruesewitz M, Daly T, Zink F. Motion Artifacts in Subsecond Conventional CT and Electron- Beam CT : Pictorial Demonstration of Temporal Resolution. Radiographics. 2000;20:1675-1681.

2.   Arvidsson I, Åkesson I, Hansson GÅ. Wrist movements among females in a repetitive, non-forceful work. Appl Ergon. 2003. doi:10.1016/S0003-6870(03)00042-5

3.   Taguchi K, Chiang BS, Hein IA. Direct cone-beam cardiac reconstruction algorithm with cardiac banding artifact correction. Med Phys. 2006;33(2):521-539. doi:10.1118/1.2163247

4.   Mori S, Endo M, Asakura H. Improvement in banding artefacts in four-dimensional computed tomography for radiotherapy planning. Phys Med Biol. 2006;51:5231-5244. doi:10.1088/0031-9155/51/20/010

5.   Ramirez-giraldo JC, Yu L, Kantor B, Ritman EL, McCollough CH. A strategy to decrease partial scan reconstruction artifacts in myocardial perfusion CT: Phantom and in vivo evaluation. Med Phys. 2012;39(1):214-223. doi:10.1118/1.3665767

Curriculum Vitae

Name: Sydney Robinson

Post-Secondary   Mechanical Engineering, BASc
Education and   Queen's University, Kingston, Ontario
Degrees: 2015-2019

                       Biomedical Engineering, MESc
                       The University of Western Ontario, London, Ontario
                       2019-2021

Honours and   Ontario Graduate Scholarship
Awards: 2019-2020, 2020-2021

                       Top Poster Presentation
                       Wester Research Forum
                       March 2021

                       Second Place Oral Presentation
                       METRIC 2020
                       October 2020

                       Top Oral Presenter in the Special Emphasis Section: MSK
                       Imaging Innovations
                       The 4th Biennial Canadian Bone and Joint Conference, Bone and
                       Joint Institute
                       June 2020

Transdisciplinary Bone & Joint Award
Collaborative Specialization in Musculoskeletal Health Research
(CMHR), Bone and Joint Institute
2019-2020, 2020-2021

125th Engineering Excellence Award
Queen's University, Kingston, Ontario
April 2019

Dean's Scholar
Queen's University, Kingston, Ontario
2015-2019

Queen's University Excellence Scholarship
Queen's University, Kingston, Ontario
2015-2016

Related Work Experience:

Teaching Assistant
Department of Engineering Science
The University of Western Ontario
2020-2021

Lead Teaching Assistant
Department of Civil and Environmental Engineering
The University of Western Ontario
2019-2020

Publications:

Sydney Robinson, Lauren Straatman, Ting-Yim Lee, Nina Suh, Emily Lalone. (2021). Evaluation of Four-Dimensional Computed Tomography as a Technique for Quantifying Carpal Motion. Journal of Biomechanical Engineering. Published online.

Michael Riddle, Joy MacDermid, Sydney Robinson, Mike Szekeres, Louis Ferreira, Emily Lalone. (2020). Evaluation of Individual Finger Forces During Activities of Daily Living In Healthy Individuals and Those With Osteoarthritis. Journal of Hand Therapy. 33(2): 188-197

Presentations: First Listed Author. The Effect of Volar Scapholunate Tears on Carpal Kinematics. Sydney Robinson, Elizabeth Norman, Michael Rainbow, Emily Lalone, Nina Suh. Canadian Orthopaedic Research Society (CORS). 2021.

Co-Author. Examination of radiocarpal vs midcarpal contribution to flexion and extension motion of the wrist using 4-Dimensional Computed Tomography (4DCT). Elizabeth Norman, Sydney Robinson, Nina Suh, Emily Lalone. Western Research Forum. 2021.

First Listed Author. The Effect of Volar Scapholunate Tears on Carpal Kinematics. Sydney Robinson, Elizabeth Norman, Michael Rainbow, Emily Lalone, Nina Suh. Imaging Network Ontario (ImNO). 2021.

Co-Author. Examination of Radiocarpal vs Midcarpal Contribution to Flexion Motion of the Wrist using Four-Dimensional Computed Tomography. Elizabeth Norman, Sydney Robinson, Nina Suh, Emily Lalone. Imaging Network Ontario (ImNO). 2021.

First Listed Author. Evaluation of scaphoid kinematics using 4-dimensional computed tomography. Sydney Robinson, Lauren

Straatman, Ting-Yim Lee, Nina Suh, Emily Lalone. Canadian Bone and Joint Conference. 2020.

First Listed Author. Development of a Total Wrist Arthroplasty System to Improve Patient Outcomes. Sydney Robinson, Daniel Langohr, Nina Suh, Emily Lalone. Bone and Joint Institute Showcase Series. 2020.

First Listed Author. Evaluation of Scaphoid Kinematics Using Four-Dimensional Computed Tomography. Sydney Robinson, Lauren Straatman, Ting-Yim Lee, Nina Suh, Emily Lalone. METRIC. 2020.

Posters: Co-Author. Examination of Radiocarpal vs Midcarpal Contribution to Flexion and Extension Motion of the Wrist Using 4-Dimensional Computed Tomography (4DCT). Elizabeth Norman, Sydney Robinson, Nina Suh, Emily Lalone. Canadian Orthopaedic Research Society (CORS). 2021.

First Listed Author. The Effect of Volar Scapholunate Tears on Carpal Kinematics. Sydney Robinson, Elizabeth Norman, Michael Rainbow, Emily Lalone, Nina Suh. Western Research Forum. 2021.

First Listed Author. The Effect of Volar Scapholunate Tears on Carpal Kinematics. Sydney Robinson, Elizabeth Norman, Michael Rainbow, Emily Lalone, Nina Suh. Orthopaedic Research Society (ORS). 2021.

Co-Author. Examination of Radiocarpal and Midcarpal

Contribution to Flexion Motion of the Wrist using Four-Dimensional Computed Tomography. Elizabeth Norman, Sydney Robinson, Nina Suh, Emily Lalone. Orthopaedic Research Society (ORS). 2021.

First Listed Author. Evaluation of scaphoid kinematics using four-dimensional computed tomography. Sydney Robinson, Nina Suh, Emily Lalone. Canadian Orthopaedic Research Society (CORS). 2020.

First Listed Author. Development of scaphoid kinematics using four-dimensional computed tomography. Sydney Robinson, Nina Suh, Emily Lalone. Imaging Network Ontario (ImNO). 2020.

Co-Author. Investigation of Hand Forces Produced While Playing Golf: With the Use of New Wearable Sensor Technology to Assist in the Hand Function of Patients with and without Hand Arthritis. Sara Holland, Lauren Straatman, Sydney Robinson, Jim Dickey, Louis Ferreira, Emily Lalone. 6th International Congress on Sport Science Research and Technology Support. 2018.

Co-Author. Evaluating the Hand Forces in Individuals with and without Hand Arthritis using a New Wearable Sensor Technology in Golfers. Sara Holland, Lauren Straatman, Sydney Robinson, Jim Dickey, Louis Ferreira, Emily Lalone. 20th Biennial Meeting of the Canadian Society for Biomechanics. 2018.